NOTE TO USERS

Université d'Ottawa · University of Ottawa

Université d'Ottawa · University of Ottawa

FACULTÉ DES ÉTUDES SUPÉRIEURES ET POSTDOCTORALES

FACULTY OF GRADUATE AND POSTDOCTORAL STUDIES

Candice SY

AUTEUR DE LA THÈSE - AUTHOR OF THESIS

M. Sc. (Cellular and Molecular Medicine)

GRADE - DEGREE

Department of Cellular and Molecular Medicine

FACULTÉ, ÉCOLE, DÉPARTEMENT - FACULTY, SCHOOL, DEPARTMENT

TITRE DE LA THÈSE - TITLE OF THE THESIS

The Cloning of *Notch1* and *Groove* in *notophthalmus viridescens*, the Red-spotted Newt, and an Examination of the Expression Profiles of Both Genes in the Regenerating Forelimb through Real Time RT-PCR

C. Tsilfidis

DIRECTEUR DE LA THÈSE - THESIS SUPERVISOR

CO-DIRECTEUR DE LA THÈSE - THESIS CO-SUPERVISOR

EXAMINATEURS DE LA THÈSE - THESIS EXAMINERS

M.-A. Akimenko

V. Wallace

J.-M. De Koninck, Ph.D.

LE DOYEN DE LA FACULTÉ DES ÉTUDES SUPÉRIEURES ET POSTDOCTORALES

SIGNATURE

DEAN OF THE FACULTY OF GRADUATE AND POSTDOCTORAL STUDIES

THE CLONING OF *NOTCH1* AND *GROOVE* IN *NOTOPHTHALMUS VIRIDESCENS*, THE RED-SPOTTED NEWT, AND AN EXAMINATION OF THE EXPRESSION PROFILES OF BOTH GENES IN THE REGENERATING FORELIMB THROUGH REAL TIME RT-PCR

by

Candice Sy

A thesis is submitted in partial fulfillment of the Master of Science program in Growth and Development, Department of Cellular Molecular Medicine

July 15, 2003

University of Ottawa, Canada

Your file Votre référence
ISBN: 0-612-90351-6
Our file Notre référence
ISBN: 0-612-90351-6

ABSTRACT

Limb regeneration in urodeles is a complex process that involves the reinduction of a number of genes that are expressed during limb development. *Notch* is an essential developmental gene that is likely to play a pivotal role in the genetic control of forelimb regeneration in the red-spotted newt, *Notophthalmus viridescens*. In this thesis, a partial cDNA of the newt homologue of *notch1* was cloned, as well as a complete cDNA containing only 5 EGF repeats and a NIDO domain which also showed homology to *notch1*. This truncated version of *notch1* is suspected, based on its functional domains, to act as a secreted dominant negative regulator of Notch signaling. Real time RT-PCR detection of expression of both genes revealed that *notch* is expressed at relatively high levels in both the 24 hour and the 2 week regenerate. This may point towards a functional role for Notch signaling in the wound healing process, through activation of cell migration and mobilization, and in the regeneration blastema, through induction of cell proliferation and repression of differentiation. The truncated notch isoform is expressed at low levels in all the tissues that express *notch*, but whether this results in dominant negative regulation of Notch signaling is currently unknown. Together, these data point towards a functional role for *notch* in epimorphic limb regeneration.

TABLE OF CONTENTS

APPENDIX 4 – PCR PROGRAMS

LIST OF FIGURES

LIST OF ABBREVIATIONS

BIOLOGICAL TERMINOLOGY

AEC	apical epithelial cap
AER	apical ectodermal ridge
DNA	deoxyribonucleic acid
CNS	central nervous system
Ct	threshold cycle
PCR	polymerase chain reaction
RACE	rapid amplification of cDNA ends
RNA	ribonucleic acid
RT-PCR	reverse transcription polymerase chain reaction
ZPA	zone of polarizing activity

GENETICS

bHLH	basic helix-loop-helix
DlEC	Delta extracellular
DNER	Delta/Notch-like Epidermal Growth Factor-related receptor
EGF	epidermal growth factor
FGF	fibroblast growth factor
HDAC	histone deacetylase
HES	hairy enhancer of split
JNK	c-jun N-terminal kinase
LNR	Lin-12/Notch related
MET	methionine
ORF	open reading frame
PSORT	prediction of protein sorting signal localization sites in amino acid sequences
Rb	retinoblastoma
shh	sonic hedgehog
SMRT	silencing mediator of retinoid and thyroid hormone receptors
sns	sticks-and-stones
Su(H)	suppressor of hairless
TAD	transcriptional activator domain
UTR	untranslated region

CHEMICALS AND REAGENTS

DMSO	dimethylsulfoxide
FCS	fetal calf serum
IPTG	isopropylthio-B-D-galactoside
LB	Luria broth
MS222	3-aminobenzoic acid ethyl ester
PBS	phosphate buffered saline
PFA	paraformaldehyde

TAE	tris/acetic acid/EDTA
X-gal	5-bromo-4-chloro-3-indolyl-B-D-galactoside

ACKNOWLEDGEMENTS

First and foremost, my thanks goes out to my supervisor, Cathy, for giving me the freedom and autonomy to guide my own project. Thank you for all the ways in which you helped me learn and grow as a scientist. Thank you also for all the kindness and support you have shown in helping me towards my future. For that I am truly grateful.

Thank you to members of my examining committee, Dr. Valerie Wallace and Dr. Marie-Andrée Akimenko for their time and contributions.

Thank you to Dr. Alan Mears for the SYBR green and for his help with the real time RT-PCR.

Thanks to the members of the Tsilfidis Lab, in particular:

Shawn Beug, my partner in crime through these two years, thanks for your help, and more importantly for your friendship. It's been fun. Thanks also for the GapDH primers; someone had to clone it, I'm glad it was you.

Adam Baker, thanks for your unconditional help in everything related to the lab, and for all those times you've helped bail me out of some mess or other.

Sandy Vascotto, thanks for the original *notch* fragment, the double stranded adapter ligated RACE cDNA template, and for the excellent technical advice.

Thank you to my mother, my father and sister for their unconditional love and support.

Thank you to Adam Leverette for being my emotional support through thick and thin. Thank you for being there for me, for listening to my unending complaining, and for telling me that it would be alright (you were right).

Thanks to Erin Koen and Stephanie Desilets for being the best roommates ever, and for making my time in Ottawa truly memorable. In the darkest hours, it was the ice cream and the gummies that pulled me through.

Finally, thank you to all the red-spotted newts whose participation (albeit unwilling) in my project earned me a master's degree. We couldn't have done it without you.

INTRODUCTION

Basic types of regeneration

Wound healing and stem cell mobilization

In order to survive, organisms are constantly faced with the challenge of repairing and replacing tissue that has been damaged due to environmental stress or physical injury. Organisms display a wide array of mechanisms for dealing with tissue damage that range from basic wound healing and scarring, to more complex forms of healing such as regeneration. On the most fundamental level, many mammals and "higher" vertebrates deal with tissue damage by initiating an immune response which attenuates the damage and results in the formation of scar tissue. This tissue is not functional, but serves to protect the site of injury from infection and further damage. However, many mammals also have very limited abilities to regenerate tissue, by activating populations of progenitor cells that reside in respective tissues (Campion, 1984). For example, in mature muscle tissue, there exists a population of satellite cells which, upon muscle damage, populate the area of damage and differentiate into mature muscle cells (Carlson, 2003). In addition, it has been shown that many mammals also have the ability to initiate hyperplasia in response to liver tissue damage (Stocum, 2001). Liver hyperplasia is characterized by a partial reversion of mature hepatocytes back to a more primitive state, followed by proliferation to compensate for the damaged tissue (Stocum, 2001). However, the tissue that ensues from hyperplasia is not patterned, and does not lose its functional properties while it is proliferating, indicating only a partial regenerative response (Stocum, 2001).

Morphallaxis

A more interesting form of regeneration, called morphallaxis, is found in metazoans such as planarians, *Hydra*, and echinoderms (Brockes, 1997). Morphallactic regeneration is initiated when the organism is bisected. From the plane of amputation, the remaining cells are re-patterned, then grow into the proper dimensions of the original. Interestingly, in *Hydra*, the capacity to regenerate is limited to the area of the body column, where normal cells are continually dividing in the adult *Hydra*, either to replace cells being sloughed off, or to replace cells budded off for asexual reproduction (Bode, 2003). Since these cells regularly undergo cell division and patterning to maintain the adult organism, they may in some respects be classified as stem cells, which never fully differentiate and exit the cell cycle (Bode, 2003). Consequently, there is no point where differentiated cells re-enter the cell cycle to produce the regenerated *Hydra*. In this sense, morphallaxis in *Hydra*, while impressive, is not necessarily more complex than mammalian regeneration, in that mobilization of undifferentiated stem cells is still required to form the new regenerate.

Epimorphic regeneration

The most complex form of regeneration is epimorphic regeneration. This type of regeneration is seen in only a limited number of vertebrates, most of which are urodeles. Epimorphic regeneration differs from stem cell mobilization, hyperplasia, or morphallaxis in that terminally differentiated mesenchymal (often post-mitotic) cells at the plane of amputation dedifferentiate and revert back to a pleuripotent, embryonic-like state. Following this, the cells re-enter the cell cycle and proliferate to form a blastema, then are re-patterned and re-differentiate in order to form the new regenerate. Most

urodeles combine mechanisms of stem cell mobilization with epimorphic regeneration to regenerate different organs in their body. For example, it is thought that damaged blood, epithelia, bone and muscle tissue are typically replaced by the mobilization of reserve populations of stem cells, whereas whole organs such as limbs, jaws, tails and lenses are replaced by epimorphic regeneration (Nye *et al.*, 2003).

Limb regeneration: rebuilding a complex structure

At the height of the spectrum of epimorphic regeneration is limb regeneration. The asymmetric morphology of the limb, as well as the fact that it is comprised of multiple tissue types, makes it an extraordinarily complex system to rebuild and a fascinating system to study. The fact that it is readily accessible and easy to manipulate also makes it ideal for studying epimorphic regeneration. Limb regeneration exhibits all the phases of classical epimorphic regeneration. Immediately after the limb is amputated, epithelial cells from the surrounding epidermis migrate to cover the wound stump in a process termed wound healing (Figure 1). Wound healing is initiated immediately after amputation and may continue for up to 5 days post-amputation (Iten and Bryant, 1973). Following this, cells are induced to lose their differentiated characteristics and revert back to a pleuripotent, embryonic-like state. This phase is called dedifferentiation, and begins 6-8 days after amputation (Iten and Bryant, 1973). Dedifferentiated cells re-enter the cell cycle, and begin to proliferate to form a mass called the blastema. During blastema formation, cells remain undifferentiated while they proliferate. The peak of blastema formation is thought to be at 15 days (approximately 2 weeks) post amputation (Iten and Bryant, 1973). Following this, the dedifferentiated cells begin to grow outwards from the stump. The cells form a spike, which begins to flatten into a palette

Figure 1. Photographic representation of different stages of *Notophthalmus viridescens* forelimb regeneration (taken from Goss, 1969). The panel on the left depicts a typical regenerative profile when the adult forelimb is amputated at the level of the mid-radius/ulna. The panel on the right represents the standard regenerative profile when the limb is amputated at the level of the mid-humerus. Note that regardless of the level of amputation along the proximodistal axis, the regenerate retains positional information. This means that the newt only regenerates structures distal to the plane of amputation, such that proximal structures are not duplicated, and the new regenerate is a perfect replica of the original.

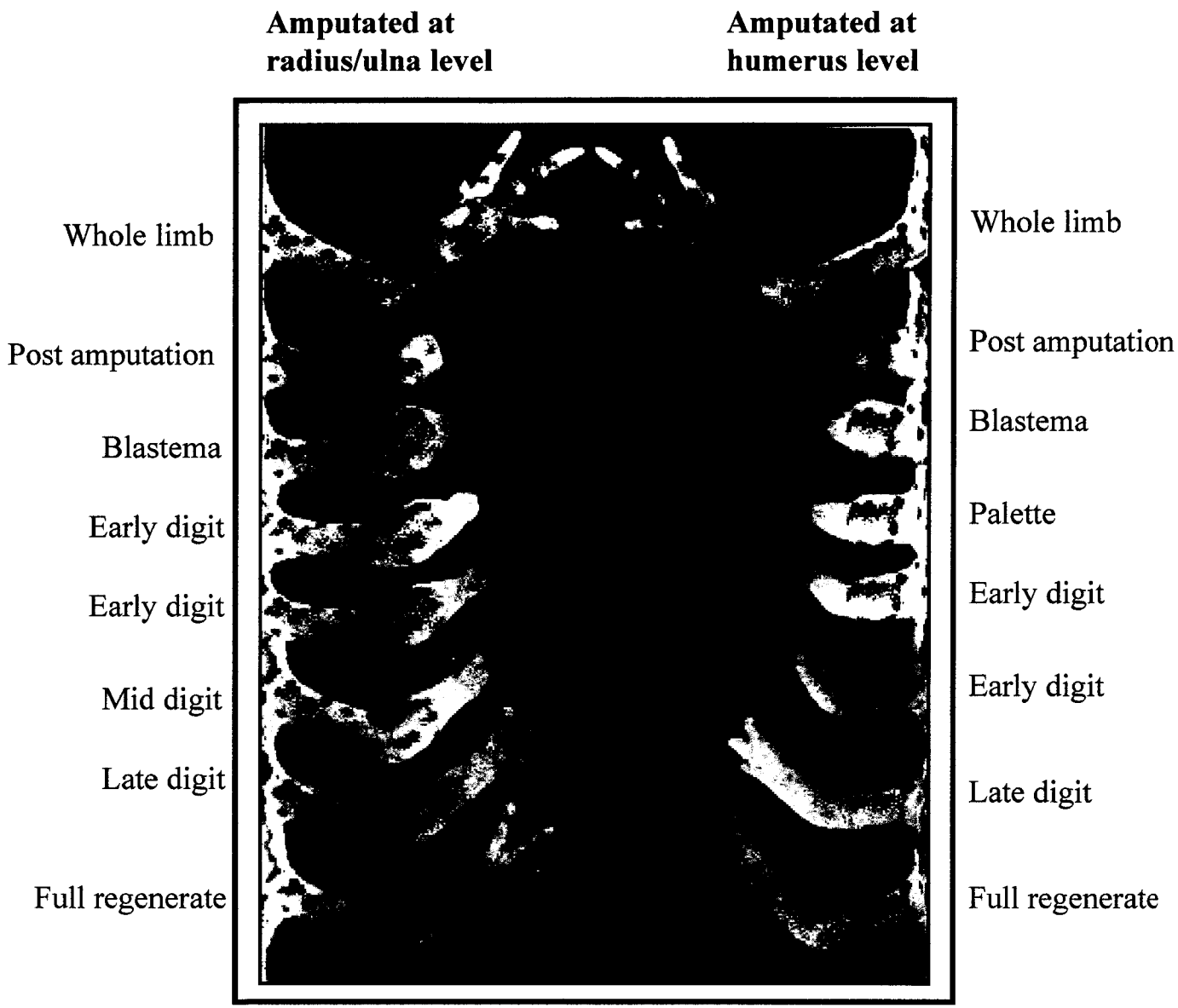
Amputated at radius/ulna level
Amputated at humerus level
Whole limb
Post amputation
Blastema
Early digit
Early digit
Mid digit
Late digit
Full regenerate
Whole limb
Post amputation
Blastema
Palette
Early digit
Early digit
Late digit
Full regenerate

between 18-24 days post amputation (Iten and Bryant, 1973). During this time, the cells are beginning to be re-patterned, starting with the ones most proximal to the amputation site. By 22-28 days post amputation the distal tip of the limb has flattened into a visible palette. By this stage, termed the palette stage, early transdifferentiation of cells is beginning, and dedifferentiated cells are re-differentiating to form cartilage which has started to condense at the proximal end of the new regenerate (Iten and Bryant, 1973). Note that the rate of regeneration is subject to variations in temperature and fitness of the individuals, hence the large time interval encompassing each stage. Anywhere from 24-33 days post amputation, digit formation and outgrowth begins. At this time, extensive re-differentiation of the dedifferentiated cells is occurring in the regenerate, as well as re-patterning. Again, patterning and maturation of the regenerate occurs in a proximal to distal fashion, with the cells at the proximal tip being the most mature, and the cells at the distal tip being the least. Complete regeneration takes approximately 2.5 to 3 months.

Transferring regenerative potential to higher vertebrates: barriers

Was regenerative ability "lost" through evolution?

The fact that the most exceptional regenerative ability is limited to a small subset of "lower" vertebrates raises the question of whether regenerative ability has been lost through evolution. It is thought that the immune system of many "higher" vertebrates initiates a protective inflammatory response which interferes with processes which are necessary for regeneration (Harty *et al.*, 2003). This immune response often involves the recruitment of neutrophils to the site of injury, which control for bacterial invasion and infection, but also release proteases and other cytokines which interfere with regeneration (Harty et al., 2003). The platelets that are responsible for initiating the blood clotting

cascade which initially closes the wound and also attract macrophages to the site of injury, which phagocytocize dead cells and activate fibroblasts (Singer and Clark, 1999). These fibroblasts eventually begin to lay down a granular matrix by producing a number of substances such as fibronectin, hyaluronate and collagen (Singer and Clark, 1999; Harty et al., 2003). Eventually, the fibroblasts become myofibroblasts, which, in conjunction with macrophages, serve to compact the collagen matrix and create the tightly woven, non-functional scar tissue (Singer and Clark, 1999). During this stage of collagen deposition, many cells die by apoptosis, further contributing to the non-functional quality of scar tissue (Singer and Clark, 1999). In addition, some scars such as glia scars in the central nervous system (CNS) actually produce chondroitin sulfate proteoglycan molecules such as NG2, neurocan and phosphacan, which inhibit neurogenesis and further impede regeneration (Chen *et al.*, 2002).

If it is the inflammatory immune response of "higher" vertebrates that impedes regeneration, then it would follow that prevention of the immune response would lead to an increased ability to regenerate, provided that the underlying programs that mediate regeneration are still conserved. Our ability to artificially initiate regeneration in "higher" vertebrates will then depend on two factors: 1) understanding the mechanisms which control regeneration, which will then allow us to manipulate these variables, and 2) the extent to which our body system is capable of naturally adapting to the regenerative mechanisms instigated.

Regenerative potential in "higher" vertebrates

It has been shown that children and rats (non-regenerative mammals) have the ability to regenerate the distal tips of their digits, so long as the amputated wound surface

is not covered with tissue grafts of any sort (Borgens, 1982; Illingworth, 1974). This regenerative capacity of the distal digit tip has also been shown to still be present in adult humans (Muller *et al.*, 1999). This suggests that many mammals and "higher" vertebrates intrinsically possess the genetic and physiological programs that allow for appendage regeneration, albeit to a limited degree. More recently, it has been demonstrated that terminally differentiated mammalian myotubes can be induced to re-enter the cell cycle and lose their differentiated characteristics (MyoD, myogenin and troponin T expression) when cultured in the presence of an extract from regenerating newt limbs (McGann *et al.*, 2001). This is further evidence that mammalian cells may still possess the intrinsic capacity to regenerate when induced by the proper signals, and leads to the hypothesis that it is either the lack of proper regenerative stimuli or the prevention of regeneration by specific factors (such as an immune response) that limits regenerative potential in higher vertebrates.

Sequential barrier model of regeneration

In 1999, Muller et al. proposed a sequential barrier model for regenerative potential, wherein progressive maturation of tissues creates barriers to regeneration that must be overcome (or reverted) in order for vertebrates to regenerate. In young vertebrates, only a few barriers may exist which must be overcome to allow for regeneration. This is demonstrated by various species which have impressive regenerative ability in their developmental phase of life, but lose it as they mature. For example, *Xenopus laevis* possess the ability to regenerate entire hindlimbs when amputated in their larval phase, but lose this ability as they develop towards metamorphosis (Dent, 1962). Similarly, the developing limbs of embryonic chicks and

mice have limited regenerative capacity when amputation occurs in areas where cells have not yet differentiated (Bryant et al., 2002). However, this limited regenerative ability is soon lost as the cells begin to differentiate. As vertebrates mature, more barriers (such as terminal differentiation) may arise, which will be harder to overcome, as it involves more steps backwards in the developmental process in order to recapitulate the patterning programs that are required for regeneration.

One possible solution lies in the newt

The ability of newt to overcome this barrier through dedifferentiation is extremely valuable to us, as it poses a potential solution to the problem of tissue maturation which limits our ability to regenerate. Further, the ability of the newt to re-induce the developmental programs that pattern the new regenerate is paramount to reinstating the functional ability of the newly regenerated tissue. By understanding the genetic mechanisms by which the newt controls dedifferentiation, re-patterning and re-differentiation, we may be able to overcome some of the major barriers to regeneration in higher vertebrates. This, in combination with suppressing the immune response, may be the key to eventually artificially inducing regeneration in higher vertebrates. This is of tremendous medical relevance, as the ability to regenerate all or part of an organ may some day abolish the need for organ transplants. Further, the ability to regenerate entire appendages may abolish the need for prosthetics, while greatly improving the quality of life for those who suffer from extremity amputations due to injury or disease. In addition, the ability to regenerate ocular structures may some day make blindness a thing of the past.

While it seems unlikely that we will be able to fully decipher all the genetic control mechanisms that underlie the regenerative process in the near future, it has been recently suggested that perhaps we will not have to do so in order to use regeneration in medical science. Bryant et al. (2002) maintain that dedifferentiated newt cells may be classified as a type of stem cell, in that they are renewable and maintain a high level of plasticity. Because of this, the authors argue that studying these cells will enhance our understanding of stem cell biology, and may increase our ability to manipulate mammalian stem cells. Further, they cite recent work which shows that human adult stem cells such as bone marrow stem cells are far more pleuripotent than once believed, and have the capacity to differentiate into blood vessels, heart, brain, liver and muscle tissue (Blau et al., 2001). The discovery that human stem cells still retain a broad plasticity brings us one step closer to actually being able to induce regeneration in humans, in that our cells seem to possess intrinsic capabilities to transdifferentiate and regenerate. We simply need to learn how to initiate, manipulate and direct the process. Altogether, this points to the importance of studying regeneration biology, and highlights the potential medical application of any discoveries made in the field.

Cellular and genetic control of limb regeneration

Wound healing

Having outlined the value of studying urodele limb regeneration, it is important to take a closer look at the basic framework in which regeneration takes place. The first step in regeneration is wound healing, where cells from the epidermis surrounding the plane of amputation migrate to cover the wound stump. This step, while simple, is crucial to the regeneration process. It has been observed that if bits of bone protruding

from the amputation stump physically interfere with the formation of a wound epithelium, then full epimorphic regeneration is prevented. Similarly, if the amputation surface is immediately covered with mature skin, such as a graft, regeneration is also prevented (Stocum, 2001). The reason why the wound epithelium is so important is that it acts as a source of signaling molecules that communicates with the underlying mesenchyme. In the regenerate, the distal wound epithelium eventually thickens and forms into a structure called the apical epithelial cap (AEC), which has been compared to the apical ectodermal ridge (AER) in developing amniote limbs. The AER also acts as a source of developmentally important genes that are necessary for limb outgrowth. Cross-signaling between the AER/AEC and the underlying mesenchyme is made possible by the lack of a basement membrane between the two, and is necessary for both regeneration and development. Removal of the AER/AEC leads to an arrest in limb outgrowth in both development and regeneration, respectively (Saunders, 1948; Stocum and Dearlove, 1972).

Both the AEC and the AER produce members of the fibroblast growth factor (FGF) family that are crucial for limb outgrowth. In embryonic chickens, it has been shown that replacement of the AER with a bead soaked in FGF suffices to promote normal outgrowth in a limb which would otherwise not grow at all (Niswander et al., 1993). In *Xenopus,* treating regeneration-competent *Xenopus* limbs with FGF receptor inhibitors can prevent regeneration (D'Jamoos *et al.*, 1998). Yokoyama et al. (2000) showed that expression of *fgf10* in the mesenchyme of regenerating *Xenopus* correlates to the animal's ability to regenerate. In addition, they showed that epidermis transplanted from an older heteromorphic *Xenopus* tadpole can be induced to re-express *fgf8* when

placed onto mesenchyme from a younger staged, regeneration-competent limb (Yokoyama et al., 2000). This reinforces the importance of FGFs as signaling molecules in the regeneration process. In addition, it also highlights the importance of the cross-talk between the mesenchyme and the AEC in regeneration.

Dedifferentiation

The next stage of limb regeneration is dedifferentiation, which is characterized by the cells of the mesenchyme underlying the wound epidermis losing their differentiated cellular characteristics and re-entering the cell cycle. The point at which cells typically re-enter the cell cycle is at the S phase of DNA synthesis. This transition point is usually regulated by retinoblastoma (Rb), a protein that normally prevents cells from making the transition from G1 to S phase. It has been shown that in regenerating newt limbs, Rb is phosphorylated upon serum stimulation, which relieves G1 to S phase arrest and promotes S phase re-entry (Tanaka et al., 1997). Thrombin, a member of the cascade that leads to blood clotting after injury, has also been shown to induce newt myotubes to re-enter the cell cycle (Tanaka et al., 1999). It is unknown whether thrombin is the factor that is initiating the signaling cascade that leads to Rb phosphorylation and S phase re-entry, but the fact that it also results in S phase re-entry suggests that it may be an upstream component of the signaling pathway which initiates dedifferentiation.

Blastema formation

Once the cells dedifferentiate, they must remain in an undifferentiated state while they proliferate to form a blastema. Several lines of evidence point to the importance of maintaining this undifferentiated state for a certain amount of time prior to re-differentiation. Post-metamorphic *Xenopus* limbs also form a blastema after amputation,

but the cells begin to differentiate immediately, which results in the formation of a heteromorphic spike, instead of a full regenerate as seen in younger, regenerative larvae (Dent, 1962). In 1999, Shimizu-Nishikawa *et al.* shed further light on the importance of maintaining this undifferentiated state by comparing the expression patterns of genes which may regulate differentiation in both the regeneration-competent urodele *Cynops pyrrhogaster* and the non-regenerative adult *Xenopus laevis*. Id2 and Id3 act as repressors of differentiation by binding to and sequestering basic helix-loop-helix factors (bHLHs) which activate differentiation-promoting genes such as *myoD* and *achaete-scute* (Shimizu-Mishikawa et al., 1999). In this manner, Id2 and Id3 expression serves to maintain the blastema in an undifferentiated state. Both genes were shown to be expressed in the blastema of both *Xenopus* and *Cynops* (Shimizu-Mishikawa et al., 1999). However, Id3 expression decreases as the *Xenopus* heteromorphic spike begins to form, whereas levels still remain high in the regenerating *Cynops* limb (Shimizu-Mishikawa et al., 1999). The authors suggest that the decrease in Id3 promotes early re-differentiation of cartilage in *Xenopus*, which pre-empts the proper re-patterning of the blastema which is necessary for complete functional regeneration (Shimizu-Mishikawa et al., 1999).

Similarly, Reginelli et al. (1995) performed experiments that correlate the expression of *Msx1* to the ability of embryonic mice to regenerate digit tips. They found that positional regenerative ability along the proximal-distal axis corresponds spatially to the expression domain of *Msx1* but not *Msx2,* which was expressed more proximally (Reginelli et al., 1995). As *Msx1* is a negative regulator of differentiation, the authors proposed that *Msx1* permits regeneration by maintaining cells in an undifferentiated, proliferating state before re-patterning and regeneration occurs (Reginelli et al., 1995).

Indeed, *Msx1* has been shown to be upregulated in the late bud stage of regeneration in axolotls, where maximal dedifferentiation is taking place (Koshiba et al., 1998). In addition, *Msx1* is expressed throughout the entire mesenchyme at this stage of regeneration, which lends further evidence to its role in maintaining the undifferentiated state of the entire blastema (Koshiba et al., 1998). As an interesting aside, *Msx1* also displays the same expression pattern (throughout the mesenchyme) in the developing axolotl limb bud (Koshiba et al., 1998). In this way, it seems that at least some genes responsible for the development of embryonic limbs are re-used in regeneration in the same manner as they appear to be used in development. Altogether, these data highlight the importance of the blastema formation stage of epimorphic regeneration.

The role of nerves in limb regeneration

It has long been known that nerves play a crucial role in the blastemal formation stage of limb regeneration. Experiments wherein adult axolotl forelimb regenerates were denervated prior to the early bud stage of regeneration resulted in a resorption of the developing blastema and a complete failure of the limb to regenerate (Nye et al., 2003). Denervation after the early limb bud stage produced a miniaturized limb, which is thought to be the result of cells arresting in the G1 stage of the cell cycle (Nye et al., 2003). From these experiments, it is evident that nerves are producing a factor or substance that is essential to blastemal outgrowth and formation, but which is not as crucial in the later stages of regeneration following blastema formation. Several candidate factors have been identified, including Fgf2, Ggf2, substance P and transferrin (Nye et al., 2003). Of these factors, transferrin appears to currently hold the most promise as a blastema promoting factor. One reason why is that it has been shown to be

neurally localized, and is transported on sciatic axons and released into the limb regenerate (Nye et al., 2003). Further, it has been shown to promote high levels of blastema cell proliferation in denervated cells that would otherwise stop proliferating (Nye et al., 2003). These effects on cell proliferation can be specifically reversed by blocking transferrin activity with anti-transferrin antiserum and chelating agents (due to the fact that transferrin activity requires iron as a cofactor) (Nye et al., 2003).

Re-patterning and transdifferentiation

The next and final stage of regeneration involves a plethora of genes that all work together to re-pattern different aspects of the new regenerate. All the genes that are used to re-pattern the regenerate, with one exception (*Hoxc10*), are also involved in the patterning of developing limbs (Bryant et al , 2002); however, this does not mean that they necessarily display the same spatial or temporal expression patterns that they did in the developing limb bud. While some genes do display the same expression patterns, others do not. Here I will present a brief overview of some of the basic genetic networks involved in the complicated task of re-patterning the regenerating newt limb.

Perhaps one of the most amazing features of epimorphic regeneration is the ability of the newt to conserve positional identity. Regardless of the level of amputation along the proximodistal axis, the newt will only regenerate structures distal to that point of amputation in a manner that replaces the original, but does not duplicate proximal structures (see Figure 1). The most renown molecule implicated in the control of positional specification is retinoic acid. First known for its ability to proximalize and duplicate regenerating structures (Maden, 1982), it has since been shown to be able to ventralize and posteriorize limbs, depending on the concentration administered (Nye et al

, 2003). The ability of retinoic acid to dictate positional identity along the proximodistal axis may be conferred through a gene called *Prod1*, which is responsive to retinoic acid, and is located at the cell surface (da Silva et al, 2002). The ability of a ligand to confer positional identity, however, is useless without the presence of the appropriate receptor to mediate signal transduction. Retinoic acid receptors α and β are expressed in the newt blastema, as well as $\delta 1$ and $\delta 2$ (Nye et al., 2003). Of these retinoic acid receptors, it has been shown (through experiments involving activation of individual retinoic acid receptors in chimeric T3 receptor constructs) that $\delta 1$ is responsible for mediating proximodistal specification (Pecorino et al, 1996).

Other genes which are known for their role in establishing pattern include members of the *Hox* family of genes. In particular, the colinear expression pattern of *hoxA* genes usually dictate the positional identity of limb structures along the proximodistal axis. *HoxA9* expression is usually seen in tissues that will give rise to structures of the forelimb including the hand, the forearm, and parts of the humerus (Gardiner et al., 1995). The expression of *hoxA13*, on the other hand, is restricted to a distal part of the tissue and is nested within the region of *hoxA9* expression (Gardiner et al., 1995). It is thought that the combination of *hoxA9* and *hoxA13* expression in the presumptive distal hand tissue determines the identity of the hand structure, whereas the expression of only *hoxA9* in proximal tissues identifies tissues fated to become proximal structures (Gardiner et al., 1995). In agreement with this hypothesis, Gardiner et al. (1995) showed that treatment of the regenerating axolotl blastema with retinoids proximalized the tissue by decreasing levels of *hoxA13* expression, but not *hoxA9* expression. In addition, *hoxA9* expression appears earlier in the developing limb than

hoxA13 (Gardiner et al., 1995). The expression patterns of *hoxA9* and *hoxA13* in the developing axolotl forelimb are consistent with these patterns, which have been previously observed in chicks and mice (Gardiner et al., 1995). However, the regenerating axolotl forelimb interestingly displays an alternate expression pattern for *hoxA9* and *hoxA13*. Instead of displaying colinear expression, *hoxA9* and *hoxA13* are expressed simultaneously in the early regenerate in a colocalized manner (Gardiner et al., 1995). Later in the regenerate, *hoxA13* eventually becomes restricted to distal cells, and thus the pattern of *hoxA* expression begins to resemble that of development again (Gardiner et al., 1995). However, this shows that while some of the genes expressed during development are reinstated in regeneration, their patterns of expression may not be recapitulations of development. This may be indicative of fundamental differences between the physiological processes of development and regeneration which we have yet to fully understand.

Another developmentally important signaling molecule is Sonic hedgehog (shh). In chicks, it is produced in the zone of polarizing activity (ZPA), which is a major signaling center that is responsible for patterning along the anteroposterior axis (Riddle et al, 1993). *shh* expression in both the developing and the regenerating axolotl limb is similar to that of chicks in that it is localized within the posterior mesenchyme (Torok et al, 1999). However, Nye et al. (2003) note that the fairly limited and late expression pattern of *shh* in the axolotl limb does not seem to be sufficient for it to be responsible for establishing anteroposterior patterning in the limb. This is confirmed by recent experiments performed by Roy and Gardiner (2002), where *shh* signaling was blocked, and the resulting limb displayed correct anteroposterior patterning, but incorrect digit

formation. Therefore, *shh* in the regenerating limb is responsible for the specification of the digits, but not for the determination of patterning along the anteroposterior axis.

Other potentially important genes involved in pattern formation are *Wnt7a*, *En1*, and *Lmx2* (Nye et al, 2003). These genes establish patterning in the regenerate along the dorsal-ventral axis (Nye et al., 2003). Interestingly, En1 is also known to dorsally restrict the expression of another gene called *radical fringe* (*Rfng*) in chicks (Gardiner et al., 2002). *Rfng* is one of the genes that is involved in the control of dorsal-ventral pattern formation in the developing *Drosophila* wing, through its modulatory effects on another gene called *notch* (Bray, 1998). *Notch* is a very important gene which acts as a central controller of many developmental events, and regulates the development of a wide range of tissues from all three germ layers (Artavanis-Tsakonas et al., 1995). Its potential role in regeneration extends far beyond that of simple dorsal-ventral patterning, as we will see later.

Notch in development: a potential role in regeneration?

Notch: master regulator of development

Having established that many of the genes that control regeneration are the same as those that guide development, the importance of investigating developmentally significant genes for their possible role in regeneration becomes apparent. At the zenith of the list of developmentally important genes is *notch*. First isolated in *Drosophila*, it has been found in every organism from *C.elegans*, to *Xenopus*, to sea urchins, to humans. Its evolutionary conservation underscores its importance as a developmental regulatory molecule. It has been implicated in such a wide array of developmental processes that it has come to be known more as a general "arbiter of cell fate" which acts as a "master

switch" for controlling developmental decisions, rather than for any one particular function that it performs in development (Miele and Osborne, 1999). In most cases, *notch* mutants are embryo lethal, however an analysis of the embryos reveals interesting patterning and lineage abnormalities, such as the neurogenic phenotype, where too many cells adopt a neural fate (Artavanis-Tsakonas et al., 1999). Depending on the system, *Notch* regulates the spatial organization of developing tissues, boundary formation, cell fate and lineage decisions, the timing of specific developmental events as they relate to cell proliferation and differentiation, and events related to apoptosis. Notch mediates these events through specific interactions at both the ligand binding level as well as the signal transduction level. These will be discussed in more detail later.

The molecular structure of notch

Notch is a single pass transmembrane receptor (Miele and Osborne, 1999). *Drosophila* have only one *notch* gene, while mammals have four *notch* genes, the longest of which is *notch1* (Miele and Osborne, 1999). The extracellular domain of Notch consists of multiple repetitive domains that are similar to Epidermal Growth Factor (EGF) (Figure 2). There are 36 EGF repeats in *Drosophila* Notch and mammalian Notch1 and Notch2, while Notch3 and Notch4 contain fewer repeats (Weinmaster, 1997). These repeats mediate ligand binding; different repeats confer specificity to different ligands, though two ligands may also bind common EGF repeats (Baron et al., 2002). 3' to the EGF repeats lie three Lin-12/Notch related regions (LNR), which are *notch*-specific and are conserved in all species from *C. elegans* (where Notch is named Lin) to humans (Weinmaster, 1997). These domains do not appear to interact with other signaling molecules, however, they are nevertheless important in regulating receptor

Figure 2. Molecular structure of the Notch1 receptor. The extracellular domain is comprised of 36 tandem EGF repeats followed by 3 Lin/notch related (LNR) repetitive motifs. The intracellular domain consists of a RAM domain, 6 ankyrin repeats, and a TAD domain, followed by a PEST domain that is responsible for protein turnover. Flanking the ankyrin repeats are two nuclear localization sequences. Shown below in blue are notch ligands (serrate, delta) and ligand modulators (fringe), as well as downstream effectors of Notch signal transduction (CBF1, numb, deltex, PCAF/GCN5) and regulators of Notch protein turnover (Sel10). The blue components of Notch signaling are positioned below the Notch fragment according to the relative areas where they bind to the Notch receptor.

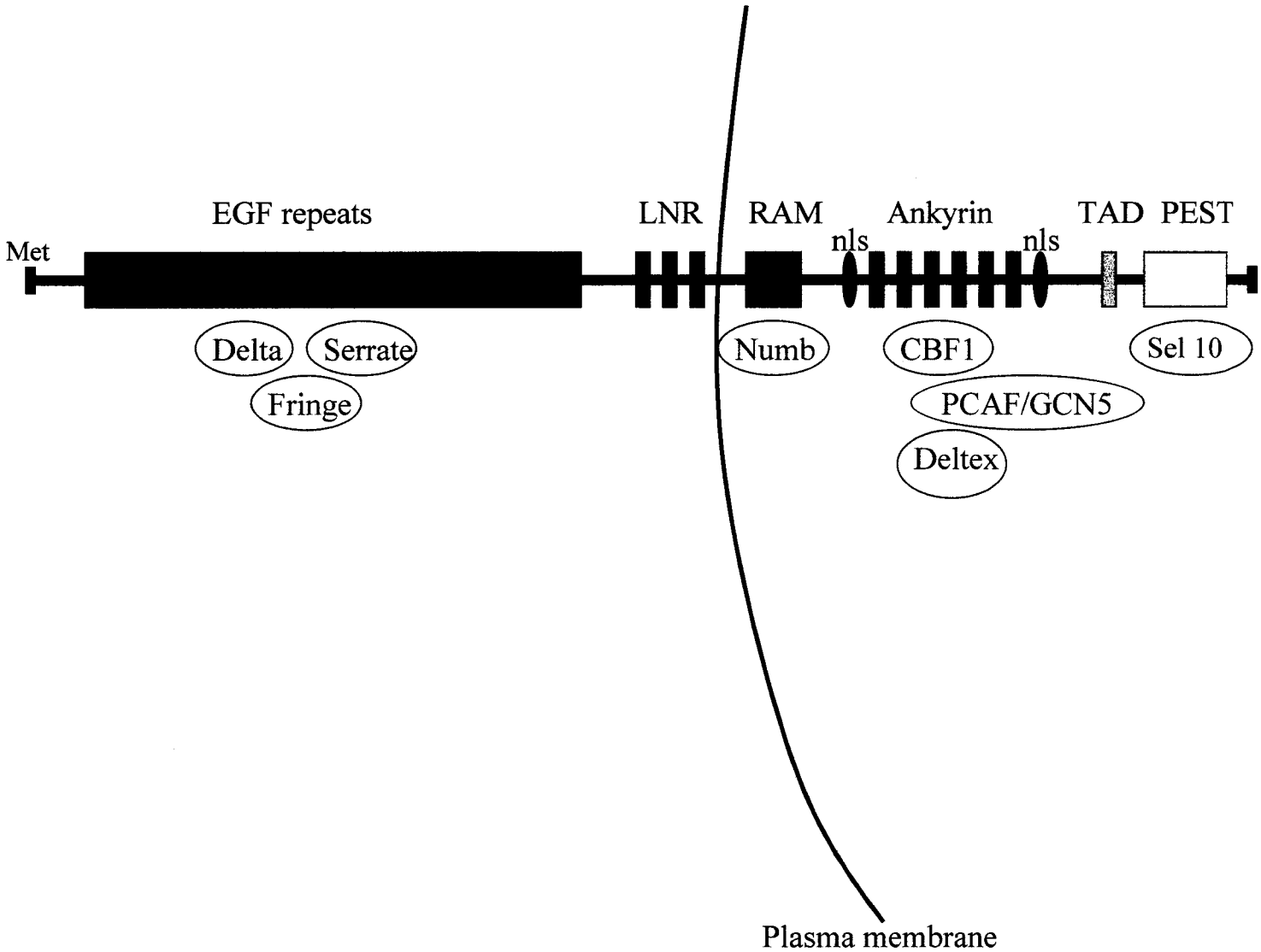
EGF repeats
LNR
RAM
Ankyrin
TAD
PEST
Met
nls
nls
Delta
Serrate
Fringe
Numb
CBF1
Sel 10
PCAF/GCN5
Deltex
Plasma membrane

activation, since mutating these elements creates constitutive activation of the Notch receptor (Weinmaster, 1997). Following these repeats is the transmembrane region, and immediately after that, the RAM domain, where some of the major downstream effectors of Notch signaling bind (Miele and Osborne, 1999). After the RAM domain lie six ankyrin repeats, which also interact with several downstream signaling molecules to propagate signal transduction (Baron et al., 2002). Flanking the ankyrin repeats are two nuclear localization sequences, of obvious function (Baron et al., 2002). Following the ankyrin repeats is the transcriptional activator domain (TAD), which also mediates intermolecular interactions with downstream signal transduction molecules (Baron et al., 2002). Finally, at the 3' end of the gene is the PEST domain, which is thought to control protein turnover, possibly through its interactions with Sel10, a protein that stimulates ubiquitin-mediated degradation (Baron et al., 2002).

Notch signal transduction

Notch is presented at the cell surface as a heterodimer consisting of an extracellular subunit and an intracellular subunit that includes the transmembrane domain (Miele and Osborne, 1999). Interestingly, these two subunits are fully separated, and are held together by calcium-dependent interactions (Baron et al., 2002). The functional purpose of this post-translational cleavage event that gives rise to the Notch heterodimer is currently unclear. Upon ligand binding, the Notch receptor is cleaved again in two separate locations: once in the extracellular domain by an ADAM protease, and another time inside the transmembrane domain by a complex of enzymes that includes Presenilin (Arias et al., 2002). This releases the intracellular domain, which then translocates to the nucleus where it interacts with its main downstream transcriptional activator, Suppressor

of Hairless (Su(H)), or CBF 1 in mammals (Figure 3) (Artavanis-Tsakonas et al., 1999; Baron et al., 2002). CBF1 normally functions to repress transcription by complexing with a co-repressor called silencing mediator of retinoid and thyroid hormone receptors (SMRT) and a histone deacetylase (HDAC1) (Baron et al., 2002). Interestingly, the mechanism by which Notch activates transcription is twofold: first, it binds CBF 1 and displaces the CBF1/SMRT/HDAC complex, thereby relieving CBF1-mediated transcriptional repression (Miele and Osborne, 1999). Following this, however, the Notch/CBF1 complex acts as a transcriptional activator of various genes such as hairy enhancer of split (HES) (Miele and Osborne, 1999). HES is a basic helix-loop-helix (bHLH) transcription factor that functions to suppress differentiation through the inhibition of other bHLHs (Miele and Osborne, 1999). The exact mechanism by which CBF1 functions as both a transcriptional repressor and a transcriptional activator (depending on the binding status of Notch) is not fully understood, however, it is thought to involve several other molecules in the activator complex. In addition to binding CBF1, the intracellular domain of Notch also promotes transcription by binding histone acetylases, which then work directly on the histone-bound chromatin to induce an open conformation and facilitate transcription (Baron et al., 2002).

Various studies have identified another CBF1-independent signal transduction pathway that is mediated by the gene *deltex*, which binds to the ankyrin repeat region of Notch from inside the cell (Miele and Osborne, 1999). Deltex signaling does not involve Notch translocation to the nucleus; instead, the signal may be transmitted through a different pathway involving c-jun N-terminal kinase (JNK) and Ras (Miele and Osborne, 1999). Mutations in *deltex* do not produce severe phenotypes; instead, the wide range of

Figure 3. Molecular mechanisms of Notch signal transduction. Upon ligand binding, the Notch intracellular region is cleaved and translocates to the nucleus, where it relieves transcriptional repression by binding to CBF1 and dissociating the CBF1/SMRT/HDAC complex that suppresses transcription. The Notch/CBF1 complex then acts as a transcriptional activator through downstream signaling molecules such as HES. In addition, Notch recruits the histone acetylases PCAF and GCN5, which work on histone-bound chromatin to induce an open conformation and promote transcription. Notch also works through a separate, deltex-mediated signal transduction pathway, which may involve downregulation of JNK and RAS (Baron et al., 2002).

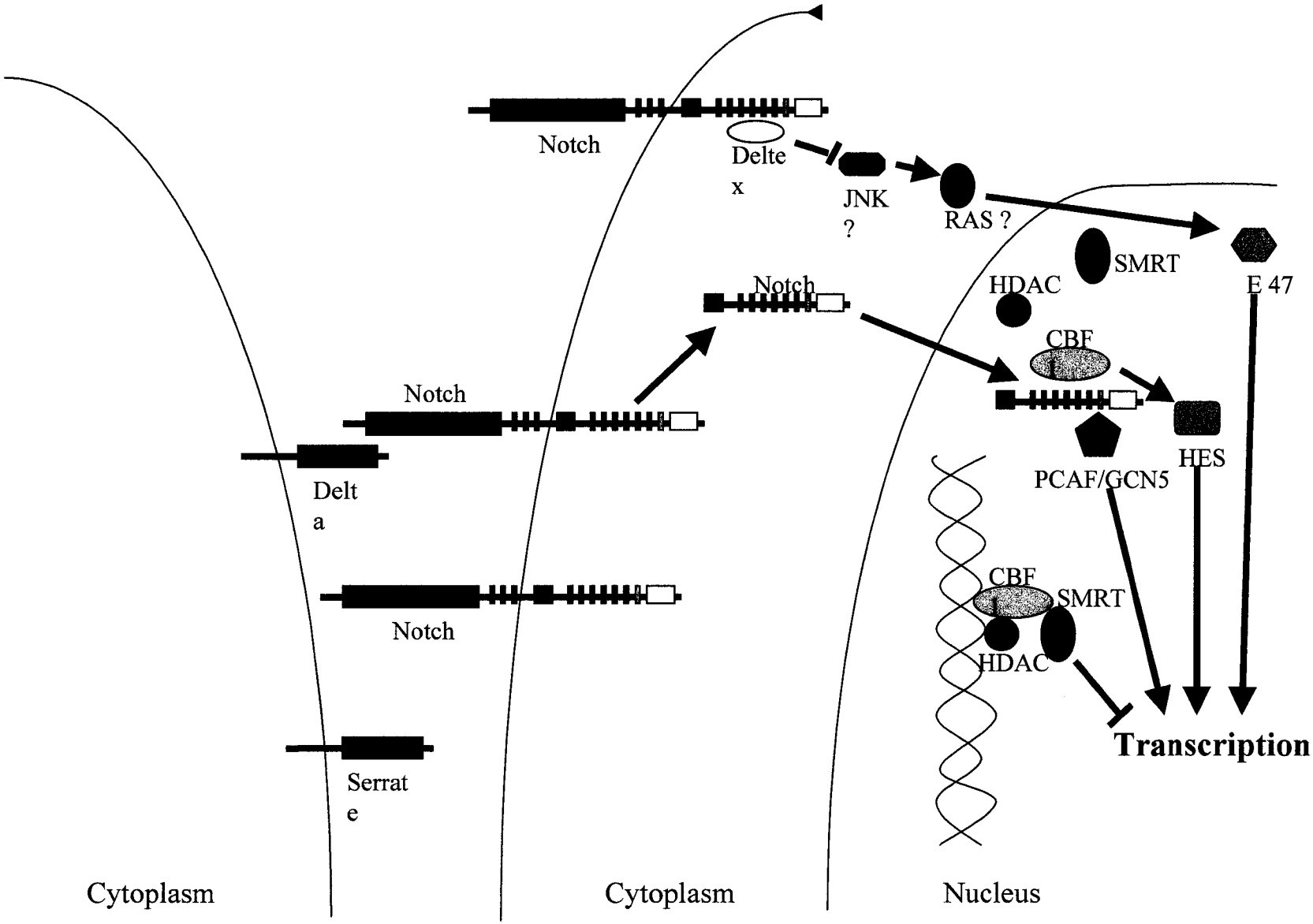
Notch
Delte
x
JNK
?
RAS ?
SMRT
HDAC
E 47
Notch
CBF
Notch
HES
PCAF/GCN5
Delt
a
Notch
CBF
SMRT
HDAC
Transcription
Serrat
e
Cytoplasm
Cytoplasm
Nucleus

mild phenotypes observed lends to the conclusion that *deltex* may be a gene which connects two cross-talking pathways, rather than a crucial signaling molecule in a particular developmental pathway (Panin and Irvine, 1998). Artavanis-Tsakonas et al. (1999) point out that due to the diversity of the signal transduction pathways that Notch is involved in, it may be more useful to view Notch signaling as a network, rather than as any number of individual pathways. Deltex may present one example of a molecule that Notch uses to interplay between the pathways in this network.

Ligands

The two major ligands of Notch are Serrate (Jagged in mammals) and Delta. Both of these ligands are membrane-tethered in their predominant form, and therefore only mediate Notch signaling at short ranges (Weinmaster, 1997). Soluble forms of Delta (DlEC) have been found which consist of only the extracellular ligand binding domain. However, reports indicate that these molecules seem to act more as Notch receptor antagonists rather than as long range signaling molecules, possibly through competitively binding and sequestering available Notch receptor (Artavanis-Tsakonas et al., 1999; Baron et al., 2002). However, even as such, DlEC represents another level of control of Notch signaling which may be exerted by cells which are not directly adjacent to *notch*-expressing cells.

Mechanisms of notch action

Bray (1998) maintains that the mechanisms by which Notch mediates its wide range of developmental activities can be grouped into three basic categories of action. The first of these three is lateral inhibition. This is demonstrated in neurogenesis in *Drosophila*, where *notch* identifies cells fated to become neurons from clusters of

undifferentiated, pro-neural cells (Miele and Osborne, 1999). Initially, each cell in the cluster expresses *notch* as well as its ligand *delta*, and therefore each cell acts as both a stimulator and a recipient of Notch signaling. However, cells which are destined to become neurons begin to express higher levels of *delta*, which then increases the signal stimulation received by the Notch receptors on the cells surrounding the *delta*-expressing cell (Miele and Osborne, 1999). This Notch activation generates a positive feedback loop where activated cells are stimulated to express more *notch*, and less *delta* (Miele and Osborne, 1999). In this manner, one cell becomes the primary signaling source, while other cells around it become inhibited from signaling. High levels of Notch activation result in increased expression of *enhancer of split*, a downstream transcription factor that binds to Groucho and forms a complex that represses *achaete-scute* expression (Brennan and Gardner, 2002). Since high levels of *achaete-scute* expression shuttles cells towards a neural fate, only the *delta*-expressing cell in the center of the signaling complex will adopt a neural fate. The cells around it which express *notch* will be repressed through Notch activation which in turn represses *achaete-scute* expression. Thus, through the respective inhibition of its neighbors, one cell out of a group of competent precursors is selected to act as a signaling center that establishes a pattern for the surrounding tissue by preventing the cells around it from adopting the same fate.

The second typical mechanism through which Notch regulates developmental events is through inductive signaling (Artavanis-Tsakonas et al., 1995). This type of signaling typically dictates lineage specification for groups of cells arising from the same embryonic tissue (Bray, 1998). It is set up when proteins such as *Drosophila* Numb segregate asymmetrically in the early embryo (Weinmaster, 1997). Numb binds to the

intracellular RAM domain of the Notch receptor and acts as a negative regulator of Notch signaling (Panin and Irvine, 1998). In this manner, activation of Notch is asymmetric according to the segregation pattern of *numb*.

Finally, Notch is involved in boundary formation in developing systems. This type of patterning is typically achieved using the same ligands that are involved in lateral inhibition, however, it also utilizes the ligand modulating protein Fringe (Bray, 1997). Fringe modulates ligand activation of Notch by adding a GlcNAc group to EGF repeats 24 – 26 of the Notch extracellular domain that are necessary for Serrate binding, but not for Delta (Baron et al., 2002). In this manner, Fringe inhibits Serrate/Notch signaling, while potentiating Delta/Notch signaling. Both secreted and membrane-bound forms of Fringe exist (Panin and Irvine, 1998). In *Drosophila*, boundary formation is seen in the developing wing, where Notch is responsible for setting up the dorsal-ventral axis (Bray, 1997). Expression of *fringe* in the dorsal cells of the developing wing restricts the range of Notch/Serrate signaling, thus establishing a boundary that is determined by Notch activation (Bray, 1997).

Potential roles for notch in regeneration

Given the abundance of regulatory roles that *notch* undertakes during development, it follows naturally that *notch* is likely to play a significant role in the regulation of regeneration as well. Having established that many of the genes expressed during limb development are also re-expressed during limb regeneration, it is almost certain that *notch*, too, will be re-expressed. There are several areas where it seems probable that *notch* will play a pivotal role either in the arbitration of cell fate or in the establishment of patterns that are crucial for proper regeneration. Specifically, *notch* is

known to downregulate expression of the myogenic marker MyoD (Hirsinger et al., 2001). By doing this, *notch* serves to maintain avian myogenic cells in an undifferentiated state. It was established above that the maintenance of cells in an undifferentiated state for a period of time during blastema formation is necessary for proper regeneration. This points to a possible role for *notch* in the regulation of blastema formation by suppressing differentiation of cells during this critical period. Further, *notch* has been implicated in maintaining the plasticity of differentiated neurons (Sestan et al., 1999). Given the extraordinary plasticity of post-mitotic newt cells, it is possible that *notch* is one of the factors that confers and/or regulates this plasticity.

Later in development, *notch* is responsible for regulating numerous patterning and cell fate decisions. Neurogenesis, myogenesis and angiogenesis are among the list of developmental processes which require *notch* to proceed (Artavanis-Tsakonis, 1999). Later in regeneration, the cells of the blastema undergo re-differentiation to form the blood vessels, neural and muscle tissues of the new regenerate, and it is quite possible that here as well, *notch* functions to specify cell fate determination. Finally, it is quite likely that *notch* also plays a role in directing the spatial patterning of the new regenerate, through the mechanisms of spatial signaling discussed above. Specifically, *notch* may play a role in specifying dorsal-ventral patterning boundaries through interactions with the ligand modulating protein Fringe.

Interestingly, it has been shown that ectopic Notch activation can trigger the formation of accessory eyes in *Drosophila* (Artavanis-Tsakonas et al., 1999). Whether inducing *notch* expression will be sufficient to stimulate regeneration of an eye in an adult fly whose tissues are differentiated remains to be seen. Even if ectopic *notch*

expression alone is not sufficient to generate entire organ systems, an understanding of *notch* function will greatly increase our ability to engineer and manipulate tissues. Given that *notch* controls many cell fate decisions, it is not inconceivable that one day we may be able to use this information to direct or bias cells towards a particular fate. This is, after all, the goal of those of us in pursuit of the elusive goal of understanding the genetics of regeneration.

Investigating the role of *Notophthalmus viridescens notch1* in forelimb regeneration

Objectives and hypotheses

It is almost certain that *notch* will play a functional role in regulating one or more of the processes comprising limb regeneration. Further evidence for a functional role for *notch* in regeneration comes from the recent cloning of *notch1* in the Japanese firebelly newt, *Cynops pyrrhogaster.* The expression pattern of *Cynops notch1* was examined in the regenerating newt retina (Kaneko et al., 2001). *notch1* expression was found in the early stages of regeneration in proliferating retinal precursor cells, but decreased later as differentiation progressed (Kaneko et al., 2001). Based on these data, one may speculate that *notch* expression serves to control the fate of retinal precursor cells, possibly by maintaining them in an undifferentiated state. In addition to this, the gene for *radical fringe* has been cloned and its expression pattern characterized in the regenerating limb of *Notophthalmus viridescens,* the red-spotted newt (Cadinouche et al., 1999). Newt *radical fringe* expression is weak in the early blastema, peaks at the mid-digit stage, then decreases again as cells begin to differentiate in the late-digit stage regenerate (Cadinouche et al., 1999). Finally, the *Notophthalmus viridescens* homologue of the *notch* ligand *serrate* has recently been cloned, and its expression confirmed in the

regenerating newt forelimb (Sandy Vascotto, unpublished results). The presence of both the ligand modulating gene *radical fringe* and the *notch* ligand *serrate* in the *Notophthalmus viridescens* regenerating limb system is compelling indication that *notch1* will also be present and active in the regenerating limb.

Based on these data, I have decided to investigate the potential role of *notch1* in regeneration, using the *Notophthalmus viridescens* regenerating forelimb as a model system. My goals are threefold:

1) To clone the *Notophthalmus viridescens* homologue of *notch1*.
2) To examine its expression pattern in the regenerating *N. viridescens* forelimb using real time reverse transcription polymerase chain reaction (RT-PCR).
3) To extrapolate possible functional roles for *notch1* in regeneration using the data from the experiments above.

In pursuit of these goals, my hypothesis is the following:

- *Notch1* is expressed in the regenerating *N. viridescens* forelimb. The expression pattern of *notch1* is indicative of a role for *notch1* in regulating regeneration.

Through these experiments, I hope to further our understanding of the genetic control mechanisms that underlie the fascinating process of regeneration.

METHODS

Basic animal care

Male and female *Notophthalmus viridescens* were wild caught from Tennessee, U.S.A. by Charles Sullivan and shipped to our animal care facility at the University of Ottawa. Animals were kept in clear plastic aquaria in dechlorinated tap water. Partial water changes were performed weekly, replacing no more than three quarters of the total volume of the aquarium at any given time. Animals were fed live blackworms from Aquatic Foods Inc. weekly; volume of blackworms added was scaled according to the number of newts in the individual aquaria. Excess blackworms were allowed to live in the tanks and act as a continual source of live food for the newts.

Amputations

Animals were anesthetized with a mixture of 0.5 g 3-aminobenzoic acid ethyl ester (MS222) and 0.6 g sodium hydrogen carbonate in 1L of dechlorinated tap water. Unused portions of MS222 were refrigerated at 4°C. MS222 was warmed to room temperature prior to amputations. MS222 solution was discarded after refrigeration for longer than three months. Newts were immersed in MS222 until all movement ceased (approximately 10 minutes). As soon as the newts were anesthetized, they were placed on a sterile petri dish on kimwipes soaked in MS222. The petri dish was then placed under a dissecting microscope. Newt limbs were amputated at either the level of the radius/ulna or at the level of the humerus with scissors that had been sterilized in 70% ethanol. After a few minutes, any protruding bone or skin was trimmed from the amputation surface in order to generate a flat amputation plane, which is essential for complete regeneration. Newts were then placed in a recovery tank containing shallow dechlorinated tap water. After the newts had revived, they were placed back in their

respective aquaria. The same procedure was used for re-sampling tissue from previously amputated newts. Sampled tissue was immediately frozen in liquid nitrogen for RNA extractions later.

Tissue culture

Maintenance of cell lines and subculture

B1H1 cell lines were a gift from Jeremy Brockes. All tissue culture protocols and reagent recipes are modified from Brockes (personal communication, 1999). Cells were maintained in 100 mm sterile tissue culture dishes (Falcon) in 10 ml of newt medium containing 10% fetal calf serum (FCS) (see Appendix 2 for newt media recipe). Plates were kept in humidified incubators at 28°C. Media was changed every four days. Cells were subcultured once a week, or when they reached confluency. Subculturing consisted of aspirating media from the plates, then washing cells with 10 ml A. PBS (see Appendix 2 for A. PBS recipe). After aspirating off the A. PBS, 1 ml of 0.1% trypsin/EDTA diluted in A. PBS was added to each plate. Cells were given 2-3 minutes to detach from the plate. Following this, 9 ml of newt media with 10% FCS was added to the plates to stop the reaction. 3 ml of this was plated directly on to gelatin-coated plates (see Appendix 2 for gelatin plate recipe). 7 ml of newt media with 10% FCS was then added to each plate. When cells were to be harvested for RNA, they were placed in a sterile tissue culture tube, instead of being plated onto new plates. Cells were then spun down in a centrifuge at 1000 rpm for 5 minutes. Media was aspirated off, and 1 ml Trizol ® (Invitrogen) reagent was added. Tissue was stored immediately at –70°C.

Thawing and freezing down cells

Cells to be frozen were trypsinized as described above, followed by centrifugation at 1000 rpm for 5 minutes. Media was aspirated off, and cells were re-suspended in 1.8 ml of newt media with 10% FCS. 0.2 ml DMSO was added, pipetted up and down to mix, then frozen in –70°C freezer for a few hours. After this, samples were transferred to liquid nitrogen. Cells to be thawed were placed in a 37°C water bath until ice had melted. Following this, 9 ml of newt medium with 10% FCS was added, then cells were centrifuged in a Beckman J6-MC centrifuge at 1000 rpm for 15 minutes. Supernatant was aspirated off, and cells were re-suspended in 1 ml newt medium with 10% FCS, then plated directly onto gelatin coated plates. 9 ml of newt media with 10% FCS was then added to the plates.

Myotube induction and re-supplementation

B1H1 cells were induced to differentiate into myotubes by adding newt media with 1% FCS (Figure 4) (see Appendix 1 for newt media recipe, however, use 4 ml FCS instead of 40 ml). Myotube cells were harvested either 4 or 8 days post serum drop by trypsination as described above. Myotubes could also be induced to dedifferentiate by re-supplementing the media with 10% FCS four days after the drop to 1% FCS. Following this, the myotubes were collected by trypsination 4 days after serum re-supplementation.

Primer design, oligonucleotide synthesis, and sequencing

All primers were designed using the PrimerSelect program from Lasergene. Primer sequences are listed in Appendix 3. Primers were synthesized by either the University of Ottawa Biotechnology Institute or by Qiagen Operon. All primers were synthesized to a salt free purity and were subsequently re-suspended in ddH_2O that had

Figure 4. Subconfluent, mononucleated B1H1 cells derived from the regenerating newt blastema (a) can be induced to differentiate into multinucleated myotubes (b) by lowering the media FCS concentration from 10% to 1%.

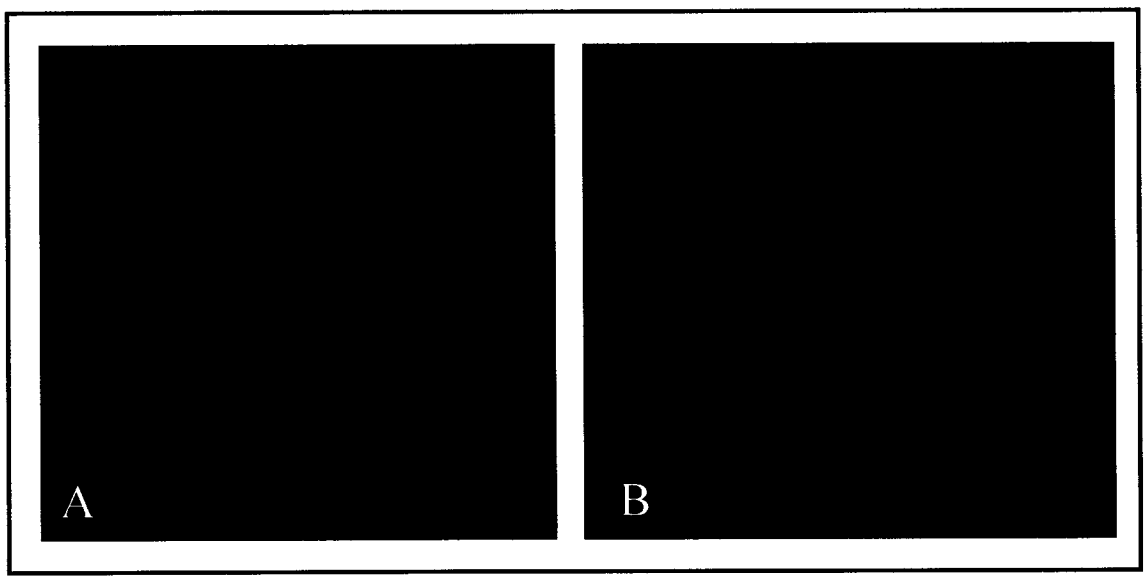
A
B

been autoclaved and filter sterilized at 0.2 μm. All samples were sent away for sequencing either with the University of Ottawa Biotechnology Institute or with Canadian Molecular Research Services Inc.

3' and 5' rapid amplification of cDNA ends (RACE)

The RACE procedure creates a double stranded cDNA population from oligodT primed poly A^+ mRNA, which has AP1 external and AP2 nested primers ligated to either ends of the cDNA. These ligated primer sites were then used in combination with gene specific external and nested primers to independently amplify the 5' and 3' ends of the gene of interest. Initially, I was given a 1294 bp fragment of cDNA, which had been cloned by Sandy Vascotto through the screening of a *Notophthalmus viridescens* 15 day regenerating λgt10phage blastema cDNA library with an EcoRV digested *Xenopus notch* probe. From this 1294 bp fragment, I designed primers to amplify a 741 bp fragment roughly corresponding to the middle of the 1294 bp sequence. These primers were used to sequence the middle of the 1294 bp fragment in order to confirm sequence ambiguities. Once a consensus sequence had been compiled, external and nested RACE primers were designed to amplify both the 3' and the 5' ends of the cDNA. 3' external and nested RACE primers were named 3'RACEex and 3'RACEnes, respectively, and 5' external and nested RACE primers were named 5'RACEex and 5'RACEnes (Figure 5) (see Appendix 3 for primer sequences). Two separate populations of cDNA were generated by Sandy Vascotto from B1H1 cells and 15 day regenerating newt forelimb tissue according to the procedure outlined in the Clontech manual for RACE. The 3' and 5' external primers were used in conjunction with the AP1 primer from Clontech to perform 3' and 5' RACE on 1:50 and 1:10 dilutions of the double stranded adapter

ligated cDNA. The basic RACE protocol is listed in Appendix 1, while the basic nested and external RACE PCR programs are detailed in Appendix 4. 3' and 5' RACE experiments were performed separately. Single primer or no template controls confirmed the specificity of PCR amplification. PCR products were visualized on a 2% agarose gel. Following this, 3' and 5' nested RACE was performed using the 3'and 5' nested RACE primers in conjunction with the AP2 nested primer from Clontech. These primers were used to amplify 1µl, 1:5 and 1:10 dilutions of the respective 3' and 5' external RACE PCR products generated earlier. Controls included additional reactions without the AP2 primer or the 3' or 5' nested RACE primers using 1 µl of external RACE product as template. Nested RACE PCR products were cloned using the PGEM-T easy vector system. E. *coli* was transformed with the ligation products and screened with M13 forward and reverse primers (M13F and R) according to the procedure listed below for "cloning and sequencing" (see Appendix 3 for M13F and R primer sequences). In addition, selected clones were screened with gene-specific PCR primers corresponding to the 3' and 5' ends of the 1294 bp fragment (Figure 5). These primers were named 5'PCRfwd, 5'PCRrev, 3'PCRfwd and 3'PCRrev, and can be found in Appendix 3. The thermal cycler program (entitled CSPCRSC) can be found in Appendix 4. Clones that were positive for this internal PCR screen were grown, miniprepped, and sent for sequencing. 3' and 5' RACE experiments were performed using B1H1 cell template cDNA as well as 15 day regenerating forelimb template cDNA. 3' RACE experiments were repeated on B1H1 cDNA template.

Figure 5. External and nested primers (5'RACEex, 5'RACEnes, 3'RACEex, and 3'RACEnes) were designed from the 1294 bp *notch* fragment cloned by Sandy Vascotto in order to perform 5' and 3' RACE. Internal PCR primers (5'PCRfwd, 5'PCRrev, 3'PCRfwd and 3'PCRrev) were also generated from the 5' and 3' ends of the 1294 bp fragment in order to confirm the specificity of any RACE products generated. Following this, external and nested primers (5'UTRex, 5'UTRnes, 3'UTRex and 3'UTRnes) were designed from the 5' and 3' ends of the new cDNA fragments cloned through 5' and 3' RACE, in order to verify the 5' and 3' RACE fragments through RT-PCR. Primer sequences can be found in Appendix 3.

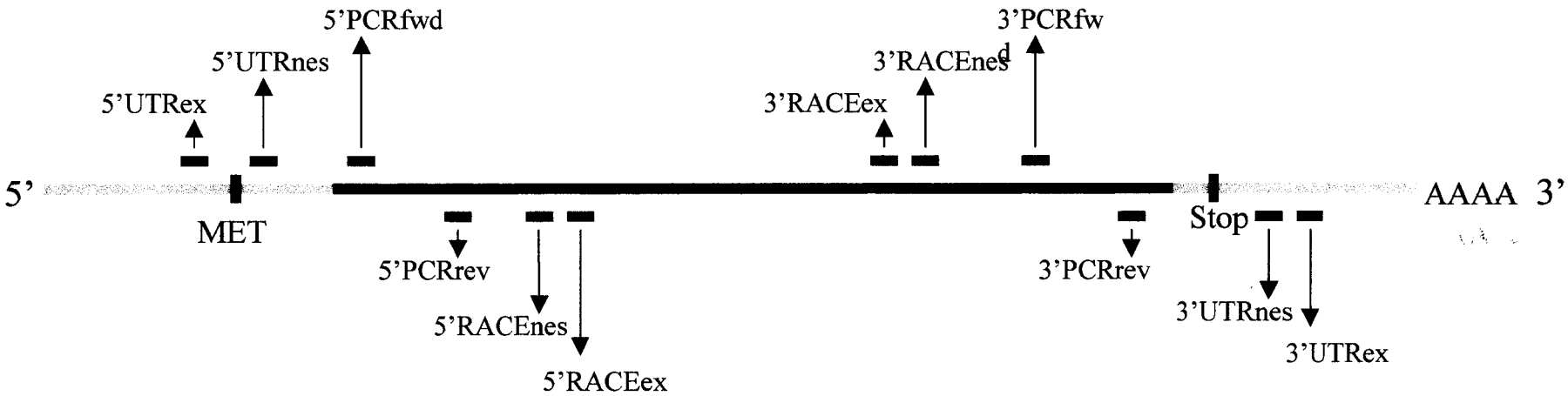
5'PCRfwd
5'UTRnes
5'UTRex
3'PCRfwd
3'RACEnes
3'RACEex
5'
AAAA 3'
MET
Stop
5'PCRrev
3'PCRrev
5'RACEnes
3'UTRnes
5'RACEex
3'UTRex
Cloned by RACE
Original 1294 bp fragment

Cloning and sequencing

PCR products were cloned directly into the PGEM-T easy vector system (Promega) by adding 3 μl of fresh PCR products to 5 μl of 2x ligation buffer, 1 μl PGEM-T Easy vector (50 ng/μl) and 1 μl T4 DNA ligase. PCR products were ligated at 4°C overnight. When fresh PCR products were not available, older PCR products were A-tailed prior to ligating into PGEM-T easy vector by combining 8 μl of old PCR product with 1 μl Taq polymerase and 1μl 2mM dATP. This mixture was then incubated at 70°C for 20 minutes. Following this, the A-tailed PCR products were ligated into PGEM-T easy vector in the same manner as described above. After the overnight ligation reaction, 3 μl of the ligated mixture was added to 100 μl of DH5α competent *E.Coli* cells and 2 μl of DMSO. The components were mixed and then incubated on ice for 30 minutes. Following this, cells were heat shocked for 2 minutes at 42°C, then chilled on ice for 1 minute. The cells were then transferred to 1.5 ml LB, and incubated at 37°C for 1 hour with shaking at 200 rpm (see Appendix 2 for LB recipe). Cells were then plated onto LB- Ampicillin plates containing IPTG and Xgal (see Appendix 2 for LB-amp plate recipe). Plates were incubated inverted at 37°C overnight. The next day, white colonies were selected and PCR screened using M13 forward and M13 reverse primers that are specific to PGEM-T easy vector arm sequences (see Appendix 3 for M13 F and R primer sequences). Colonies were inoculated directly into a standard PCR reaction mix (see Appendix 1 for general PCR protocol). Screening was performed using the PCR program CTCONDI (see Appendix 4). Screened colonies were replica plated onto a LB-amp plate with a paper grid taped onto it. The replica plate was grown inverted at 37°C overnight. Plates were then wrapped in parafilm and kept at 4°C for

long term storage. Selected colonies were grown in 3 ml LB with 50μg/ml ampicillin for no more than 18 hours at 37°C with shaking at 230 rpm. Plasmids were extracted using either the QIAprep spin miniprep kit (Qiagen) or the GenElute plasmid miniprep kit (Sigma). Resulting plasmid DNA was quantified using spectrophotometry. 1μg of plasmid was run on a 1% agarose gel for visual confirmation of plasmid purity. Plasmids were then sent for sequencing using the M13 forward and reverse primers.

Reverse transcription polymerase chain reaction (RT-PCR)

RNA extractions

Total RNA was extracted (using Trizol ®, Invitrogen) from subconfluent B1H1 cells, as well as from 2 week regenerating forelimb tissue (see Appendix 1 for RNA extraction protocol). Total RNA was quantified using spectrophotometry, and was run on a 1% agarose gel for verification (see Appendix 1 for quick RNA gel protocol).

RT-PCR of 3' RACE product for verification

In order to independently verify the existence of the 3' end of the cDNA obtained by 3' RACE, external and nested reverse primers were designed from the sequence of the 3' fragment cloned through RACE. These primers were called 3'UTRex and 3'UTRnes (Figure 5) (see Appendix 3 for primer sequences). 2 μg of total RNA from confluent B1H1 cells was used in conjunction with the 3'UTRnes primer to generate first strand cDNA according to the protocol listed in Appendix 1. The 3'UTRnes primer was then used in combination with the 3'RACEex and 3'RACEnes primers in a PCR reactions using 5 μl of the B1H1 first strand cDNA generated above as template (see Appendix 1 for general PCR protocol). The thermal cycler PCR program used (entitled 3'UTRconf) can be found in Appendix 4. The results were run on a standard 1% agarose gel.

RT-PCR of 5'RACE clone for verification

Using the DNA sequence of the clone generated by 5' RACE, external and nested forward primers were designed and named 5'UTRex and 5'UTRnes, respectively (Figure 5) (see Appendix 3 for primer sequences). 2 μg of total RNA from confluent B1H1 cells was used in conjunction with 5'PCRrev and 5'RACEex primers (individually) to generate first strand cDNA (see Appendix 1 for first strand cDNA synthesis protocol). From here, three combinations of primers were used (5'UTRex and 5'PCRrev, 5'UTRnes and 5'PCRrev, 5'UTRnes and 5'RACEex) to PCR amplify different fragments of cDNA using 5 μl of the respective first strand templates generated above. The thermal cycler program (called 5'UTRconf) can also be found in Appendix 4. PCR products were run on a standard 1% agarose gel.

RT-PCR spanning the 3' and 5' RACE contig

The resulting contig generated from 3' and 5' RACE was assembled using the SeqMan program from Lasergene. In order to verify the fact that the assembled contig truly represents a full length cDNA, 2 μl of total RNA from confluent B1H1 cells was used to generate first strand cDNA with the 3'UTRex primer (see Appendix 1 for first strand cDNA synthesis protocol). 5 μl of the first strand reaction was used as template in a PCR reaction with the 3'UTRex and 5'UTRex primers which span the contig generated by both 5' and 3' RACE (see Appendix 2 for general PCR protocol). The PCR program (UTRcontig) can be found in Appendix 4. A gradient of six different annealing temperatures was tested in order to obtain the optimal conditions for PCR amplification of the contig using these primers. The PCR products were run on a standard 1% agarose gel. The annealing temperature that gave the sharpest band of the appropriate size was

chosen. 1 μl of these PCR products were used as template in a subsequent PCR with the nested primers 3'UTRnes and 5'UTRnes. Again, a gradient of annealing temperatures was tested using the same thermal cycler program (UTRcontig). Results were run on a standard 1% agarose gel.

Degenerate primer RT-PCR

Degenerate primers were designed from regions of high protein and nucleic acid sequence conservation of *Notch1* in various species (*Xenopus laevis, sea urchin, Danio rerio, Gallus gallus, Homo sapiens, Mus musculus and Cynops pyrrhogaster* for protein sequence; *Xenopus laevis, Danio rerio, Gallus gallus, Homo sapiens, Mus musculus* and *Cynops pyrrhogaster* for cDNA sequence). Sequences were aligned using the MegAlign program from Lasergene. All primers had a degeneracy of <500 fold. Seven degenerate primers were designed; they are listed in Appendix 3. The primer pairs Notch2F and Notch2R, Notch3F and Notch3R, and Notch4F and Notch4R each represent the same primers designed in both the forward (F) and the reverse (R) orientation. Notch5R was only designed in the reverse orientation. First strand cDNA was generated using 2 μg of confluent B1H1 cell total RNA with 500 ng of random hexamers (Promega) (see Appendix 1 for first strand cDNA synthesis protocol). 5 μl of this first strand cDNA was used as template to PCR amplify *notch1* using different combinations of the seven degenerate primers (see Appendix 1 for general PCR protocol). For primers whose degeneracy was <100 fold, 1 μl of primers diluted to 10 μM was used in each reaction, while for primers whose degeneracy was >100 fold, 1.5 μl of primers diluted to 10 μM was used in each PCR reaction. The thermal cycler program used (CANDEGN) is listed in Appendix 4. Products were run on a 2% agarose gel. Samples which displayed strong

bands of the expected size were cloned directly into PGEM-T easy vector, screened using M13F and R, and sequenced according to the procedure described above. However, samples which displayed weak banding or multiple bands (at least one of which was the expected size) were re-run on a 0.6% low melting point agarose gel. The band of the appropriate size was then cut out of the gel, and was mixed with an equivalent amount of TE buffer (10mM Tris.Cl/1mM EDTA). The TE/gel mixture was heated to 37°C in a water bath in order to dissolve the agarose. 1 µl, 3 µl and 5 µl of this mixture were used as template in subsequent PCR reactions with the same primers originally used to amplify the respective bands. Primer and thermal cycler conditions were as above. The same thermal cycler program was used (CANDEGN). The products were run on a standard 2% agarose gel. PCR products which displayed stronger bands of the expected size (relative to the original RT-PCR) were cloned into PGEM-T easy vector, screened using M13F and R, and sequenced.

The overlapping fragments generated by random primed RT-PCR with degenerate primers were assembled using the SeqMan program from Lasergene. Sequence ambiguities resulting from the inability of the sequencing reaction to span the full length of the cDNA fragments were clarified by designing primers to amplify the middle of each of the clones. Eight primers were designed for sequencing the middle regions of 4 different cloned fragments. These primers are named 2F4R79midFwd, 2F4R79midRev, 4F5R7midFwd, 4F5R7midRev, 2F3R26midFwd, 2F3R26midRev, 4F5R26midFwd, and 4F5R26midRev (see Appendix 3 for primer sequences). The resulting contig was assembled using the SeqMan program and was manually checked for any remaining sequence discrepancies.

Real time RT-PCR

RNA extractions

Total RNA was extracted from subconfluent, confluent, and superconfluent B1H1 cells, as well as B1H1 cells that had been collected 4 days and 8 days post serum drop, and B1H1 cells that had been re-supplemented with 10% FCS after being induced to differentiate into myotubes. In addition, total RNA was also extracted from whole limbs, 24 hour post-amputation tissue, and 1 week, 2 week, 3 week, and 4 week regenerating forelimbs. RNA was extracted using Trizol® reagent (Invitrogen) above (see Appendix 1 for RNA extraction protocol). Total RNA was quantified using spectrophotometry, and RNA integrity was verified by running the RNA on a 1% agarose gel (see Appendix 1 for quick RNA gel protocol).

First strand cDNA generation

2 μg of total RNA from each tissue was DNAse-treated with Amplification Grade Deoxyribonuclease 1 (Sigma) (see Appendix 1 for DNAse treatment protocol). Subsequently, the DNAse-treated RNA reaction mix was incubated at 65°C for 10 minutes to denature both the RNA and the DNAse. Random hexamers (Promega) and oligodT primers (Promega) were also denatured simultaneously at 65°C for 10 minutes in separate tubes. After this, both the RNA samples and the primers were snap cooled on ice, then 500 ng of random hexamers (Promega) and 500 ng of oligodT primers (Promega) primers were added to each RNA sample. First strand cDNA was generated according to the protocol listed in Appendix 1, using 3 μl of DEPC treated filter sterilized water instead of 9 μl in order to compensate for the increased volume of the denatured primer/RNA mixture. Controls consisted of generating first strand cDNA from 2 μg of

DNAse treated RNA without M-MLV reverse transcriptase enzyme (substitute with DEPC-treated filter sterilized water).

Real time RT-PCR primer design and verification

Primers specific to the *notch1* contig (degenerate RT-PCR product) and *groove* contig (RACE product) were designed using the PrimerSelect program (Lasergene). These primers, named NotchRTfwd, NotchRTrev, GrooveRTfwd, and GrooveRTrev, can be found in Appendix 3. In the case of *groove*, the cloned contig sequence was compared to the *Cynops pyrrhogaster notch1* sequence using the dot plot function from MegAlign (Lasergene). Primers were specifically designed in areas of low sequence homology in order to ensure for gene-specific amplification of the *groove* cDNA. In the case of *notch1*, the primers were designed in areas that fell between conserved domains and functional motifs, in order to similarly ensure for gene-specific amplification. Primers specific to *Notophthalmus viridescens GapDH* were generated by Shawn Beug (see Appendix 3 for primer sequences). All three primer sets (*groove*, *notch1* and *GapDH* were tested in a real time RT-PCR using 0.5 μl of the myotube first strand cDNA template generated above (see Appendix 1 for real time RT-PCR protocol). Negative controls consisted of the same reaction replacing the cDNA template with nuclease-free water (Ambion). All reactions were performed in a BioRad iCycler using the CSmelt57 program found in Appendix 4. All reactions were performed in triplicate. Specificity of the PCR amplification was determined using the melt curve analysis function of the iCycler iQ Optical System software (BioRad; version 3.0) as well as by running 5 μl of the PCR products on a standard 1.5% agarose gel.

Real time RT-PCR

Random and oligodT primed first strand cDNA generated from all of the respective tissue types above was diluted with equivalent amounts of nuclease-free water (Ambion). 1 µl of this diluted first strand was then used to perform real time RT-PCR (see Appendix 1 for real time RT-PCR protocol) with each of the three sets of primers and iQ SYBR® green supermix (BioRad). Negative controls included reactions using the first strand myotube cDNA template generated above without reverse transcriptase enzyme, as well as reactions with no first stand cDNA template. Reactions were performed in a BioRad iCycler using the program CSmelt57 (see Appendix 4). All reactions were performed in triplicate. A master mix was created from each specific tissue type containing a specific set of primers, which was then aliquotted three times into 96 well plates. Specificity of the PCR amplification was determined using the melt curve analysis function of the iCycler iQ Optical System software (BioRad; version 3.0) as well as by running 5 µl of the PCR products on a standard 1.5% agarose gel. Data was processed by averaging the triplicate threshold cycle (Ct) values, and by subtracting the averaged GapDH Ct values from the averaged Notch or Groove Ct values. This number (ΔCt) was then subtracted from the lowest ΔCt value of the tissue samples tested to give $\Delta\Delta$Ct. Fold overexpression was then calculated by taking 2 raised to the $\Delta\Delta$Ct power.

RESULTS

The original fragment

I began this project with a 1294 bp fragment of cDNA that had been isolated from a λgt10phage cDNA library generated from *Notophthalmus viridescens* 15 day regenerating blastemas. The library had been screened with an EcoRV digested *Xenopus notch* probe by Sandy Vascotto. The resulting 1294 bp fragment shared 65% identity with a protein isolated from mouse stromal cells called SST3, and 64% identity with a human protein called FLJ00133. The 1294 bp fragment showed 36% identity with sea urchin *notch*, and 34% identity with *Danio rerio notch1*. NCBI Conserved Domain Search revealed 5 EGF repeat motifs, as well as 14 N-terminal amino acids which corresponded to part of a NIDO domain. From this original fragment, primers were designed in order to clone the rest of the cDNA through RACE.

5' RACE

5'RACE using B1H1 cell cDNA template yielded a fragment of 1011 bp, of which 568 bp was new sequence extending in the 5' direction past the original 1294 bp fragment (Figure 6). 5'RACE using 15 day regenerate cDNA template yielded a comparable fragment of similar size. The 5' RACE consensus fragment is characterized by an additional 409 bp of open reading frame (ORF) extending past the 5' end of the original *notch* fragment. Preceding this in the 5' direction is 180 bp of additional sequence. There is a putative MET translational start site 262 bp after the stop codon that marks the 5' boundary of the ORF at position 181 of the consensus sequence. There is no identifiable Kozak sequence (ACCATGG).

Figure 6. Nucleotide sequence of the contig generated from 3'and 5' RACE. The contig, named *groove,* contains an open reading frame of 1563 bp and a putative coding region of 1302 bp. At the 5' end of the coding region is a MET translational start site. At the 3' end, features of the contig include a 3'UTR destabilizing sequence, a transcription termination signal, and a poly A^{++} tail.

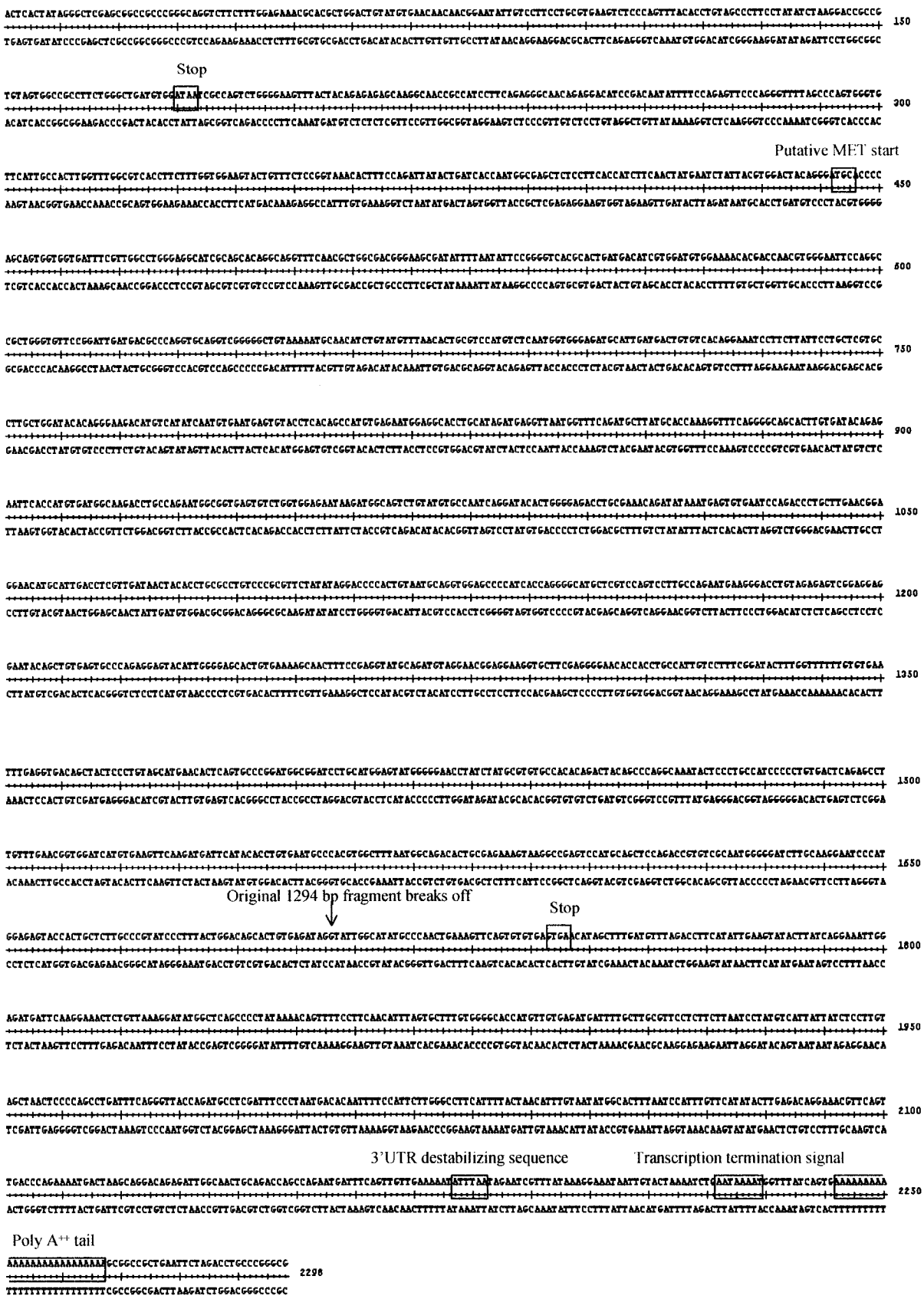
Stop
Putative MET start
Original 1294 bp fragment breaks off
Stop
3'UTR destabilizing sequence
Transcription termination signal
Poly A++ tail

3'RACE

Two independent 3' RACE experiments using the B1H1 cell cDNA template produced two comparable fragments of 718 and 725bp respectively (Figure 6). 3'RACE using the 15 day regenerating tissue cDNA template resulted in a comparable fragment of similar length. Interestingly, all three 3' RACE fragments share a similar feature: after the nested gene specific *notch* primer 3'RACEnes (see Figure 5), the sequence follows the original 1294 bp *notch* fragment for 98 bp, whereafter all the clones suddenly diverge at exactly the same point (at bp 1117 of the original 1294 bp *notch1* fragment) and acquire a new sequence. In other words, none of the 3' RACE clones actually follow the original 1294 bp fragment to the end. This new sequence remains in an open reading frame for only 37 bp before the first stop codon begins. Following this, the putative 3' untranslated region (UTR), littered with stops, extends for an additional 475 bp until the transcription termination signal (AATAAAA) is seen, followed by a poly A^+ tail 13 bp after that. Additional features of this 3' RACE fragment include a 3' UTR destabilizing sequence (ATTTA) 470 bp after the point where the sequence diverges from the original *notch1* clone.

5' and 3' RACE contig alignment and sequence analysis

Contig alignment produces what appears to be a complete cDNA containing a putative MET translational start site, an open reading frame of 1563 bp, a putative coding region of 1302 bp, and a poly A^+ tail. The cDNA was given the name *groove*, which is indicative of a smaller version of a *notch*. Domain mapping using NCBI Conserved Domain Search reveals that *groove* consist of only 5 EGF repeats contained by the area of the original 1294 bp Notch fragment (Figure 7). 5' to these EGF repeats is an

Figure 7. Results of the NCBI Conserved Domain Search reveal that Groove contains 5 EGF repeats and a NIDO domain. Functional domains were assigned a random number in red corresponding to the sequence in which they are found on the contig (i.e. EGF1, EGF2, etc). This number is matched with the particular details regarding their sequence homology below. NIDO domains are extracellular regions of unknown function that are present in Nidogen and Entactin, basement membrane proteins that also contain EGF repeat domains.

Groove amino acid sequence

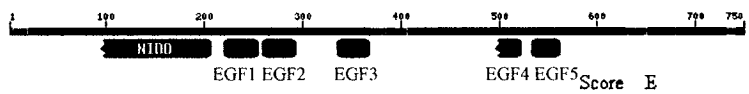

PSSMs producing significant alignments:		Score (bits)	E value
1)	gnl|CDD|488 smart00539, NIDO, Extracellular domain of unknown function in ...	124	4e-29
2)	gnl|CDD|14791 cd00054, EGF_CA, Calcium-binding EGF-like domain, present in a...	44.1	5e-05
3)	gnl|CDD|14791 cd00054, EGF_CA, Calcium-binding EGF-like domain, present in a...	41.4	3e-04
4)	gnl|CDD|14791 cd00054, EGF_CA, Calcium-binding EGF-like domain, present in a...	38.7	0.002
5)	gnl|CDD|14791 cd00054, EGF_CA, Calcium-binding EGF-like domain, present in a...	37.6	0.005
6)	gnl|CDD|14791 cd00054, EGF_CA, Calcium-binding EGF-like domain, present in a...	37.6	0.006

1) NIDO domain

```
CD-Length = 153 residues, only  71.9% aligned
Score =  124 bits (312), Expect = 4e-29

Query:  93   AQWVFIATWFGVTFFGGSTVSPVNTFQIILITNGELSFTIFNYESITWTTGMHPSSGGDF  152
Sbjct:  44   AKSVVIVTWENVAAYGAQGSSGTNTFQAVLATDGSRTYAIFLYPSLGWTWDV------TA  97

Query:  153  VGLGGIAAQAGFNAGDGK-RYFNIPGSRTDDIVDVENTTNVGIPGRWVFRIDDAQV  207
Sbjct:  98   GGDDGVPARAGFNGGDGTFLSYTLPASGEENIKNLAEGSNVGIPGRWMFRVDGAEI  153
```

2) EGF 2

```
CD-Length = 38 residues, 100.0% aligned
Score = 44.1 bits (104), Expect = 5e-05

Query:  258  NVNECTS-QPCENGGTCIDEVNGFRCLCTKGFRGSTCD  294
Sbjct:  1    DIDECASGNPCQNGGTCVNTVGSYRCSCPPGYTGRNCE  38
```

3) EGF 3

```
CD-Length = 38 residues,  94.7% aligned
Score = 41.4 bits (97), Expect = 3e-04

Query:  334  DINECESR-PCLNGGTCIDLVDNYTCACPAFYIGPH  368
Sbjct:  1    DIDECASGNPCQNGGTCVNTVGSYRCSCPPGYTGRN  36
```

4) EGF 4

```
CD-Length = 38 residues, only  76.3% aligned
Score = 38.7 bits (90), Expect = 0.002

Query:  496  PCLNGGSCEVQDDSYTCECPRGFNGRHCE  524
Sbjct:  10   PCQNGGTCVNTVGSYRCSCPPGYTGRNCE  38
```

5) EGF 5

```
CD-Length = 38 residues,  84.2% aligned
Score = 37.6 bits (87), Expect = 0.005

Query:  532  SSRPCRNGGSCKESHGEYHCSCPYPFTGQHCE  563
Sbjct:  7    SGNPCQNGGTCVNTVGSYRCSCPPGYTGRNCE  38
```

6) EGF 1

```
CD-Length = 38 residues,  86.8% aligned
Score = 37.6 bits (87), Expect = 0.006

Query:  219  CLTLRPCLNGGRCIDDCVTGNPSYSCSCLAGYTGKTC  255
Sbjct:  5    CASGNPCQNGGTCVN----TVGSYRCSCPPGYTGRNC  37
```

extracellular NIDO domain. NIDO domains are extracellular sequences of unknown function found in nidogen/entactin related proteins. Nidogen and entactin are basement membrane proteins that also contain EGF repeats. An examination of the protein structure with the Prediction of Protein Sorting Signals and Localization Sites in Amino Acid Sequences program (PSORT version 6.4; Kenta Nakai, 2000) reveals an uncleavable N-terminal signal sequence, but no transmembrane region. This is indicative of a secreted protein. BLAST analysis (blastx) of *groove* revealed that it shows highest homology (62%) to a stromal cell-derived secreted protein called SST3 in the mouse. Unfortunately, very little is known about this protein, as the publication is currently in press. *groove* also shows very high homology to the protein FLJ00133 in *Homo sapiens* (61-65%). This protein interestingly also contains a NIDO domain as well as an EGF repeat domain. *groove* shows strong homology to FLJ00133 in both the regions of the NIDO domain and the EGF repeat area. *groove* shows homology to *notch1,* as well as slightly more distant similarity to the other Notch isoforms (*notch2*, *3* and *4*, respectively) and other Notch-related proteins (*serrate* and/or *jagged*).

Independent verification of the 3' and 5' RACE clones

In order to validate the identity of the 3' RACE clone, RT-PCR was performed on cDNA derived from B1H1 cells using the 3'UTRnes primer designed from the new regions of the 3' RACE clone (see Figure 5 for primer map). Two subsequent PCR reactions using the 3'UTRnes primer in conjunction with 3'RACEex and 3'RACEnes primers yielded single bands of the appropriate size: 581 bp and 466 bp, respectively (Figure 8). This confirms the presence of the 3'RACE clone in a different RNA preparation of blastema-derived newt B1H1 cells. Similarly, RT-PCR was performed

Figure 8. RT-PCR verification of the fragment cloned by 3' RACE. First strand cDNA was generated from B1H1 cell RNA using the 3'UTRnes primer. PCR was then performed using different sets of primer pairs on the cDNA template generated above. The first primer pair, 3'UTRnes and 3'RACEex, produced a single band of the appropriate size: 581 bp. The second primer pair, 3'UTRnes and 3'RACEnes, yielded a single band of 466 bp. Negative controls consisted of a PCR reaction with one of the primer sets without cDNA template. This confirms the presence of the 3' RACE fragment in B1H1 cells.

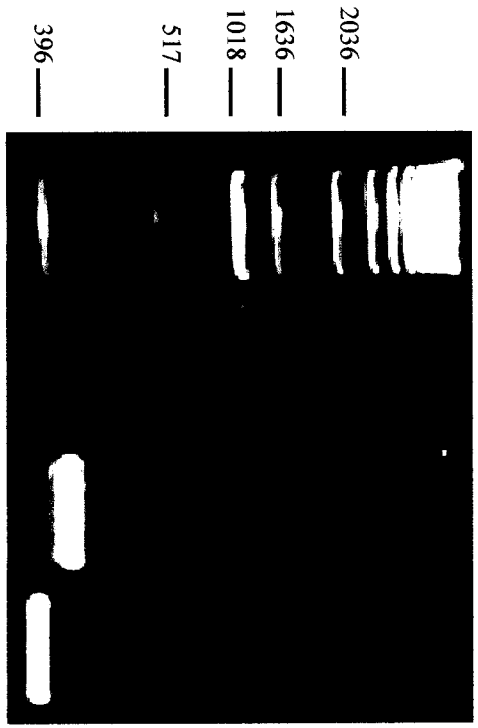
396
517
1018
1636
2036
1kb ladder
Negative control
3'UTRnes + 3'RACEex
3'UTRnes + 3'RACEnes

using two different populations of cDNA generated from B1H1 cell RNA in conjunction with the primers 5'PCRrev and 5'RACEex to prime first strand cDNA, respectively. Three subsequent PCR reactions were performed using the primer pairs 5'UTRex and 5'PCRrev, and 5'UTRnes and 5'PCRrev in conjunction with the B1H1 cell cDNA generated with the 5'PCRrev primer, as well as the primer pair 5'UTRnes and 5'RACEex in conjunction with the B1H1 cell cDNA generated with the 5'RACEex primer (see Figure 5 for primer map). These PCR reactions generated bands of the appropriate sizes: 626 bp, 499 bp and 773 bp, respectively (Figure 9). While other fainter bands also appear (possibly as a result of primers binding non-specifically to other sites on the cDNA), the predominant band in each reaction is indicative of the correct sized fragment.

Verification of the contig through RT-PCR

Finally, external and nested primers designed from the sequence of the 3' and 5' RACE clones were used to RT-PCR amplify the entire contig in order to verify the existence of a single cDNA in an RNA population derived from B1H1 cells. cDNA generated from B1H1 cell RNA using the 3'UTRex primer was used as template in a PCR reaction with the 3'UTRex and 5'UTRex primers (see Figure 5 for primer map). Following this, an aliquot of the PCR products of the external PCR reaction was used as template in a nested PCR using the primers 3'UTRnes and 5'UTRnes. This resulted in a single band of the appropriate size: 1657 bp (Figure 10). This single PCR product spans the entire coding region of the cDNA, and encompasses 300 bp of putative 3'UTR and 52 bp of potential 5'UTR. This further confirms the existence of a single *groove* contig in blastema-derived newt B1H1 cells.

Figure 9. RT-PCR verification of the fragment cloned by 5' RACE. Two different sets of cDNA were generated using B1H1 cell RNA in conjunction with two separate primers: 5'PCRrev and 5'RACEex. Different primer pairs were then tested by PCR using the first strand cDNA template generated above. The primer pair 5'UTRex and 5'PCRrev was used in combination with the B1H1 cell cDNA generated with the 5'RACEex primer; this produced a band of 626 bp. The primers 5'UTRnes and 5'PCRrev were also used with the B1H1 cell cDNA generated with the 5'PCRrev primer, which produced a band of 499 bp. Finally, the primers 5'UTRnes and 5'RACEex were used in conjunction with the B1H1 cell cDNA generated with the 5'RACEex primer, which resulted in a band of 773 bp. Negative controls consisted of a PCR reaction with one of the primer sets without cDNA template. This confirms the presence of the fragment generated by 5' RACE in B1H1 cells.

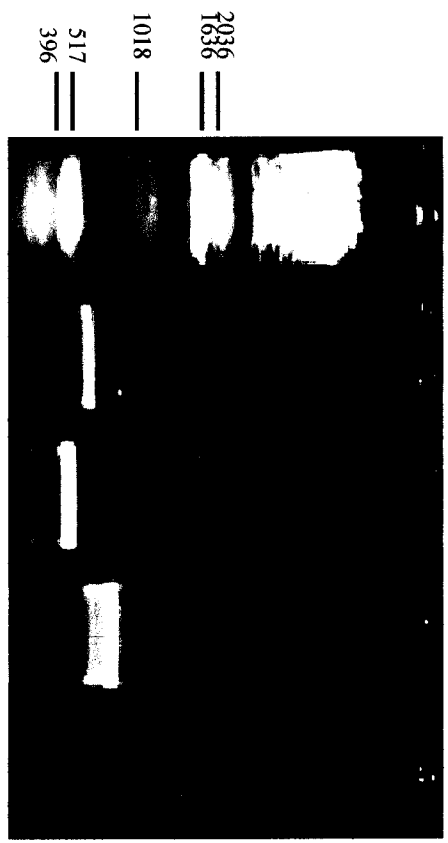

1kb ladder

5'UTRex + 5'PCRrev

5'UTRnes + 5'PCRrev

5'UTRnes + 5'RACEex

Negative control

Figure 10. Nested RT-PCR verification of the *groove* contig. cDNA was generated from B1H1 cell RNA using the 3'UTRex primer. This cDNA was then used as template in a PCR with the primers 3'UTRex and 5'UTRex, which span the length of the contig generated by 3' and 5' RACE. A fraction of this PCR product was then used as template in a nested PCR with the primers 3'UTRnes and 5'UTRnes, which also span the length of the contig. The annealing temperature was varied to obtain the optimal results. The products of the nested reaction are shown in the figure; the temperatures refer to the annealing temperatures varied across the different samples. Regardless of the annealing temperature used, a single band of the expected size (1657 bp) was generated. Negative controls consisted of a PCR reaction at one of the annealing temperatures with no external PCR product template. This confirms the existence of a single *groove* transcript in B1H1 cells, the ends of which were cloned through 3' and 5' RACE.

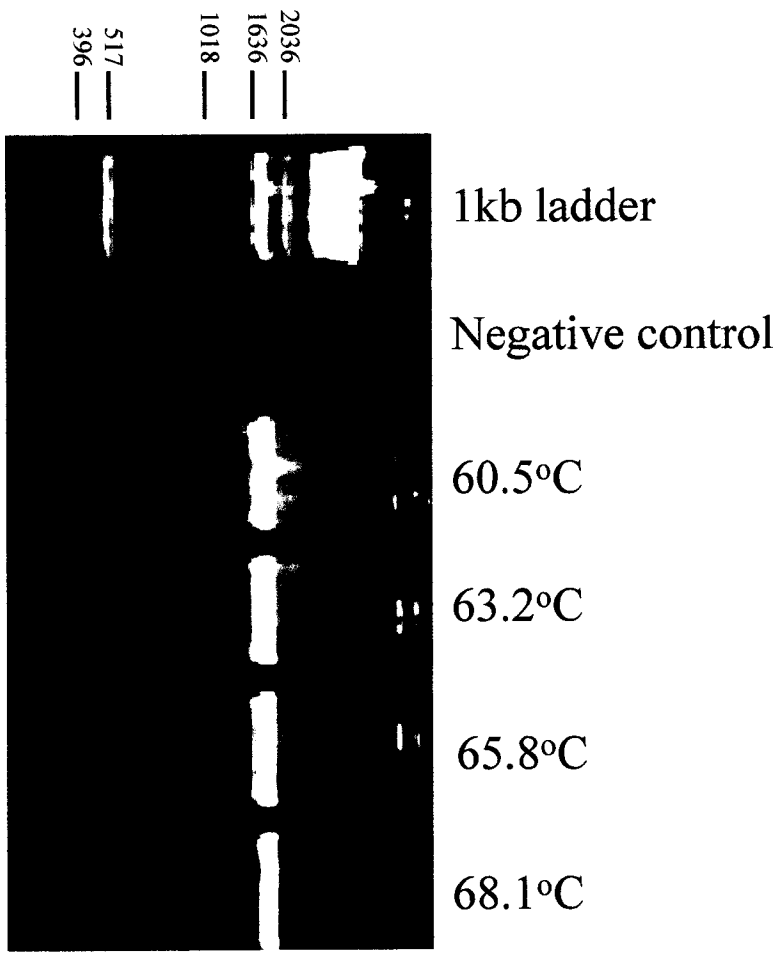
2036
1636
1018
517
396
1kb ladder
Negative control
60.5°C
63.2°C
65.8°C
68.1°C

Degenerate random-primed RT-PCR: alignment and sequence analysis

Random-primed B1H1 cell cDNA was used as template in a PCR reaction with different combinations of degenerate primers synthesized from consensus regions of both the Notch1 protein and the *notch1* nucleotide sequences. This resulted in the generation of 4 overlapping clones that show high homology to *notch1*. The resulting contig was 4158 bp or 1386 amino acids long (see Figure 11). It represents about 55% of the full length *notch1* cDNA when compared to *Cynops pyrrhogaster notch1*. Blast analysis (blastx) reveals that the contig shows strongest homology (92%) to *Cynops pyrrhogaster notch1*. Following this, it also shows strong homology (77%) to the *Xenopus laevis notch* homologue *Xotch*. Domain searching using the NCBI Conserved Domain Search shows that the *N. viridescens notch1* contig contains 19 EGF repeats and 3 LNR repetitive regions (Figure 11). However, a look at the alignment of the translated protein using blastx shows that *N. viridescens* Notch1 displays strong homology with *Xenopus laevis* Xotch throughout the area that spans from EGF repeat 13 to EGF repeat 36, through the three LNR domains, as well as through the transmembrane region (Figure 12). This suggests that the contig contains 24 EGF repeats and 3 LNR domains, even though these are not detected using the NCBI Conserved Domain Search. Analysis of protein sequence using PSORT (version 6.4; Kenta Nakai, 2000) reveals one transmembrane region close to the C-terminus end of the contig. PSORT also identified a number of residues indicative of nuclear targeting. All this is consistent with the molecular structure and features of the Notch receptor.

Upon obtaining the sequences of the *notch* and *groove* cDNA contigs, attempts were made to align the two sequences. However, the *notch* and *groove* cDNA sequences

Figure 11. The NCBI Conserved Domain Search of the *N. viridescens* Notch1 contig reveals that it contains 19 EGF repeats, as well as 3 LNR repeat regions. Functional domains were assigned a random number in red corresponding to the sequence in which they are found on the contig (i.e. EGF1, EGF2, etc). This number is matched with the particular details regarding their sequence homology below. Note that while the NCBI conserved domain search locates only 19 EGF repeats, the *Notophthalmus viridescens* Notch1 contig displays high homology to *Xenopus laevis* Xotch throughout the regions which correspond to EGF repeats 13-36. This indicates that 4 additional EGF repeats may be present in the Notch1 contig that are not detected by the NCBI Conserved Domain Search.

Notophthalmus viridescens Notch1 amino acid contig sequence

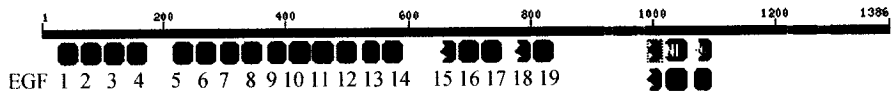

PSSMs producing significant alignments:		Score (bits)	E value
gnl|CDD|14791	cd00054, EGF_CA, Calcium-binding EGF-like domain, present in a...	44.9	7e-05
gnl|CDD|14791	cd00054, EGF_CA, Calcium-binding EGF-like domain, present in a...	42.6	3e-04
gnl|CDD|14791	cd00054, EGF_CA, Calcium-binding EGF-like domain, present in a...	41.4	7e-04
gnl|CDD|14791	cd00054, EGF_CA, Calcium-binding EGF-like domain, present in a...	41.4	7e-04
gnl|CDD|14791	cd00054, EGF_CA, Calcium-binding EGF-like domain, present in a...	41.0	0.001
gnl|CDD|14791	cd00054, EGF_CA, Calcium-binding EGF-like domain, present in a...	40.6	0.001
gnl|CDD|14791	cd00054, EGF_CA, Calcium-binding EGF-like domain, present in a...	40.3	0.002
gnl|CDD|14791	cd00054, EGF_CA, Calcium-binding EGF-like domain, present in a...	37.6	0.009
gnl|CDD|14791	cd00054, EGF_CA, Calcium-binding EGF-like domain, present in a...	37.6	0.010
gnl|CDD|14791	cd00054, EGF_CA, Calcium-binding EGF-like domain, present in a...	36.8	0.015
gnl|CDD|14791	cd00054, EGF_CA, Calcium-binding EGF-like domain, present in a...	36.8	0.017
gnl|CDD|14791	cd00054, EGF_CA, Calcium-binding EGF-like domain, present in a...	36.8	0.016
gnl|CDD|14791	cd00054, EGF_CA, Calcium-binding EGF-like domain, present in a...	35.6	0.034
gnl|CDD|14791	cd00054, EGF_CA, Calcium-binding EGF-like domain, present in a...	35.2	0.047
gnl|CDD|14791	cd00054, EGF_CA, Calcium-binding EGF-like domain, present in a...	34.9	0.063
gnl|CDD|14791	cd00054, EGF_CA, Calcium-binding EGF-like domain, present in a...	34.5	0.077
gnl|CDD|14791	cd00054, EGF_CA, Calcium-binding EGF-like domain, present in a...	34.1	0.13
gnl|CDD|14791	cd00054, EGF_CA, Calcium-binding EGF-like domain, present in a...	32.2	0.45
gnl|CDD|14791	cd00054, EGF_CA, Calcium-binding EGF-like domain, present in a...	31.8	0.52
gnl|CDD|3	smart00004, NL, Domain found in Notch and Lin-12; The Notch pr...	43.0	2e-04
gnl|CDD|3	smart00004, NL, Domain found in Notch and Lin-12; The Notch pr...	40.3	0.002
gnl|CDD|3	smart00004, NL, Domain found in Notch and Lin-12; The Notch pr...	37.2	0.013

EGF 10

```
CD-Length = 38 residues, 100.0% aligned
Score = 44.9 bits (106), Expect = 7e-05

Query:  404   DINECV-KSPCRNGAVCQNTDGGYRCNCKPGYSGRHCE  440
Sbjct:  1     DIDECASGNPCQNGGTCVNTVGSYRCSCPPGYTGRNCE  38
```

EGF 14

```
CD-Length = 38 residues, 100.0% aligned
Score = 42.6 bits (100), Expect = 3e-04

Query:  556   DVNECDSK-PCLNGGTCQDSYGTYKCSCPQGYTGLNCQ  592
Sbjct:  1     DIDECASGNPCQNGGTCVNTVGSYRCSCPPGYTGRNCE  38
```

EGF 12

```
CD-Length = 38 residues, 100.0% aligned
Score = 41.4 bits (97), Expect = 7e-04

Query:  480   DINECAS-NPCKNGANCTDCVNSYTCTCPSGFSGILCE  516
Sbjct:  1     DIDECASGNPCQNGGTCVNTVGSYRCSCPPGYTGRNCE  38
```

EGF 2

CD-Length = 38 residues, 100.0% aligned
Score = 41.4 bits (97), Expect = 7e-04

```
Query:  63    DIDECAS-TPCKNGAKCVDGANSYTCDCAEGYTDVHCE  99
Sbjct:  1     DIDECASGNPCQNGGTCVNTVGSYRCSCPPGYTGRNCE  38
```

EGF 5

CD-Length = 38 residues, 97.4% aligned
Score = 41.0 bits (96), Expect = 0.001

```
Query:  213   NIDECNS-NPCHNGGTCKDGINGFTCVCPQGYQDPTC  248
Sbjct:  1     DIDECASGNPCQNGGTCVNTVGSYRCSCPPGYTGRNC  37
```

EGF 17

CD-Length = 38 residues, 100.0% aligned
Score = 40.6 bits (95), Expect = 0.001

```
Query:  718   EINECQS-HPCQNRGTCIDLVNTYKCSCPRGTQGVHCE  754
Sbjct:  1     DIDECASGNPCQNGGTCVNTVGSYRCSCPPGYTGRNCE  38
```

EGF 4

CD-Length = 38 residues, 100.0% aligned
Score = 40.3 bits (94), Expect = 0.002

```
Query:  138   DVNECQSM-PCQNGGECQDRKNSYSCRCPKGTTGVNCE  174
Sbjct:  1     DIDECASGNPCQNGGTCVNTVGSYRCSCPPGYTGRNCE  38
```

EGF 11

CD-Length = 38 residues, 100.0% aligned
Score = 37.6 bits (87), Expect = 0.009

```
Query:  442   DIDDCL-PNPCHNGGSCSDGINEFFCICLAGFRGPKCE  478
Sbjct:  1     DIDECASGNPCQNGGTCVNTVGSYRCSCPPGYTGRNCE  38
```

EGF 7

CD-Length = 38 residues, 94.7% aligned
Score = 37.6 bits (87), Expect = 0.010

```
Query:  290   NECDS-NPCMNGGTCKDMTSGYLCSCRDGFSGPNCQ  324
Sbjct:  3     DECASGNPCQNGGTCVNTVGSYRCSCPPGYTGRNCE  38
```

EGF 18

CD-Length = 38 residues, only 73.7% aligned
Score = 36.8 bits (85), Expect = 0.015

```
Query:  773   CFNNGKCIDRVGGYNCNCPPGFVGERCE  800
Sbjct:  11    CQNGGTCVNTVGSYRCSCPPGYTGRNCE  38
```

EGF 16

CD-Length = 38 residues, 94.7% aligned
Score = 36.8 bits (85), Expect = 0.017

```
Query:  681   VDECL-PNPCQXXATCTDYLGGYSCECVAGYHGVNC  715
Sbjct:  2     IDECASGNPCQNGGTCVNTVGSYRCSCPPGYTGRNC  37
```

EGF 8

CD-Length = 38 residues, 97.4% aligned
Score = 36.8 bits (85), Expect = 0.016

```
Query:  326   NINECAS-NPCLNQGTCIDDVAGYNCNCLLPYTGPTC  361
Sbjct:  1     DIDECASGNPCQNGGTCVNTVGSYRCSCPPGYTGRNC  37
```

EGF 1

CD-Length = 38 residues, 100.0% aligned
Score = 35.6 bits (82), Expect = 0.034

```
Query:  25   NTDECAS-SPCLHNGRCIDKINEFHCECPVGFNGLLCQ  61
Sbjct:  1    DIDECASGNPCQNGGTCVNTVGSYRCSCPPGYTGRNCE  38
```

EGF 3

CD-Length = 38 residues, 100.0% aligned
Score = 35.2 bits (81), Expect = 0.047

```
Query:  101  DIDECD-PDPCHY-GTCSDGIAGFTCHCEPGYTGHRCE  136
Sbjct:  1    DIDECASGNPCQNGGTCVNTVGSYRCSCPPGYTGRNCE  38
```

EGF 13

CD-Length = 38 residues, 84.2% aligned
Score = 34.9 bits (80), Expect = 0.063

```
Query:  523  TESSCFNGGTCVDGINTFTCRCPAGFIGSYCE  554
Sbjct:  7    SGNPCQNGGTCVNTVGSYRCSCPPGYTGRNCE  38
```

EGF 6

CD-Length = 38 residues, 100.0% aligned
Score = 34.5 bits (79), Expect = 0.077

```
Query:  251  EVNECNS-NPC-IHGKCHDGINGYRCDCDPGWSGTNCD  286
Sbjct:  1    DIDECASGNPCQNGGTCVNTVGSYRCSCPPGYTGRNCE  38
```

EGF 19

CD-Length = 38 residues, 97.4% aligned
Score = 34.1 bits (78), Expect = 0.13

```
Query:  802  DVNECLS-NPCDPRGTQNCIQLVNDYXCECRQGYSGRRC  839
Sbjct:  1    DIDECASGNPCQNGGT--CVNTVGSYRCSCPPGYTGRNC  37
```

EGF 9

CD-Length = 38 residues, 84.2% aligned
Score = 32.2 bits (73), Expect = 0.45

```
Query:  369  SDNPCKNGGECRESEDYESFSCSCPAGWQGQTCE  402
Sbjct:  7    SGNPCQNGGTCVNTVG--SYRCSCPPGYTGRNCE  38
```

EGF 15

CD-Length = 38 residues, only 78.9% aligned
Score = 31.8 bits (72), Expect = 0.52

```
Query:  649  NLCRNSGLCEDTGNTHHCRCQAGYTGSYCE  678
Sbjct:  9    NPCQNGGTCVNTVGSYRCSCPPGYTGRNCE  38
```

LNR 2

CD-Length = 39 residues, 94.9% aligned
Score = 43.0 bits (101), Expect = 2e-04

```
Query:  1019  DPWKNCTQSLQCWKYFNDGKCDSQCNNAGCLYDGFDCQ  1056
Sbjct:  3     DPWSRC-EDAQCWDKFGDGVCDEECNNAECLWDGGDCS  39
```

LNR 3

CD-Length = 39 residues, only 76.9% aligned
Score = 40.3 bits (94), Expect = 0.002

```
Query:  1067  DQYCRDHFQDGHCDQGCNNAECEWDGLDCS  1096
Sbjct:  10    DAQCWDKFGDGVCDEECNNAECLWDGGDCS  39
```

LNR 1

CD-Length = 39 residues, only 69.2% aligned
Score = 37.2 bits (86), Expect = 0.013

```
Query:  988   CASFAGNKICNAXCNNHACGWDGGDCS  1014
Sbjct:  13    CWDKFGDGVCDEECNNAECLWDGGDCS  39
```

Figure 12. Alignment of the contig generated by random-primed degenerate RT-PCR with Notch1 from *Cynops pyrrhogaster, Xenopus laevis, Mus musculus and Danio rerio.* The 4158 bp (1386 amino acid) contig represents about 55% of the full length *notch1* cDNA when compared to *Cynops pyrrhogaster notch1*. The contig shows strongest amino acid homology (92%) to *Cynops pyrrhogaster notch1,* followed by 77% homology to *Xenopus laevis notch* homologue *xotch.* Consensus sequences are shaded in yellow, while sequence disagreements are not shaded. Functional domains (as determined by the NCBI Conserved Domain Search) are boxed and labeled in red.

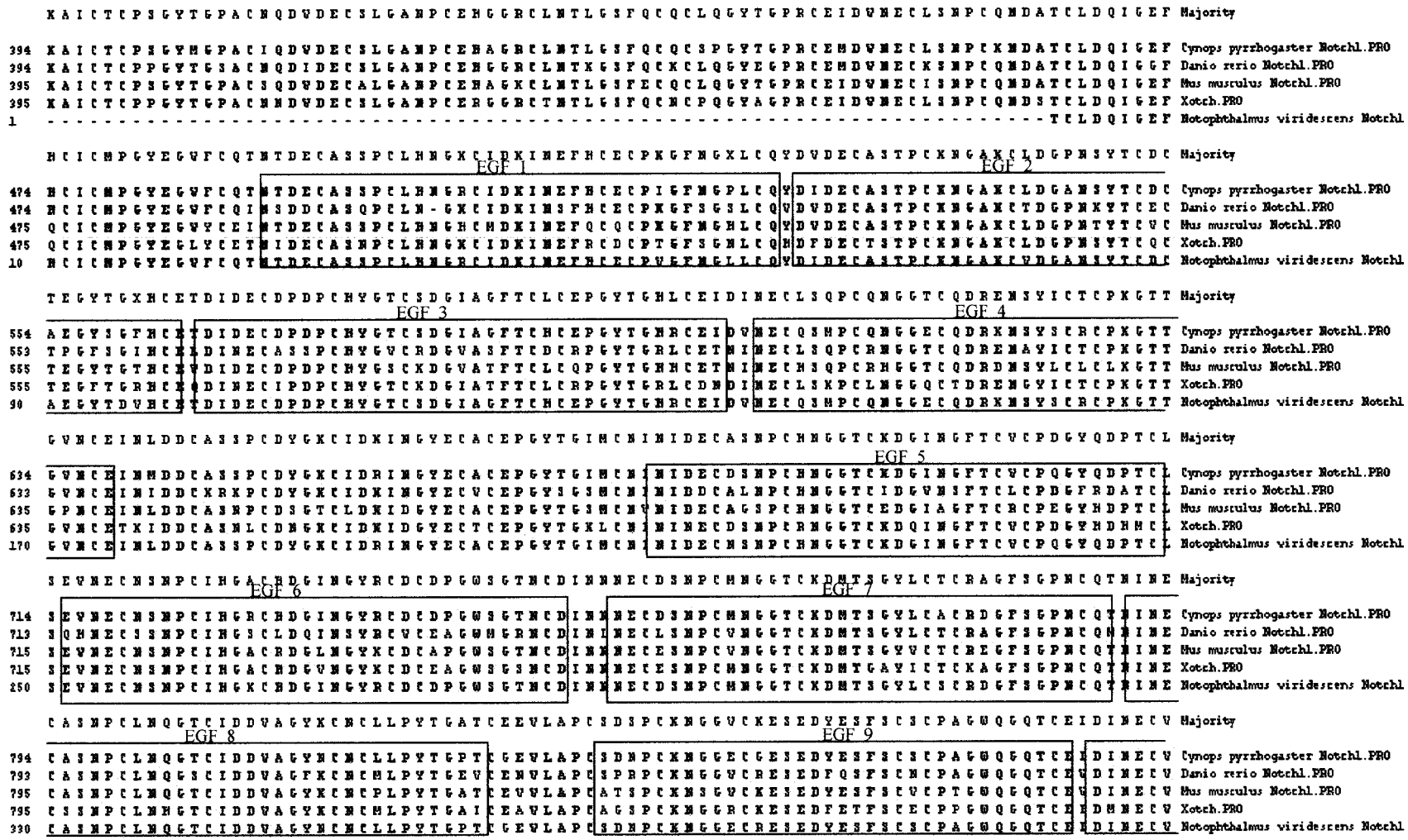
EGF 1
EGF 2
EGF 3
EGF 4
EGF 5
EGF 6
EGF 7
EGF 8
EGF 9

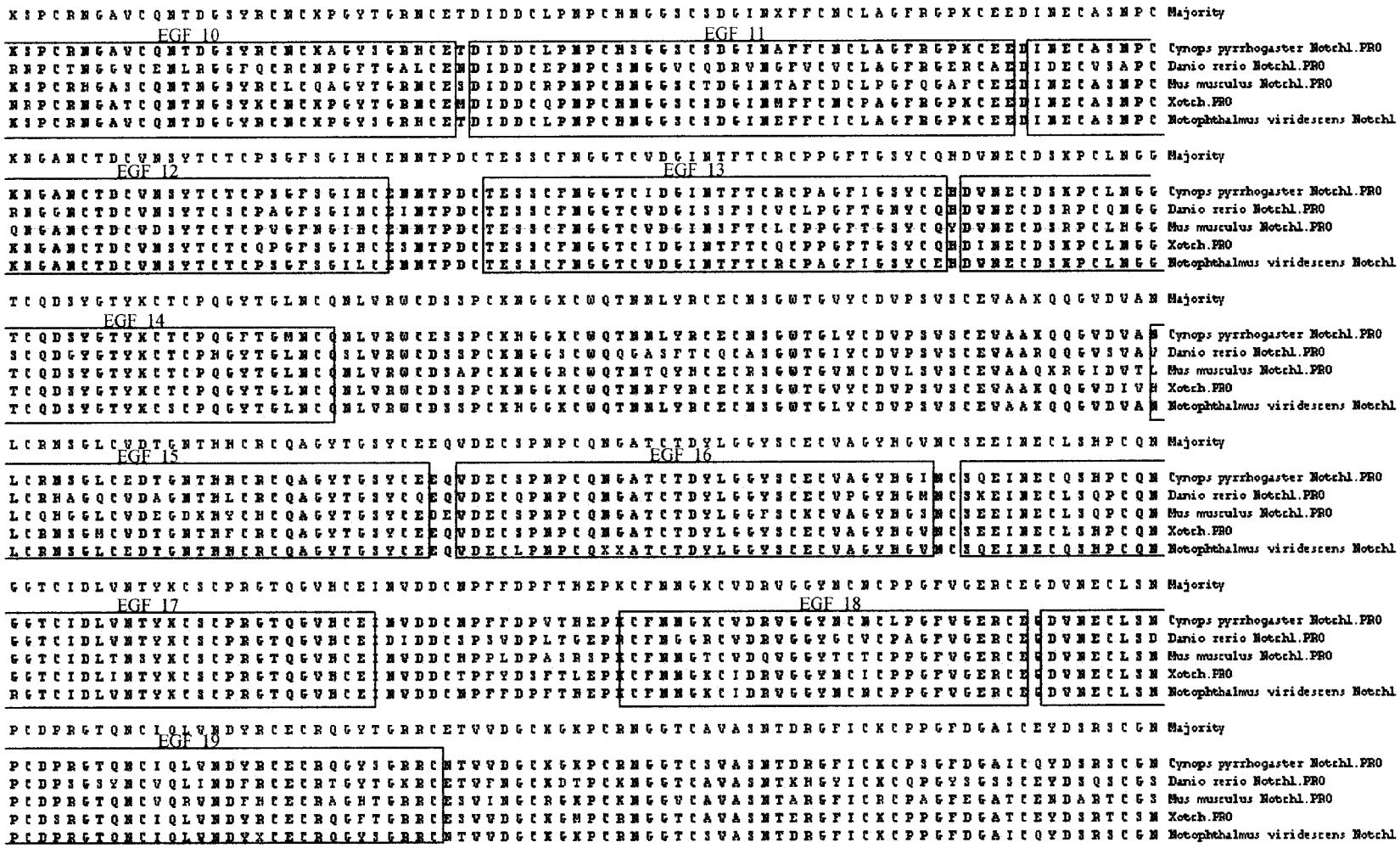
EGF 10
EGF 11
EGF 12
EGF 13
EGF 14
EGF 15
EGF 16
EGF 17
EGF 18
EGF 19
Majority
Cynops pyrrhogaster Notchl.PRO
Danio rerio Notchl.PRO
Mus musculus Notchl.PRO
Xotch.PRO
Notophthalmus viridescens Notchl

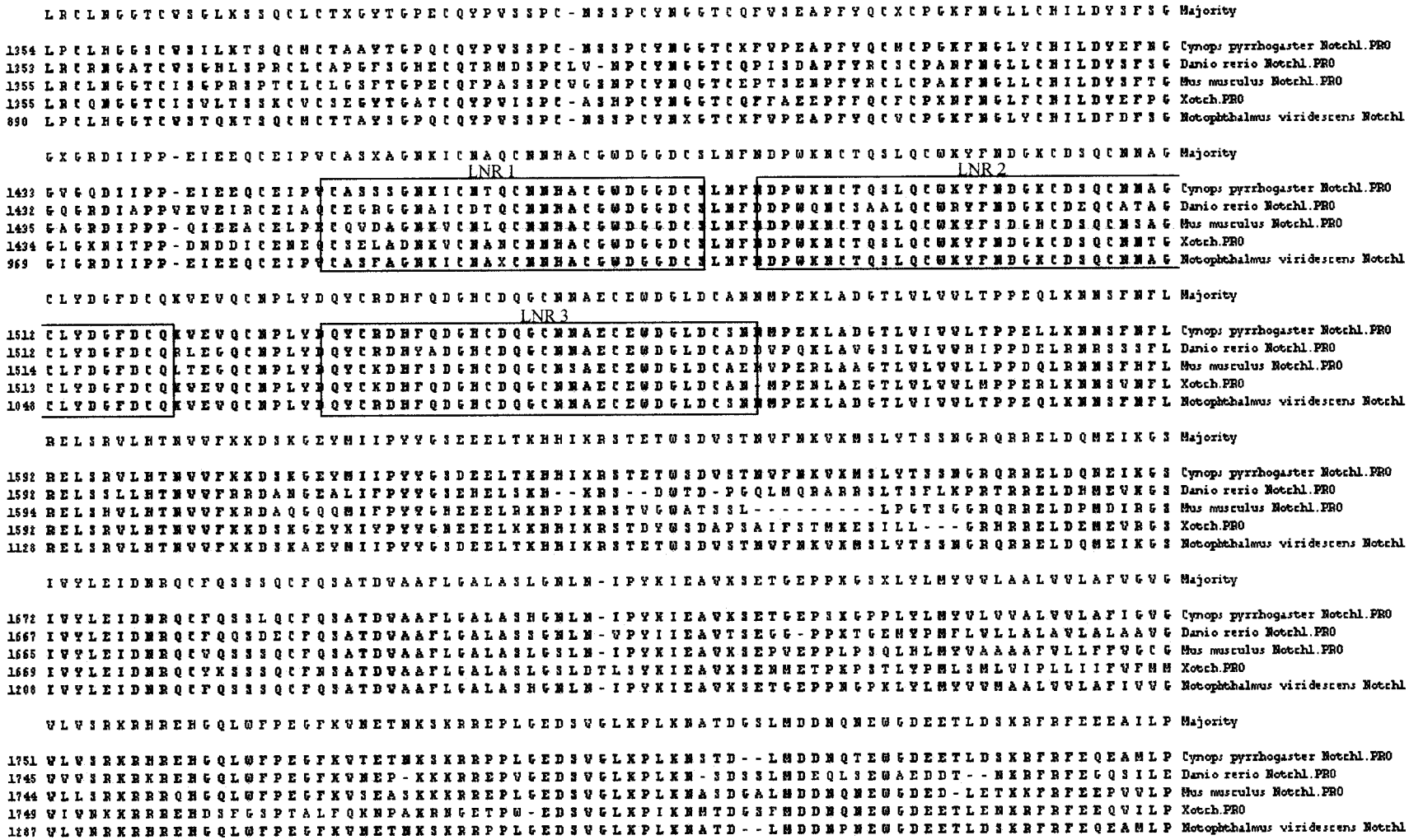
LNR 1
LNR 2
LNR 3
Majority
Cynops pyrrhogaster Notchl.PRO
Danio rerio Notchl.PRO
Mus musculus Notchl.PRO
Xotch.PRO
Notophthalmus viridescens Notchl

```
    DL-SDQTDHRQWTQQHLDAADLRISSMAPTPPQGEIDADCMDVMVRGPDGFTPLMIASCSGGGLETGMSEEEEDASAMVI Majority

1829 DM-MDQTDRRQWTQQHLDAADLRISSMAPTPPQGEIDPDCLDVMVRGPDGFTPLMIASCSGGGLETGMSEEEEDASAMVI Cynops pyrrhogaster Notchl.PRO
1821 --MSGQLDMRQWTQQHLDAADLRLMSMAPTPPQGQIEMDCMDVMVRGPDGFTPLMIASCSGGGLEMEMGEAEEDPSADVI Danio rerio Notchl.PRO
1823 DL-SDQTDMRQWTQQHLDAADLRMSAMAPTPPQGEVDADCMDVMVRGPDGFTPLMIASCSGGGLETGMSEEEEDAPA-VI Mus musculus Notchl.PRO
1828 ELVDDKTDPRQWTRQHLDAADLRISSMAPTPPQGEIEADCMDVMVRGPDGFTPLMIASCSGGGLETGMSEEEEDASAMMI Xotch.PRO
1365 DM-SDQTDRRQWTQQHLDAADLR                                                          Notophthalmus viridescens Notchl

    SDFIYQGAMLHMQTDRTGETALHLAARYARSDAAKRLLEASADAMVQDMMGRTPLHAAVAADAQGVFQILIRMRATDLDA Majority

1908 SDFLYQGAMLHMQTDRTGETALHLAARYARSDAAKRLLEASAMAMVQDMMGRTPLHAAVAADAQGVFQILIRMRATELDA Cynops pyrrhogaster Notchl.PRO
1899 TDFIYHGAMLHMQTDRTGETALHLAARYARSDAAKRLLESCADAMVQDMMGRTPLHAAVAADAQGVFQILIRMRATDLDA Danio rerio Notchl.PRO
1901 SDFIYQGASLHMQTDRTGETALHLAARYSRSDAAKRLLEASADAMIQDMMGRTPLHAAVSADAQGVFQILLRMRATDLDA Mus musculus Notchl.PRO
1908 SDFIGQGAQLHMQTDRTGETALHLAARYARADAAKRLLESSADAMVQDMMGRTPLHAAVAADAQGVFQILIRMRATDLDA Xotch.PRO
1386                                                                                    Notophthalmus viridescens Notchl
```

failed to align using either Megalign or SeqMan alignment programs (Lasergene). It is important to note that this may indicate that *groove* is not directly related to *notch*, but simply shares a high sequence similarity.

Real time RT-PCR detection of *groove* expression in B1H1 cell lines

Using primers specific to areas of *groove* that displayed low homology to *Cynops pyrrhogaster notch1*, real time RT-PCR was performed on subconfluent, confluent, and myotube B1H1 cells collected 4 days and 8 days post serum drop, as well as cells that has been re-supplemented with 10% FCS after being induced to differentiate into myotubes. *Groove* consistently reached threshold cycle (Ct) quite late: *groove* samples reached Ct anywhere from cycle 28 – 30, whereas *GapDH* consistently reached Ct at cycle 15. When *GapDH* Ct is subtracted from *groove* Ct to compensate for differences in levels of starting material, *groove* shows ΔCt values of 12-13 (indicating that *groove* reaches Ct 12-13 cycles later than GapDH). This may be indicative of generally low levels of expression. Relative to the lowest expressing tissue type, *groove* seems to show highest expression in subconfluent B1H1 cells and lowest expression in myotubes collected 4 days post serum drop (Figure 13a). However, this over-expression is only approximately 3 fold. Confluent B1H1 cells display slightly lower levels of *groove* than subconfluent, but higher levels than myotubes collected 4 days post serum drop by about 2.5 fold. B1H1 myotubes harvested 8 days after serum drop show comparable levels of *groove* expression to myotubes collected 4 days post serum drop. Myotubes that had been re-supplemented with 10% FCS (representative of differentiated cells being induced to dedifferentiate) show slightly higher *groove* levels than 4 day myotubes, but only by 1.5 fold. Altogether, the data seem to indicate that *groove* expression is quite low in B1H1

Figure 13. Real time RT-PCR detection of *groove* expression in B1H1 cell lines relative to the lowest expressing tissue type amplified with *groove* primers. A) *Groove* expression, while relatively low, is detected in all lines of B1H1 cells tested (subconfluent, confluent, myotubes collected 4 and 8 days post serum drop, and myotubes induced to dedifferentiate by resupplementing the media with 10% FCS). *Groove* levels seemed to be highest in confluent B1H1 cells and lowest in 4 day myotubes, though this difference in expression is only approximately threefold. B) Low levels of *groove* expression are again detected in different preparations of subconfluent B1H1, superconfluent B1H1 and 4 day myotube cDNA. *Groove* expression decreases from subconfluent B1H1 cells to superconfluent B1H1 cells to 4 day myotubes, however, the overall decrease in *groove* expression from subconfluent B1H1 cells to 4 day myotubes is less than 2 fold.

A

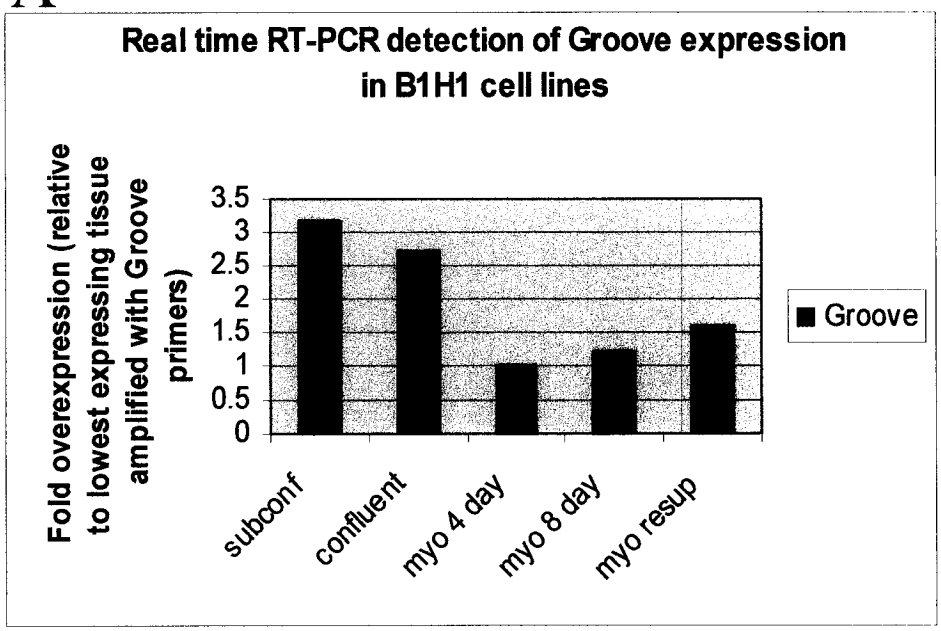
Real time RT-PCR detection of Groove expression in B1H1 cell lines
Fold overexpression (relative to lowest expressing tissue amplified with Groove primers)
3.5
3
2.5
2
1.5
1
0.5
0
subconf
confluent
myo 4 day
myo 8 day
myo resup
Groove

B

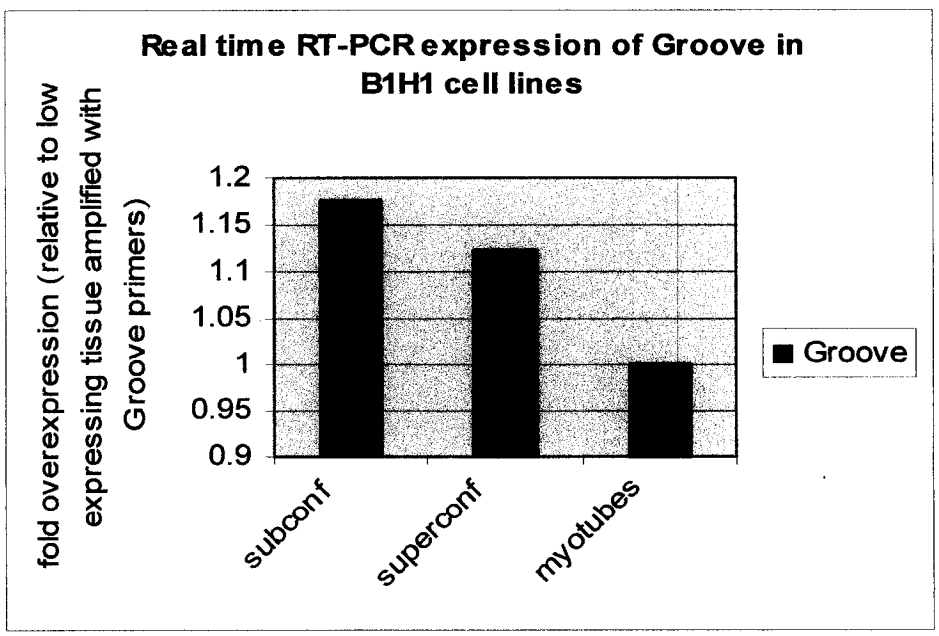
Real time RT-PCR expression of Groove in B1H1 cell lines
fold overexpression (relative to low expressing tissue amplified with Groove primers)
1.2
1.15
1.1
1.05
1
0.95
0.9
subconf
superconf
myotubes
Groove

cells, and that while it is highest in subconfluent B1H1 cells and lowest in myotubes collected 4 days post serum drop, this difference is not considerable.

When real time RT-PCR was repeated using cDNA generated from different preparations of subconfluent B1H1 cells, superconfluent B1H1 cells and 4 day myotube RNA, the *groove* expression profile obtained was similar to that of the original experiment (Figure 13b). However, in this case, the highest *groove* expressing cell lines (subconfluent) displayed less than two fold overexpression relative to the lowest *groove* expressing tissue (4 day myotubes).

Real time RT-PCR detection of *notch* expression in B1H1 cell lines

Notch expression was determined using primers designed from areas of the *Notophthalmus viridescens notch1* contig that fell between functional domains. This area was specifically chosen because it is likely to represent an area of low sequence conservation, and thus, may be more specific to the *Notophthalmus viridescens notch1* homologue. Since more than one *notch* isoforms may exist within the same species, an ideal probe should be as specific to the particular isoform of interest as possible. *Notch* expression was highest in myotubes that had been harvested 4 days after serum drop (Figure 14a). Expression was lowest in myotubes that had been induced to dedifferentiate by re-supplementing the media with 10% FCS. The 4 day myotubes showed 5 fold over-expression when compared to the re-supplemented myotubes. In between these two extremes were the myotubes harvested 8 days after serum drop, which showed 2 fold *notch* over-expression when compared to re-supplemented myotubes, but 2.5 fold less *notch* expression when compared to myotubes harvested 4 days after serum drop. *Notch* expression also seems to be high in subconfluent B1H1 cells (two fold less

Figure 14. Real time RT-PCR detection of *notch* expression in B1H1 cell lines relative to the lowest expressing tissue type amplified with *notch* primers. A) *Notch* expression was detected in all tested lines of B1H1 cells (subconfluent, confluent, myotubes collected 4 and 8 days post serum drop, and myotubes induced to dedifferentiate by resupplementing the media with 10% FCS). *Notch* expression was highest in myotubes harvested 4 days post serum drop. Expression levels decreased by 2.5 fold in the 8 day myotubes, then decreased further by 2 fold in the re-supplemented myotubes. Expression was also relatively high in the subconfluent B1H1 cells, and lower in the confluent B1H1 cells. B) *Notch* expression is again detected in each of the different preparations of subconfluent B1H1, superconfluent B1H1 and 4 day myotube cDNA. As above, *notch* expression was moderate in subconfluent B1H1 cells, low in superconfluent B1H1 cells, and highest in 4 day myotubes.

A

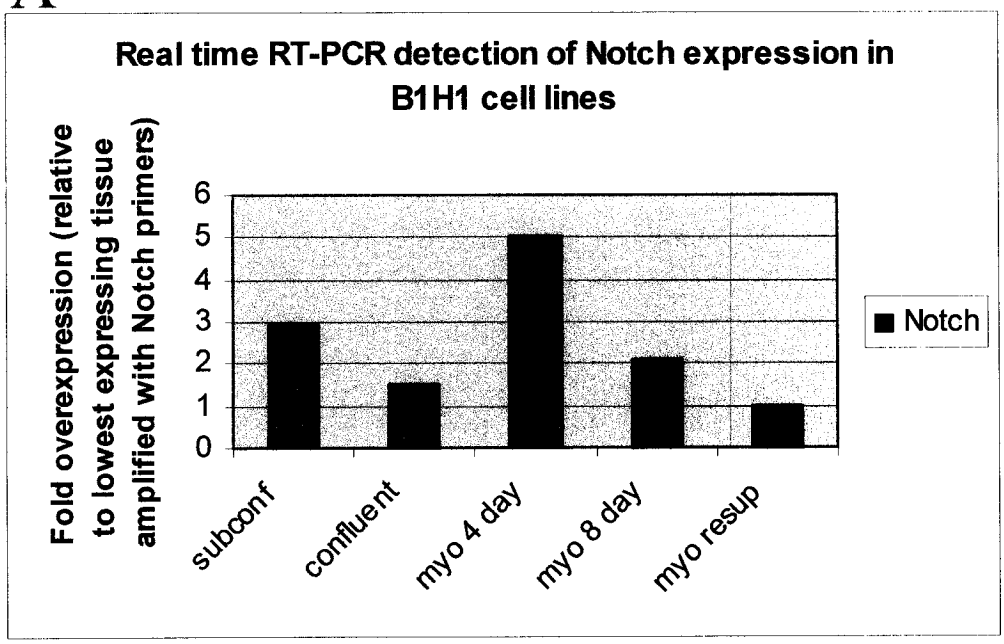
Real time RT-PCR detection of Notch expression in B1H1 cell lines
Fold overexpression (relative to lowest expressing tissue amplified with Notch primers)
6
5
4
3
2
1
0
subconf
confluent
myo 4 day
myo 8 day
myo resup
Notch

B

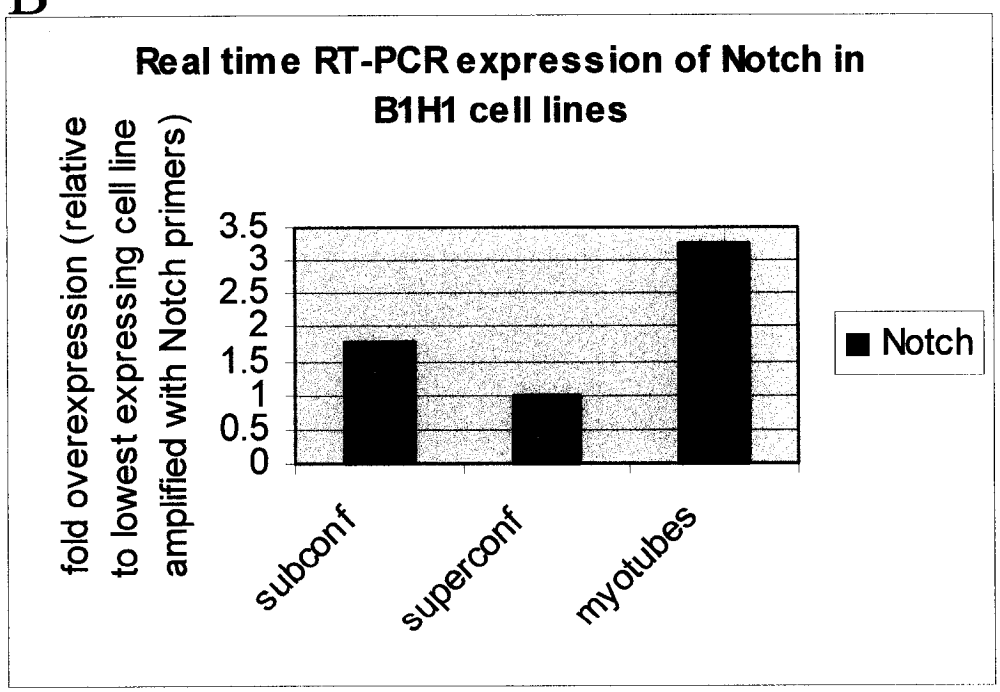
Real time RT-PCR expression of Notch in B1H1 cell lines
fold overexpression (relative to lowest expressing cell line amplified with Notch primers)
3.5
3
2.5
2
1.5
1
0.5
0
subconf
superconf
myotubes
Notch

than myotubes harvested 4 days post serum drop), but then drops in confluent B1H1 cells by approximately 2 fold (compared to subconfluent B1H1 cells).

Again, when the experiment was repeated with different preparations of subconfluent, superconfluent and 4 day myotube cDNA, the *notch* expression profile obtained matched that observed in the first real time RT-PCR experiment (Figure 14b). *Notch* expression levels were found to be moderate in subconfluent B1H1 cells, low in confluent B1H1 cells, and highest in myotubes harvested 4 days post serum drop. Subconfluent B1H1 cells displayed approximately 2 fold *notch* overexpression relative to superconfluent B1H1 cells, while myotubes harvested 4 days post serum drop displayed approximately 3 fold *notch* overexpression relative to superconfluent B1H1 cells.

Comparative expression of *notch* and *groove* in B1H1 cell lines

While these relative levels of expression may prove to be significantly indicative of differential roles for *notch* in different types of B1H1 cells, they are even more exaggerated when they are compared to levels of *groove* expression (Figure 15a). For example, in myotubes collected 4 days post serum drop, *notch* shows approximately 31 fold over-expression when compared to levels of *groove* expression. *Groove* expression appears to remain relatively low and almost negligible when compared to fluctuations in levels of *notch* expression in the same cell types. However, it is interesting to note that even while the scale magnitudes are not equivalent, levels of *groove* seem to be inversely related to levels of *notch*, in that the tissues which express relatively higher levels of *notch* express relatively lower levels of *groove* (see Figures 13a and 14a), and vice versa. For example, in myotubes collected 4 days post serum drop, levels of *groove* are at their lowest, while levels of *notch* are highest. Following this, in myotubes collected 8 days

Figure 15. Comparative real time RT-PCR detection of *groove* and *notch* expression in B1H1 cell lines relative to the lowest expressing tissue type of either gene. A) *Groove* displays low levels of expression when compared relative to levels of *notch* expression. Any fluctuations in levels of *groove* expression seem almost negligible when viewed in light of fluctuations in *notch* expression. B) *Groove* again shows relatively low expression levels when compared to *notch* expression.

A

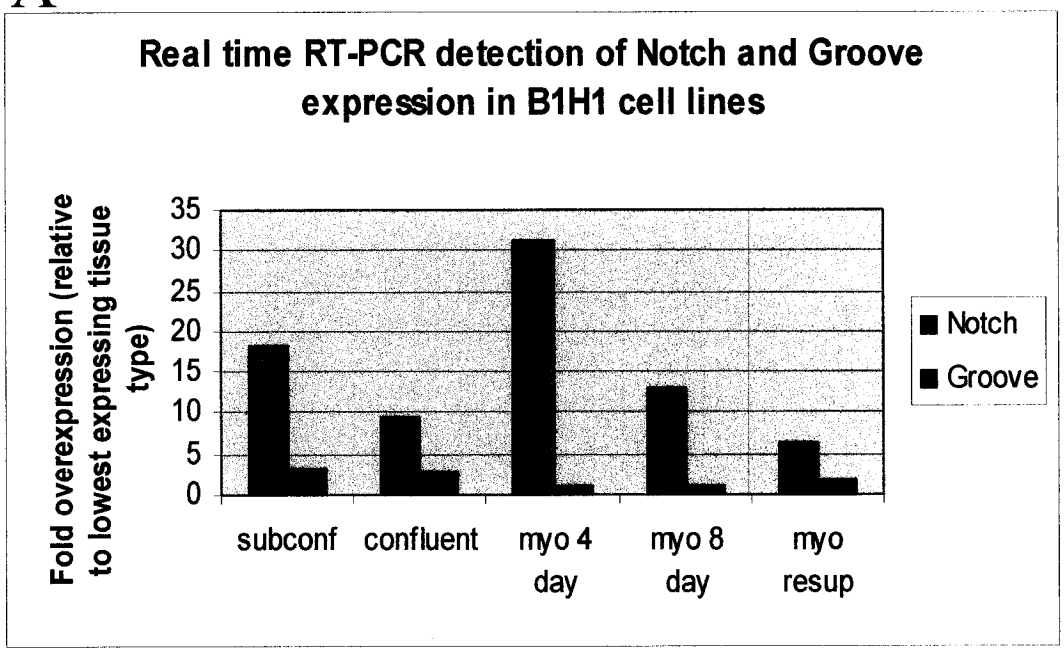
Real time RT-PCR detection of Notch and Groove expression in B1H1 cell lines
Fold overexpression (relative to lowest expressing tissue type)
35
30
25
20
15
10
5
0
subconf
confluent
myo 4 day
myo 8 day
myo resup
Notch
Groove

B

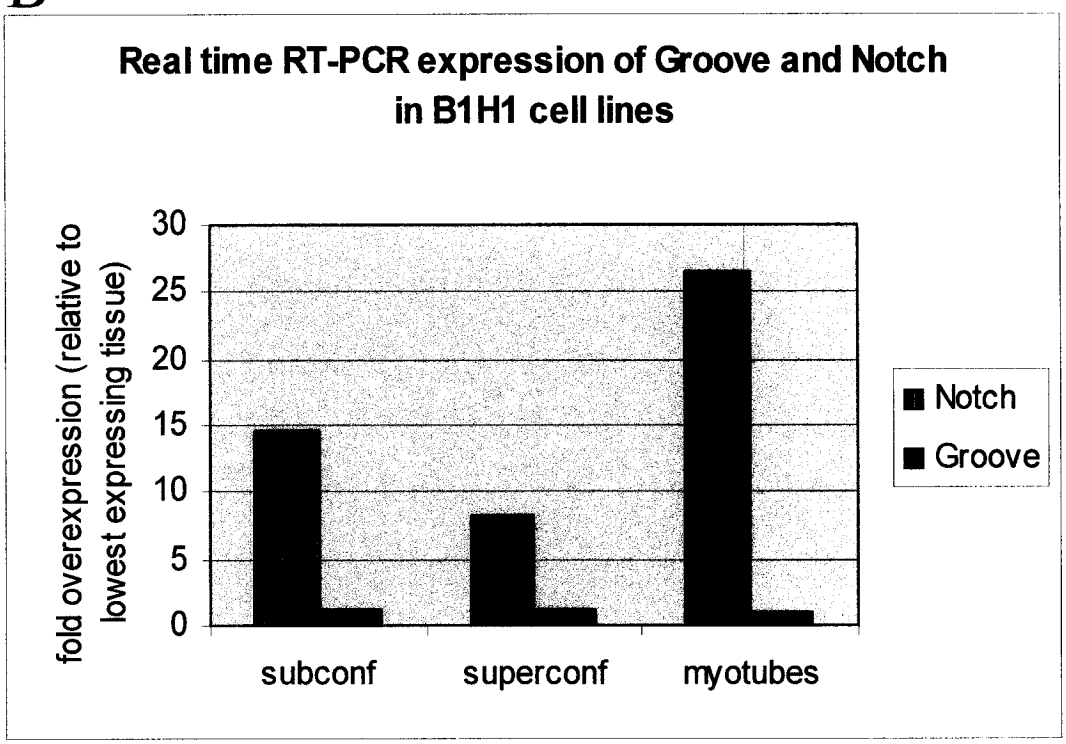
Real time RT-PCR expression of Groove and Notch in B1H1 cell lines
fold overexpression (relative to lowest expressing tissue)
30
25
20
15
10
5
0
subconf
superconf
myotubes
Notch
Groove

post serum drop, levels of *groove* increase slightly while levels of *notch* decrease. In re-supplemented myotubes, *groove* continues to increase, while *notch* levels correspondingly decrease. When these experiments were repeated with different first strand cDNA generated from different preparations of subconfluent B1H1 cell, superconfluent B1H1 cell and 4 day myotube RNA, similar trends and patterns were observed (Figure 15b).

Real time RT-PCR detection of *groove* expression in regenerating forelimb tissue

Groove expression was detected in all stages of regenerating forelimb tissue, including whole (non-regenerating) limb tissue. *Groove* expression seemed to be relatively low in whole limbs, and was comparable in the 24 hour regenerates (Figure 16a). However, following this, *groove* expression increases in the 1 week regenerate by approximately 2 fold (compared to 24 hour), then again in the 2 week regenerate by approximately 3.5 fold. In the 3 week regenerate, expression seems to decrease again, but not by much (only by approximately 1.5 fold) before it increases again in the 4 week regenerate to similar levels seen in the 2 week regenerate. Altogether, *groove* expression seems to be present in the whole limb, then increase slightly as regeneration progresses. The 4 fold increase in *groove* expression between 24 hour and 4 week regenerates, while not spectacular, may still represent a functional significance.

Different samples of cDNA were generated from whole limb RNA, as well as 24 hour, 8 day, 15 day and 21 day regenerating forelimb RNA. Real time RT-PCR was performed to determine levels of *groove* expression in these tissues. In general, the same trends were obtained with both experiments. Groove expression appeared to be lowest in

Figure 16. Real time RT-PCR detection of *groove* expression in newt forelimb regenerates relative to the lowest expressing tissue type amplified with *groove* primers. A) *Groove* was detected in all stages of the regenerating newt forelimb, including whole (non-regenerating) limbs. *Groove* expression seems to be generally low in the whole limb and 24 hour regenerate, then seems to increase as regeneration progresses. Highest levels of *groove* expression are detected in the later stages of regeneration (4 weeks). *Groove* expression in this regenerate is approximately fourfold greater than in whole limb/24 hour regenerates. B) *Groove* expression was comparably low in both the 24 hour and the 8 day regenerates. *Groove* expression was higher in the whole limb and 15 day regenerates, and peaked in the 21 day regenerate.

A

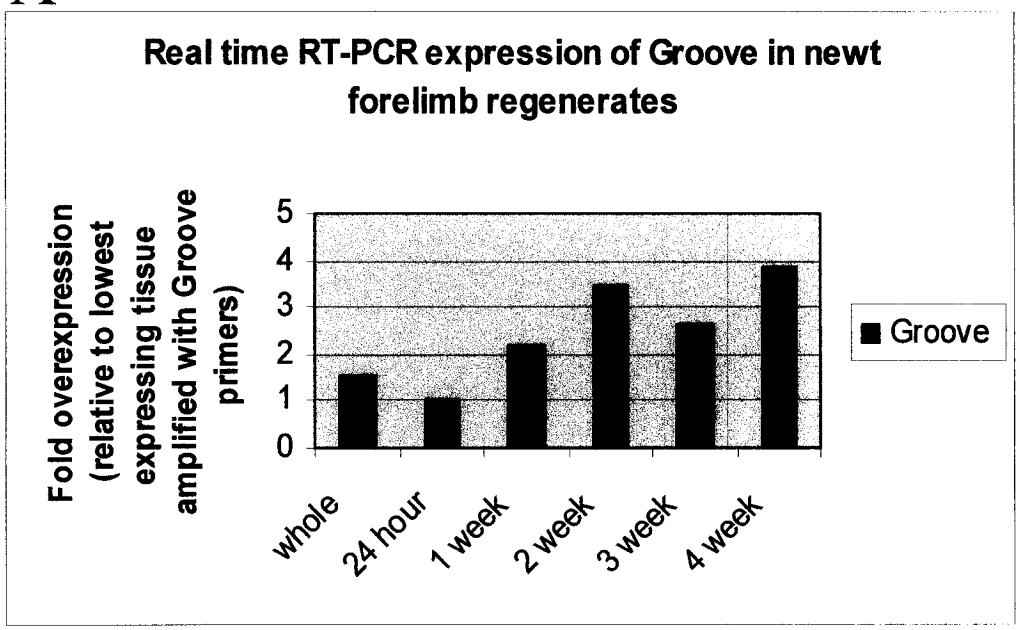
Real time RT-PCR expression of Groove in newt forelimb regenerates
Fold overexpression (relative to lowest expressing tissue amplified with Groove primers)
5
4
3
2
1
0
whole
24 hour
1 week
2 week
3 week
4 week
Groove

B

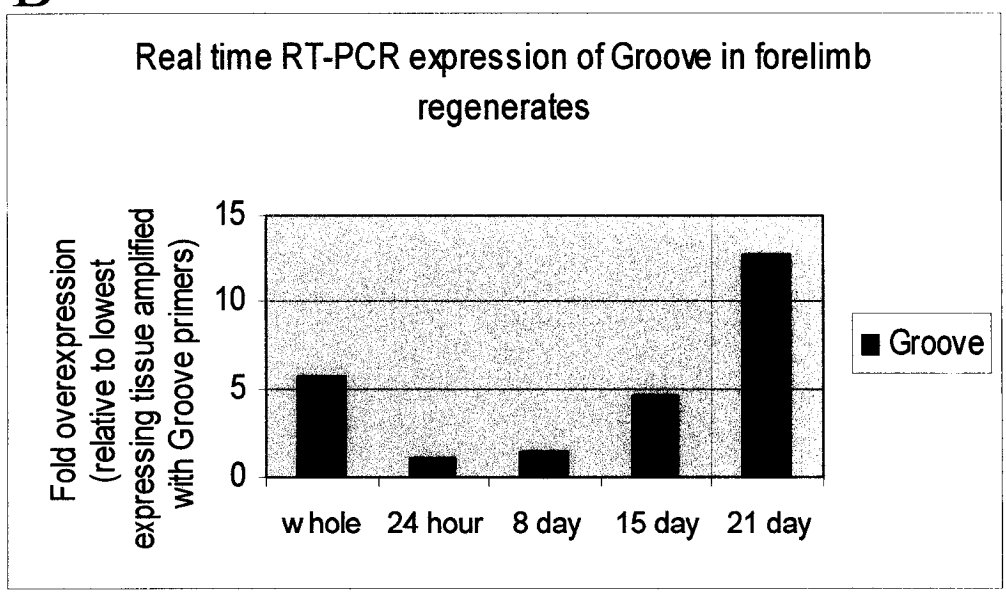
Real time RT-PCR expression of Groove in forelimb regenerates
Fold overexpression (relative to lowest expressing tissue amplified with Groove primers)
15
10
5
0
whole
24 hour
8 day
15 day
21 day
Groove

the 24 hour regenerate and then gradually increased as regeneration progressed (Figure 16b).

Real time RT-PCR detection of *notch* expression in regenerating forelimb tissue

Notch expression as detected by real time RT-PCR was relatively low (yet still present) in the whole, non-regenerating limb. Interestingly, in the 24 hour regenerate, *notch* expression suddenly increases by approximately 4 fold, which may be indicative of a role for Notch in the responsive wound healing reflex that is activated immediately following amputation (Figure 17). Following this, *notch* expression decreases in the 1 week regenerate to levels comparable to those detected in the whole limb. At 2 weeks, however, expression seems to suddenly increase again to approximately 6 fold as compared to the lowest expressing tissue amplified with the *notch* primers (4 week regenerate). At 3 weeks, expression decreases by approximately 2.5 fold, and by 4 weeks, expression further drops by about 2.5 fold more.

When the experiment was repeated on cDNA generated from different samples of whole limb, 24 hour, 8 day, 15 day and 21 day regenerating tissue, the lowest level of *notch* detection was observed in the 8 day regenerate (Figure 17b). *Notch* expression levels in the whole limb, 24 hour and 15 day regenerates were comparable; all were approximately 8 fold higher than the 8 day regenerate (Figure 17b). This differs from the previous experiment, in which levels of *notch* in the whole limb appeared to be relatively low compared to the 24 hour and 15 day regenerates (Figure 17a). Finally, *notch* expression seems to increase in the 21 day regenerate, with expression levels reaching a peak of 17 fold overexpression relative to the 8 day regenerate (Figure 17b). This is again different from the previous experiment, where *notch* expression levels decreased

Figure 17. Real time RT-PCR detection of *notch* expression in newt forelimb regenerates relative to the lowest expressing tissue type amplified with *notch* primers. A) *Notch* expression was also detected at all stages of the regenerating newt forelimb, including whole (non-regenerating) limbs. *Notch* expression seems to be relatively low in the whole limb, but then increases in the 24 hour regenerate. After decreasing slightly in the 1 week regenerate, *notch* expression then reaches its highest levels in the 2 week regenerate. Following the peak of expression at two weeks, expression decreases as regeneration progresses to the later stages. B) In this subsequent experiment, *notch* expression was clearly lowest in the 8 day regenerate. Whole limb, 24 hour and 15 day regenerating tissue all showed approximately 8 fold overexpression of *notch* when compared to the 8 day regenerating tissue. *Notch* expression then reaches its highest levels in the 21 day regenerate.

A

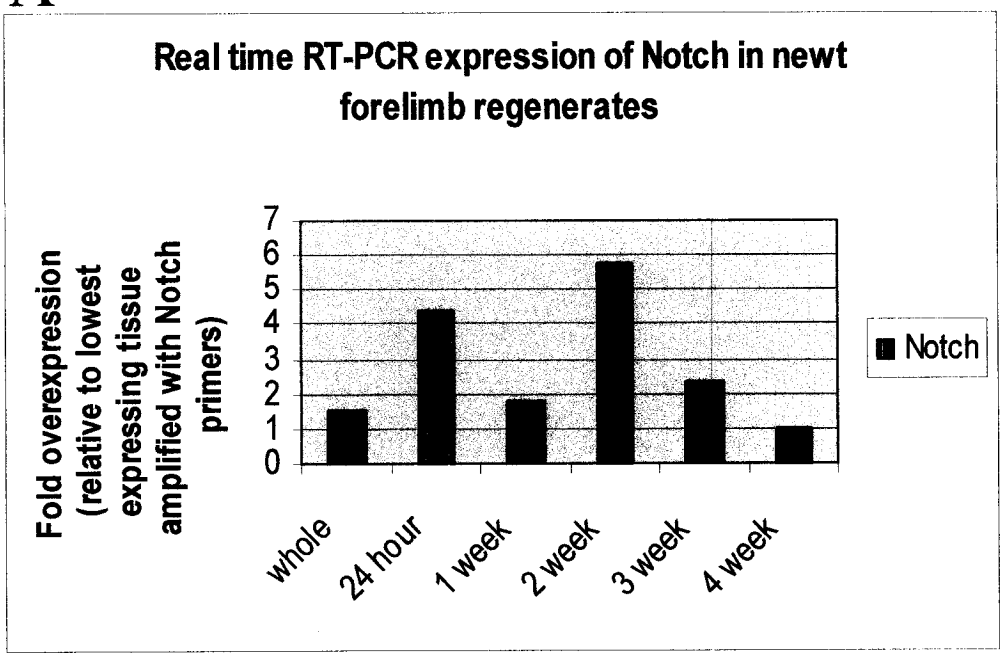
Real time RT-PCR expression of Notch in newt forelimb regenerates
Fold overexpression (relative to lowest expressing tissue amplified with Notch primers)
7
6
5
4
3
2
1
0
whole
24 hour
1 week
2 week
3 week
4 week
Notch

B

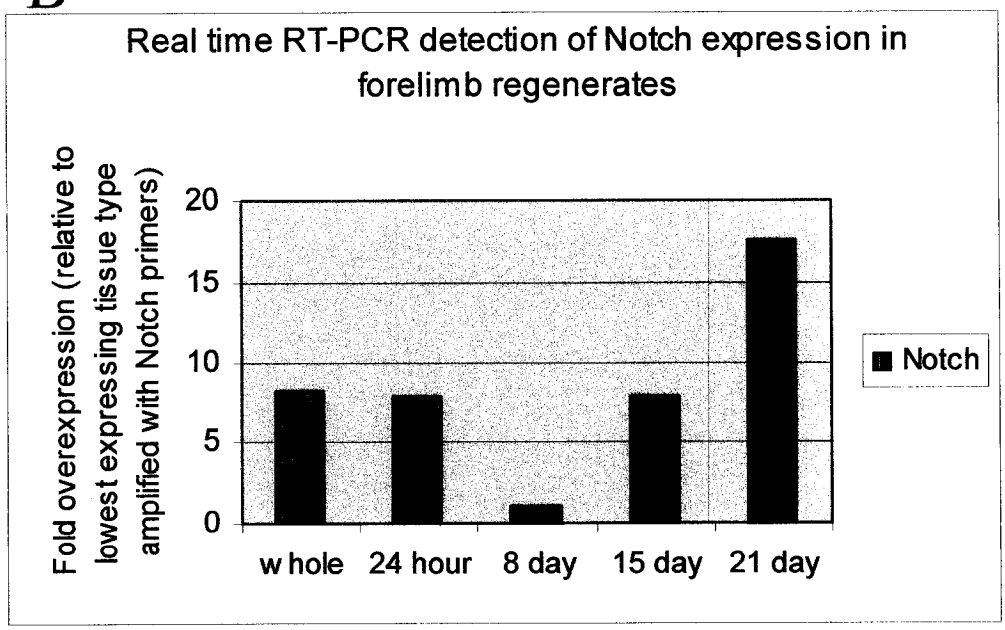
Real time RT-PCR detection of Notch expression in forelimb regenerates
Fold overexpression (relative to lowest expressing tissue type amplified with Notch primers)
20
15
10
5
0
w hole
24 hour
8 day
15 day
21 day
Notch

after 15 days (Figure 17a). Overall, in the repeated experiment, it seems that the early stages of regeneration (up to blastema formation) have been stretched over a three week period as opposed to two weeks. Unfortunately, we did not have a four week time-point in the repeat experiment so that we could determine whether the expression levels begin to drop again, as they did in the first experiment. Explanations for this apparent discrepancy between the two experiments are discussed in the next section of the thesis.

Comparative expression of *notch* and *groove* in regenerating forelimb tissue

Again, the patterns of *notch* expression become exaggerated when compared relative to levels of *groove* expression (Figure 18). In this context, levels of *groove* expression appear to remain relatively constant when compared to fluctuations in *notch* expression. *Groove* also appears to be expressed at quite low levels relative to *notch* expression. For example, in the 2 week regenerate, *notch* shows almost 19 fold over-expression when compared to the lowest levels of *groove* expression. However, despite the differences in scale magnitude, it is interesting that as in the B1H1 cell lines, levels of *groove* and *notch* expression seem to be inversely related (see Figures 16a and 17a). For example, while levels of *groove* seem to decrease in the 24 hour regenerate (relative to *groove*), levels of *notch* seem to increase (relative to *notch*). Similarly, in the 3 and 4 week regenerates, levels of *notch* seem to decrease, while levels of *groove* seem to increase. The only exception to this seems to be the 2 week regenerate, where both levels of *groove* and *notch* seem to be relatively high. Again, however, this may not be significant considering that at this stage, *notch* shows almost 19 fold over-expression when compared to *groove*.

Figure 18. Comparative real time RT-PCR detection of *groove* and *notch* expression in newt forelimb regenerates relative to the lowest expressing tissue type of either gene. Fluctuations in *groove* expression seem almost negligible when compared to fluctuations in relative levels of *notch* expression. This indicates that *groove* is, in general, a comparatively low expressing gene in the forelimb regenerate. Whether these low levels are sufficient to produce a functional effect on Notch signaling is unknown.

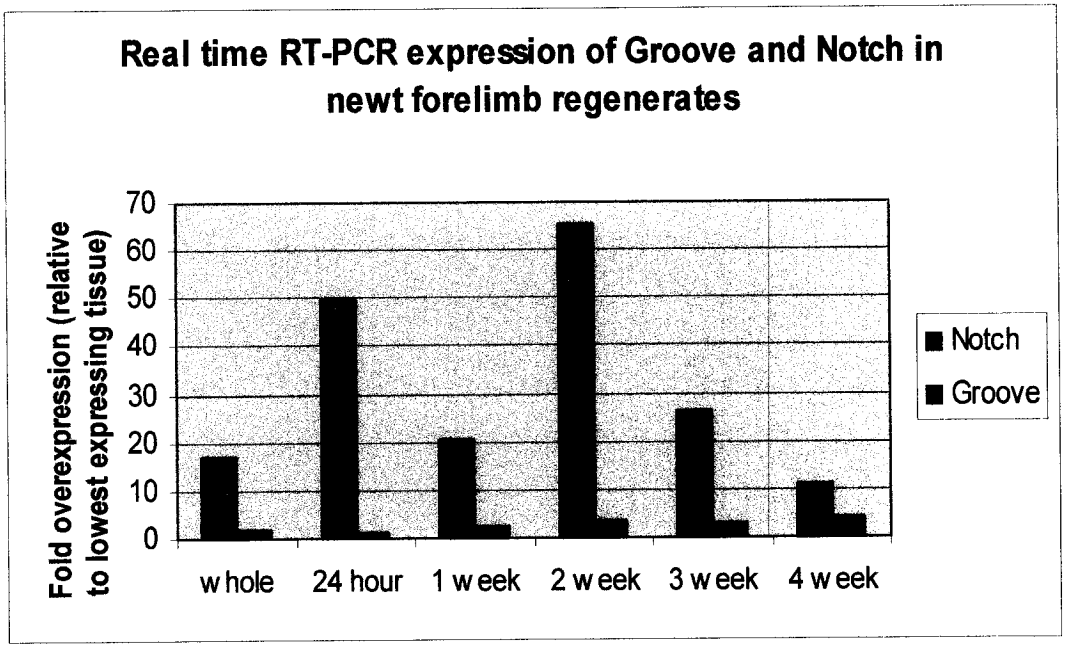
Real time RT-PCR expression of Groove and Notch in newt forelimb regenerates
Fold overexpression (relative to lowest expressing tissue)
70
60
50
40
30
20
10
0
whole
24 hour
1 week
2 week
3 week
4 week
Notch
Groove

DISCUSSION

The cloning of *groove*, a truncated version of *notch1* containing only EGF repeats

Using primers from the original 1294 bp *notch* fragment, 5' and 3' RACE produced what appears to be a truncated version of Notch1 containing only extracellular EGF repeat regions. According to the NCBI Conserved Domain Search, *groove* contains only 5 EGF repeat regions, as well as a NIDO domain. It lacks 31 of the 36 EGF repeats that are found in the full length Notch1 protein, as well as the three LNR repetitive regions that also characterize the extracellular domain of all Notch proteins. In addition, it also lacks a transmembrane region. This, in conjunction with the fact that it shows high homology to the secreted mouse protein SST3, suggests that *groove* is a secreted protein. *groove* also lacks all of the intracellular domains that are required for Notch signal transduction, including the RAM domain, the 6 ankyrin repeats, the 2 nuclear localization sequences, the TAD domain, and the PEST domain.

RT-PCR using primers designed from the 5' and 3' ends of the cloned RACE fragments in combination with the RACE primers independently verified and confirmed the presence of the 5' and 3' ends of *groove* in B1H1 cells. Further, external and nested RT-PCR using primers which spanned the length of the contig generated an appropriate sized fragment, which also confirms the existence of a single *groove* transcript in B1H1 cells. As B1H1 cells are derived from blastemal cells of the regenerating *Notophthalmus viridescens* forelimb, it can be concluded that this cDNA is likely to be found in the blastema of the regenerating forelimb, and therefore may play a role in the control of limb regeneration.

Towards a functional role for *groove* in relation to Notch signaling

While surprising, the discovery of this truncated version of *notch* containing only extracellular EGF repeat regions is not wholly unprecedented. Recently, Eiraku et al. (2002) cloned a truncated Notch-like cDNA of 2854 bp, containing only 10 EGF repeats followed by a 3' transmembrane region. This cDNA, named Delta/Notch-like Epidermal Growth Factor-related Receptor (DNER) was cloned in both mice and humans (Eiraku et al., 2002). Expression of DNER was localized to post-mitotic neurons in the central nervous system (CNS), and was absent from proliferating neuroblasts (Eiraku et al., 2002). While this suggests a role for DNER in mature neural tissues, it is uncharacteristic of Notch-related signaling, which has been shown to be specifically active in proliferating neural precursor cells (Solecki et al., 2001). However, this apparent contradiction may be explained when these data are interpreted in light of other experiments, which have shown that deletion of most of the intracellular signaling domains of Notch results in a dominant negative Notch protein (Rebay et al., 1993). Perhaps DNER is acting as a dominant negative form of Notch that suppresses Notch signaling in post-mitotic cells. This contradicts the author's conclusion that DNER is not likely to be involved in typical Notch-mediated signaling pathways during neurogenesis (Eiraku et al., 2002).

In addition, it has been shown that artificially generated secreted versions of Delta and Serrate which contain only extracellular EGF repeat regions also act as antagonists of Notch (Sun and Artavanis-Tsakonas, 1997). The effects of the secreted ligands were directly determined by measuring levels of *enhancer of split*, a downstream effector of Notch signaling. It was shown that the secreted versions of Delta and Serrate lead to a

decrease in *enhancer of split* expression, similar to Notch mutants (Sun and Artavanis-Tsakonas, 1997). The authors postulate that the secreted forms of Delta and Serrate antagonize Notch signaling by either binding to and sequestering available Notch receptor, or by respectively binding to membrane-tethered Delta and Serrate, thereby inhibiting them from signaling to Notch (Sun and Artavanis-Tsakonas, 1997). Either way, this is further evidence that soluble molecules consisting of only EGF repeats may play functional roles in the regulation of Notch signaling.

Finally, it has been reported that over-expression of the Notch receptor in a cell may act to repress Notch signaling through *cis* interactions at the cell surface (Baron et al., 2002). This is further evidence that the Notch receptor is capable of interacting with itself to modulate its own function. Following this, it is not inconceivable that a dominant negative version of Notch exists which binds to itself and similarly downregulates its own function. All these lines of evidence point towards a possible functional role for *groove* in the Notch signal transduction pathway.

Real time RT-PCR expression of *groove* and *notch* in B1H1 cell lines

Real time RT-PCR has become the gold standard technique in molecular biology for detecting and quantifying levels of mRNA expression in specific tissues of interest. It allows for direct comparison between expression levels of different genes by standardizing both genes against the expression levels of a housekeeping gene such as GapDH. However, it is limited in that it cannot be used to infer spatial expression of a gene, and in that it only measures mRNA, not protein levels. Therefore it is hard to draw conclusive inferences as to the function of a gene in a particular tissue, since one cannot discern which specific cells are expressing the gene (and to what intensity) in a

heterogeneous tissue sample, or how much functionally active protein is actually being produced. Further, fold over-expression is measured relative to the lowest expressing sample, and therefore is not a true indication of how much mRNA is actually in the tissue. For example, as was seen with *groove*, levels of mRNA expression seemed to fluctuate considerably, however, these fluctuations were minimal when compared to the fluctuations in *notch* expression. Even as such, it is entirely possible that overall *notch* expression is itself very low when compared to a more highly expressed gene, though it seems to be high when compared to *groove*.

Real time RT-PCR reveals that *groove* expression, while low, is still detectable in all samples that *notch1* is expressed in. Whether these levels of expression are sufficient to mediate a functional effect on Notch signaling is unknown. The fact that levels of *notch* and *groove* expression seem to be inversely related may support a role for *groove* in the negative regulation of *notch*. Even though fluctuations in *groove* expression seem minimal compared to fluctuations in *notch* expression, it is possible that factors such as greater mRNA stability or lower protein turnover rates may compensate for low mRNA levels to mediate a significant effect on Notch signaling in a given tissue.

In the B1H1 cell lines, *notch* expression was found at moderate levels (relative to the lowest expressing tissue amplified with *notch* primers) in subconfluent B1H1 cells. This is not surprising, as subconfluent B1H1 cells are thought to represent a population of undifferentiated, proliferating blastemal cells. *Notch* has been shown in many instances to play a role in maintaining cells in an undifferentiated state by suppressing differentiation. For example, over-expression of *notch* has been shown to suppress neurogenesis in mammalian cells (Nye et al, 1994; Kageyama and Nakanishi, 1997).

Also, *notch* is well known for its role in preventing myogenesis through the repression of the muscle specific marker, *myoD*, as well as through *myoD*-independent pathways (Nye et al, 1994; Nofziger et al., 1999; Hirsinger et al., 2001). *Notch* activation has also been shown to induce cell proliferation in the developing *Drosophila* wing (Go et al., 1998). Subconfluent B1H1 cells represent both undifferentiated cells and actively proliferating cells. In this context, it makes sense that *notch* should be expressed in subconfluent B1H1 cells. As the B1H1 cells become confluent, they begin to exit the cell cycle and align in a manner that will eventually allow them to fuse and form multinucleated myotubes. Therefore it also makes sense, in this context, that *notch* expression as detected by real time RT-PCR decreases in confluent B1H1 cells by approximately 2 fold relative to subconfluent B1H1 cells.

However, it was initially surprising that levels of *notch* expression increase in myotubes harvested 4 days post serum drop. One would expect that high levels of *notch* would prevent myotube differentiation, or that decreased levels of *notch* would be necessary to permit myotube formation. However, it has been shown that high levels of *myoD* expression can stimulate *notch* signaling in the early pre-somitic mesoderm of *Xenopus* by upregulating levels of Delta protein and mRNA (Wittenberger et al., 1999). Whether *myoD* also upregulates levels of *notch* is unknown, but this suggests a possible model wherein the drop in serum which induces myotube formation may in turn lead to increased expression of *myoD*, which may then upregulate levels of *notch* expression. Another line of evidence that may explain the relatively high levels of *notch* in 4 day myotubes comes from Bour et al. (2000), who showed that the gene *sticks-and-stones* (sns) is required specifically for *Drosophila* myoblast fusion, but not for myoblast

differentiation. As such, it acts as a marker for fusion-competent myoblasts (Bour et al., 2000). *Sns* expression was sharply reduced in *notch* mutant flies, which suggests that *sns* is regulated by *notch* (Bour et al., 2000). Following this, *notch* expression may be required in 4 day myotubes in order to regulate myotube fusion through a gene similar to *sns* in the newt. This then explains why *notch* expression decreases in 8 day (mature) myotubes, when most of the cell population should have already fused, and therefore no longer require *notch*. In fact, Fuerstenberg and Giniger (1998) show that muscle progenitor cells in the developing *Drosophila* embryo are only sensitive to *notch* until the time of myoblast fusion, as measured by the expression of muscle progenitor cell markers such as *S59*. It then makes further sense that in re-supplemented myotubes, where fusion should not be occurring at all, (on the contrary the cells should be dedifferentiating) *notch* expression continues to decrease.

Alternatively, *notch* may be playing a completely different role in myogenesis. Increasing evidence points to a role for *notch* in the control of cell migration and adhesion. Lindner et al. (2001) demonstrated that soluble forms of Jagged which act as Notch antagonists reduce cell-matrix interactions and hamper cell migration in transfected 3T3 cells. This suggests that endogenous Jagged/Notch signaling functions to propagate cell mobilization and migration. Additionally, it has been shown that activated forms of Notch confer a highly mobile, invasive phenotype on normally stationary mammary cells (Soriano et al., 2000). As B1H1 cells differentiate into myotubes, cytoskeletal rearrangements must occur in order for the cells to align and fuse into multinucleated myotubes. It is possible that *notch* is involved in directing the cell mobilization events that give rise to these cytoskeletal rearrangements that result in

myotube fusion, and that increased levels of *notch* are required to mediate this effect. Following this, it becomes clear why at 8 days post serum drop *notch* expression is reduced. By this time, the majority of cells have already fused and differentiated into myotubes, and no longer need to migrate or re-arrange themselves.

Real time RT-PCR expression of *groove* and *notch* in newt forelimb regenerates

Interestingly, *notch* expression is detected in whole non-regenerating limbs. There is no evidence for *notch* expression in whole, adult limbs in any other organism to date. It has been hypothesized that the ability of the newt to regenerate comes from its ability to re-express developmental genes. Perhaps it does this by maintaining expression of developmental genes such as *notch* at basal levels in adult tissues, such that when required, the genes do not have to be completely re-induced, and instead, they can simply be upregulated. In fact, evidence of this has been provided by studies of *hox* gene expression in regenerating newt appendages. *HoxA11* expression was detected in both the intact limb and the intact tail of the adult newt (Beauchemin et al., 1994). As regeneration is induced, *hoxA11* expression increases in the blastemas of both appendages, suggesting that it is maintained at a basal level in the intact tissue before being upregulated as required in the regenerate (Beauchemin et al., 1994).

Several discrepancies were observed in both the *groove* and *notch* expression profiles between the two data sets obtained by real time RT-PCR amplification of cDNA from regenerating forelimb tissue. These discrepancies can be explained by the fact that the second set of tissue samples (whole limb, 24 hour, 8 day, 15 day and 21 day regenerating tissue) came from a different population of younger, captive bred newts, which were all sexually mature, but still only half the physical size of a full grown adult.

As *notch* is a gene that is known to play a role in growth and development, it is entirely possible that developmental Notch signaling is still active in these younger newts, and that this extraneous Notch signaling may obscure the expression profile that would be obtained if regeneration alone were taking place in the limb. Further to this hypothesis, it can be noted that the relative levels of *notch* expression in the whole limb are much higher in the younger newts (Figure 17b) than they are in the older newts (Figure 17a). Developmental factors may also be playing a role in affecting *groove* signaling, in a similar manner. Because of these factors, the discussion below will pertain to only the data obtained in the first round of real time RT-PCR experiments (Figures 16a, 17a and 18a only), in which full grown, adult newts were used.

At 24 hours post amputation, real time RT-PCR detects that *notch* expression increases by almost 3 fold relative to the whole limb tissue. It was postulated above that *notch* signaling may play a role in activating migration and mobilization of cells by increasing the ability of cells to interact with their extracellular matrix. During the initial phases of wound healing in newts, epidermal cells at the edges of the amputation plane are mobilized and migrate to cover the amputation plane. This process may require increased levels of *notch* expression. In fact, Lindner et al. (2001) detected *in vivo* expression of *notch* at the borders of regenerating rat vascular endothelium wounds where cells similarly migrate from the edges of the wound to cover the wound surface.

Similarly, it has been shown that Notch1, Notch2, Notch3 and Delta1 are re-expressed in rat dental tissue within 24 hours after infliction of injury (Mitsiadis et al., 1999). This expression is absent in adult dental tissue, and is thought to be part of a regenerative response, since dental tissue possesses a limited ability for repair and

regeneration following injury (Mitsiadis et al., 1999). Here again, Notch expression is associated with undifferentiated cells, indicating that Notch may be playing a role in either determining cell fate by specifically marking undifferentiated precursor cells, or in maintaining cells in an undifferentiated state by preventing differentiation. Interestingly, it was found that Notch2 is the predominant Notch isoform associated with the response to injury (Mitsiadis et al., 1999). Notch1 and Notch3 were also expressed in the vasculature and in the mesenchyme flanking the site of injury, but to a lesser extent (Mitsiadis et al., 1999). In this thesis, we examine the expression of *notch1* in newt limb regenerates, however, it is entirely possible that other *notch* isoforms exist in the newt that are responsible for regulating the same or different regenerative processes. Therefore, while we may speculate as to the role of *notch1* in regeneration, we must keep in mind that this may not be the complete picture, since other isoforms may also be responsible for regulating different aspects of regeneration.

At one week, levels of *notch1* expression seem to be decrease. At this time, cells are just beginning to proliferate in the mesenchyme under the AEC and a blastema is just beginning to develop. Low levels of *notch* expression suggest that *notch* does not play a role in inducing dedifferentiation which also occurs during this time. This is in accordance with the *notch* expression data from the B1H1 cell lines, which showed that *notch* expression was relatively low in re-supplemented myotubes, which represent a population of differentiated B1H1 cells being stimulated to dedifferentiate. At about 2 weeks post amputation, a substantial blastema begins to form. By this stage, real time RT-PCR reveals that levels of *notch* expression are increasing. In the 2 week blastema, cells are both rapidly proliferating as well as dedifferentiating. As such, they need to

remain in an undifferentiated state during this time. An increase in *notch* expression at this timepoint is quite promising, since *notch* has been shown to both play an active role in the stimulation of mitotic activity and in the maintenance of an undifferentiated state through the prevention of differentiation (Nye et al, 1994; Kageyama and Nakanishi, 1997; Go et al., 1998; Nofziger et al., 1999; Hirsinger et al., 2001).

Later in the three and four week regenerates, *notch* expression progressively decreases. At this time, tissues are starting to be re-patterned and re-differentiate, and lower levels of *notch1* expression may indicate that in the regenerating newt forelimb at least, *notch1* does not play a role in the re-patterning of the regenerate.

Future directions

Due to the wide variety of functions that *notch* may mediate during regeneration, and given the plethora of ways in which Notch signaling is modulated both at the ligand binding level and at the signal transduction level, it becomes difficult to say with certainty what functional significance fluctuations in *notch* expression will have in a given tissue. In addition, the fact that it was difficult to align the *groove* fragment with the sequence obtained for *notch1* suggests that maybe the two genes are not related, and *groove* may not represent a truncated version of *notch*. In order to test whether the two genes are related and whether Groove modulates Notch function, further work needs to be done on a protein level to truly ascertain the function of Notch and Groove in limb regeneration.

Detection of Notch and Groove protein

Protein work must be done to confirm any inferences made on *notch* and *groove* function in the *Notophthalmus viridescens* regenerating forelimb on the basis of mRNA

expression. This would entail inserting selected portions of *groove and notch* into translation vectors, which would create Groove and Notch-specific amino acid sequences from which antibodies can be generated. These antibodies can then be used to run Westerns in order to validate the expression of both Groove and Notch in the same tissues that real time RT-PCR was performed on. Following this, the antibodies can be used to perform immunohistochemistry on sectioned tissue from the following stages: whole limbs, 24 hour post-amputation, 1 week, 2 weeks, 3 weeks, palette stage, early digit stage, mid digit stage, and late digit stage limbs. These data will provide us with a spatial and temporal profile of Notch and Groove expression in the regenerating newt forelimb, from which we may be able to draw inferences as to the function of these two genes, as well as their relationship to each other.

Identification of other notch isoforms

In most vertebrates, there are 4 *notch* genes. Sometimes these genes have distinct patterns of expression, while other times their expression patterns overlap. Often, the different *notch* isoforms work together in the same tissues to regulate developmental processes. It is unknown how many *notch* isoforms exist in the newt. Therefore, the other isoforms must be cloned and their expression patterns examined on both the protein and the mRNA level, in order to fully understand the role of Notch signaling in regeneration.

Viral-mediated over-expression of groove

In order to test whether or not *groove* truly functions as a negative regulator of *notch* in the newt, the complete cDNA of *groove* can be inserted into a retrovirus, which can then be allowed to infect newt blastemal B1H1 cells. Success of infection can be

assayed by Western analysis using the antibodies generated against Groove above. Alternately, real time RT-PCR can be performed to quantify levels of *groove* expression before and after retroviral infection. Following this, real time RT-PCR can be performed using primers specific to *Notophthalmus viridescens notch1* to test if over-expression of *groove* downregulates expression of *notch1*. However, even if no downregulation is observed, it is possible that Groove still acts as a dominant negative regulator of Notch1 at the protein level, for example by binding to and sequestering available Notch receptor, and thus preventing ligand-stimulated signal transduction. This can be tested by measuring the protein or mRNA expression levels of downstream effectors of Notch signal transduction such as CBF1 or HES before and after *groove* overexpression. As none of the downstream components of Notch signaling have been cloned in the newt, this would have to preclude the aforementioned experiment.

Summary

In this thesis I have cloned a partial cDNA of the newt homologue of *Notophthalmus viridescens notch1*. In the process, I also cloned *groove*, a truncated version of *notch1* containing only 5 EGF repeats and a NIDO related domain. The high level of homology that *Notophthalmus viridescens notch1* shares with *notch1* of other species suggests that this developmentally important molecule has been evolutionary conserved. The fact that it was cloned from B1H1 cells derived from regenerating newt blastemas points to a possible functional role for it in regulating regeneration. An analysis of the functional domains of the *groove* cDNA suggests that it is a secreted protein that may play a role in negatively regulating Notch signaling. Real time RT-PCR expression of *notch1* in the newt forelimb regenerate reveals that *notch* seems to be

relatively highly expressed in the 24 hour regenerate. This may be due to a functional role it plays in formation of the wound epidermis by mobilizing cells and inducing migration. *Notch* expression is also relatively high in the 2 week regenerate, which may be indicative of a functional role for the gene in blastema formation and maintenance. Notch activation has been shown to result in both initiation of proliferation and the prevention of differentiation, both of which are processes that are required in the blastema. These data point towards a functional role for *notch1* in regulating the complex process of epimorphic forelimb regeneration.

REFERENCES

Artavanis-Tsakonas, S., Matsuno, K., and Fortini, M. E. (1995). Notch signaling. Science *268*, 225-232.

Artavanis-Tsakonas, S., Rand, M. D., and Lake, R. J. (1999). Notch signaling: cell fate control and signal integration in development. Science *284*, 770-776.

Baron, M., Aslam, H., Flasza, M., Fostier, M., Higgs, J. E., Mazaleyrat, S. L., and Wilkin, M. B. (2002). Multiple levels of Notch signal regulation. Mol Membr Biol *19*, 27-38.

Beauchemin, M., Noiseux, N., Tremblay, M., and Savard, P. (1994). Expression of Hox A11 in the limb and the regeneration blastema of adult newt. Int J Dev Biol *38*, 641-649.

Blau, H. M., Brazelton, T. R., and Weimann, J. M. (2001). The evolving concept of a stem cell: entity or function? Cell *105*, 829-841.

Bode, H. R. (2003). Head regeneration in Hydra. Dev Dyn *226*, 225-236.

Borgens, R. B. (1982). Mice regrow the tips of their foretoes. Science *217*, 747-750.

Bour, B. A., Chakravarti, M., West, J. M., and Abmayr, S. M. (2000). Drosophila SNS, a member of the immunoglobulin superfamily that is essential for myoblast fusion. Genes Dev *14*, 1498-1511.

Bray, S. (1998). Notch signalling in Drosophila: three ways to use a pathway. Semin Cell Dev Biol *9*, 591-597.

Brennan, K., and Gardner, P. (2002). Notching up another pathway. Bioessays *24*, 405-410.

Brockes, J. P. (1997). Amphibian limb regeneration: rebuilding a complex structure. Science *276*, 81-87.

Bryant, S. V., Endo, T., and Gardiner, D. M. (2002). Vertebrate limb regeneration and the origin of limb stem cells. Int J Dev Biol *46*, 887-896.

Cadinouche, M. Z., Liversage, R. A., Muller, W., and Tsilfidis, C. (1999). Molecular cloning of the Notophthalmus viridescens radical fringe cDNA and characterization of its expression during forelimb development and adult forelimb regeneration. Dev Dyn *214*, 259-268.

Campion, D. R. (1984). The muscle satellite cell: a review. Int Rev Cytol *87*, 225-251.

Carlson, B. M. (2003). Muscle regeneration in amphibians and mammals: Passing the torch. Dev Dyn *226*, 167-181.

Chen, Z. J., Ughrin, Y., and Levine, J. M. (2002). Inhibition of axon growth by oligodendrocyte precursor cells. Mol Cell Neurosci *20*, 125-139.

da Silva, S. M., Gates, P. B., and Brockes, J. P. (2002). The newt ortholog of CD59 is implicated in proximodistal identity during amphibian limb regeneration. Dev Cell *3*, 547-555.

Dent, J. (1962). Limb regeneration in larval metamorphosing individuals of the South African Clawed toad. Journal of Morphology *110*, 61-77.

D'Jamoos, C. A., McMahon, G., and Tsonis, P. A. (1998). Fibroblast growth factor receptors regulate the ability for hindlimb regeneration in Xenopus laevis. Wound Repair Regen *6*, 388-397.

Eiraku, M., Hirata, Y., Takeshima, H., Hirano, T., and Kengaku, M. (2002). Delta/notch-like epidermal growth factor (EGF)-related receptor, a novel EGF-like repeat-containing protein targeted to dendrites of developing and adult central nervous system neurons. J Biol Chem *277*, 25400-25407.

Fuerstenberg, S., and Giniger, E. (1998). Multiple roles for notch in Drosophila myogenesis. Dev Biol *201*, 66-77.

Gardiner, D. M., Blumberg, B., Komine, Y., and Bryant, S. V. (1995). Regulation of HoxA expression in developing and regenerating axolotl limbs. Development *121*, 1731-1741.

Gardiner, D. M., Endo, T., and Bryant, S. V. (2002). The molecular basis of amphibian limb regeneration: integrating the old with the new. Semin Cell Dev Biol *13*, 345-352.

Go, M. J., Eastman, D. S., and Artavanis-Tsakonas, S. (1998). Cell proliferation control by Notch signaling in Drosophila development. Development *125*, 2031-2040.

Goss, R. J. (1969). Principles of Regeneration (New York, NY, Academic Press, Inc.).

Harty, M., Neff, A. W., King, M. W., and Mescher, A. L. (2003). Regeneration or scarring: An immunologic perspective. Dev Dyn *226*, 268-279.

Hirsinger, E., Malapert, P., Dubrulle, J., Delfini, M. C., Duprez, D., Henrique, D., Ish-Horowicz, D., and Pourquie, O. (2001). Notch signalling acts in postmitotic avian myogenic cells to control MyoD activation. Development *128*, 107-116.

Illingworth, C. M. (1974). Trapped fingers and amputated finger tips in children. J Pediatr Surg *9*, 853-858.

Iten, L. E., and Bryant, S.V. (1973). Forelimb regeneration from different levels of Amputation in the newt, Notophthalmus viridescens: length, rate and stages. Wilhelm Roux' Archiv fur Entwicklungsmechanik der Organismen *173*, 263-282.

Kageyama, R., and Nakanishi, S. (1997). Helix-loop-helix factors in growth and differentiation of the vertebrate nervous system. Curr Opin Genet Dev *7*, 659-665.

Kaneko, Y., Hirota, K., Matsumoto, G., and Hanyu, Y. (2001). Expression pattern of a newt Notch homologue in regenerating newt retina. Brain Res Dev Brain Res *128*, 53-62.

Koshiba, K., Kuroiwa, A., Yamamoto, H., Tamura, K., and Ide, H. (1998). Expression of Msx genes in regenerating and developing limbs of axolotl. J Exp Zool *282*, 703-714.

Lindner, V., Booth, C., Prudovsky, I., Small, D., Maciag, T., and Liaw, L. (2001). Members of the Jagged/Notch gene families are expressed in injured arteries and regulate cell phenotype via alterations in cell matrix and cell-cell interaction. Am J Pathol *159*, 875-883.

Maden, M. (1982). Vitamin A and pattern formation in the regenerating limb. Nature *295*, 672-675.

Martinez Arias, A., Zecchini, V., and Brennan, K. (2002). CSL-independent Notch signalling: a checkpoint in cell fate decisions during development? Curr Opin Genet Dev *12*, 524-533.

McGann, C. J., Odelberg, S. J., and Keating, M. T. (2001). Mammalian myotube dedifferentiation induced by newt regeneration extract. Proc Natl Acad Sci U S A *98*, 13699-13704.

Miele, L., and Osborne, B. (1999). Arbiter of differentiation and death: Notch signaling meets apoptosis. J Cell Physiol *181*, 393-409.

Mitsiadis, T. A., Fried, K., and Goridis, C. (1999). Reactivation of Delta-Notch signaling after injury: complementary expression patterns of ligand and receptor in dental pulp. Exp Cell Res *246*, 312-318.

Muller, T. L., Ngo-Muller, V., Reginelli, A., Taylor, G., Anderson, R., and Muneoka, K. (1999). Regeneration in higher vertebrates: limb buds and digit tips. Semin Cell Dev Biol *10*, 405-413.

Niswander, L., Tickle, C., Vogel, A., Booth, I., and Martin, G. R. (1993). FGF-4 replaces the apical ectodermal ridge and directs outgrowth and patterning of the limb. Cell *75*, 579-587.

Nofziger, D., Miyamoto, A., Lyons, K. M., and Weinmaster, G. (1999). Notch signaling imposes two distinct blocks in the differentiation of C2C12 myoblasts. Development *126*, 1689-1702.

Nye, H. L., Cameron, J. A., Chernoff, E. A., and Stocum, D. L. (2003). Regeneration of the urodele limb: A review. Dev Dyn *226*, 280-294.

Nye, J. S., Kopan, R., and Axel, R. (1994). An activated Notch suppresses neurogenesis and myogenesis but not gliogenesis in mammalian cells. Development *120*, 2421-2430.

Panin, V. M., and Irvine, K. D. (1998). Modulators of Notch signaling. Semin Cell Dev Biol *9*, 609-617.

Pecorino, L. T., Entwistle, A., and Brockes, J. P. (1996). Activation of a single retinoic acid receptor isoform mediates proximodistal respecification. Curr Biol *6*, 563-569.

Rebay, I., Fehon, R. G., and Artavanis-Tsakonas, S. (1993). Specific truncations of Drosophila Notch define dominant activated and dominant negative forms of the receptor. Cell *74*, 319-329.

Reginelli, A. D., Wang, Y. Q., Sassoon, D., and Muneoka, K. (1995). Digit tip regeneration correlates with regions of Msx1 (Hox 7) expression in fetal and newborn mice. Development *121*, 1065-1076.

Riddle, R. D., Johnson, R. L., Laufer, E., and Tabin, C. (1993). Sonic hedgehog mediates the polarizing activity of the ZPA. Cell *75*, 1401-1416.

Roy, S., and Gardiner, D. M. (2002). Cyclopamine induces digit loss in regenerating axolotl limbs. J Exp Zool *293*, 186-190.

Saunders, J. W. (1948). The proximo-distal sequence of the origin of the parts of the chick wing and the role of the ectoderm. Journal of Experimental Zoology *108*, 363-403.

Sestan, N., Artavanis-Tsakonas, S., and Rakic, P. (1999). Contact-dependent inhibition of cortical neurite growth mediated by notch signaling. Science *286*, 741-746.

Shimizu-Nishikawa, K., Tazawa, I., Uchiyama, K., and Yoshizato, K. (1999). Expression of helix-loop-helix type negative regulators of differentiation during limb regeneration in urodeles and anurans. Dev Growth Differ *41*, 731-743.

Singer, A. J., and Clark, R. A. (1999). Cutaneous wound healing. N Engl J Med *341*, 738-746.

Solecki, D. J., Liu, X. L., Tomoda, T., Fang, Y., and Hatten, M. E. (2001). Activated Notch2 signaling inhibits differentiation of cerebellar granule neuron precursors by maintaining proliferation. Neuron *31*, 557-568.

Soriano, J. V., Uyttendaele, H., Kitajewski, J., and Montesano, R. (2000). Expression of an activated Notch4(int-3) oncoprotein disrupts morphogenesis and induces an invasive phenotype in mammary epithelial cells in vitro. Int J Cancer *86*, 652-659.

Stocum, D. L. (2001). Stem cells in regenerative biology and medicine. Wound Repair Regen *9*, 429-442.

Stocum, D. L. and Dearlove, G.E. (1972). Epidermal-mesodermal interaction during morphogenesis of the limb regeneration blastema in larval salamanders. Journal of Experimental Zoology *181*, 49-62.

Sun, X., and Artavanis-Tsakonas, S. (1997). Secreted forms of DELTA and SERRATE define antagonists of Notch signaling in Drosophila. Development *124*, 3439-3448.

Tanaka, E. M., Drechsel, D. N., and Brockes, J. P. (1999). Thrombin regulates S-phase re-entry by cultured newt myotubes. Curr Biol *9*, 792-799.

Tanaka, E. M., Gann, A. A., Gates, P. B., and Brockes, J. P. (1997). Newt myotubes reenter the cell cycle by phosphorylation of the retinoblastoma protein. J Cell Biol *136*, 155-165.

Torok, M. A., Gardiner, D. M., Izpisua-Belmonte, J. C., and Bryant, S. V. (1999). Sonic hedgehog (shh) expression in developing and regenerating axolotl limbs. J Exp Zool *284*, 197-206.

Weinmaster, G. (1997). The ins and outs of notch signaling. Mol Cell Neurosci *9*, 91-102.

Wittenberger, T., Steinbach, O. C., Authaler, A., Kopan, R., and Rupp, R. A. (1999). MyoD stimulates delta-1 transcription and triggers notch signaling in the Xenopus gastrula. Embo J *18*, 1915-1922.

Yokoyama, H., Yonei-Tamura, S., Endo, T., Izpisua Belmonte, J. C., Tamura, K., and Ide, H. (2000). Mesenchyme with fgf-10 expression is responsible for regenerative capacity in Xenopus limb buds. Dev Biol *219*, 18-29.

APPENDIX 1 - BASIC PROTOCOLS

Total RNA extraction using Trizol® reagent (Invitrogen)

Notes: Tissue should be between 50-100 mg.
Keep all solutions on ice.
Use plugged pipetman tips at all times.

1. Add 1 ml trizol reagent to tissue in sterile, round bottom tissue culture tubes.
2. For cells, pipet up and down to homogenate. For tissue, homogenate using a hand held homogenizer that has been washed in DEPC treated water with Alconox soap, then rinsed thoroughly with DEPC treated water.
3. Transfer homogenized tissue in Trizol® to a 1.5 ml Eppendorf tube.
4. Centrifuge at 13200 rpm for 10 minutes at 4°C.
5. Collect supernatant in a fresh tube.
6. Add 200 µl chloroform.
7. Shake by hand vigorously for 15 seconds.
8. Incubate at room temperature for 2-3 minutes.
9. Centrifuge at 13,200 rpm for 15 minutes at 4°C.
10. Transfer approximately 600 µl of aqueous phase to a fresh tube.
11. Add 500 µl isopropanol.
12. Incubate 10-15 minutes at room temperature.
13. Centrifuge at 13,200 rpm for 10 minutes at 4°C.
14. Decant fluid.
15. Wash pellet with 1 ml 75% ethanol in DEPC water.
16. Centrifuge at 13,200 rpm for 5 minutes at 4°C.
17. Decant fluid.
18. Air dry pellet.
19. Resuspend in 20-40 µl of DEPC treated water.
20. Store at –70°C.
21. Quantify using spectrophotometry.

Quick protocol for verification of RNA

Prepare gel:

- Weigh out 0.5 g RNAse free agarose with RNAse free weigh dishes.
- Add 1 ml 50 X TAE and 49 ml DEPC treated water.
- Dissolve in microwave.
- Once cool, add 0.5 µl ethidium bromide.
- Pour into clean gel tray.

To clean gel box:

- Fill with DEPC treated water, add bleach, leave for >10 min.
- Decant, rinse with DEPC treated water.
- Fill with DEPC treated water, add 23M formaldehyde, leave for >10 minutes.
- Decant, rinse with DEPC treated water.

Prepare samples:

- Run 1 μg total RNA in 8-12 μl DEPC treated water.
- Denature RNA for 10 minutes at 65°C.
- Snap cool on ice for 1 minute.
- Add 1 μl loading buffer.
- Load onto gel, run with 1X TAE in DEPC treated water running buffer.
- Run for 10-15 minutes at 110 V.

Basic RACE protocol

Notes: Keep all solutions on ice at all times.
Use plugged pipetman tips.

Mix the following:

5 μl	10 X PCR buffer
1.5 μl	50mM MgCl
1 μl	10mM dNTP mixture
0.5 μl	Taq polymerase
1 μl	external or nested gene specific RACE primer (10 μM)
1 μl	AP1 or AP2 primer (10 μM)
X μl	template DNA
X μl	PCR water (ddH_2O autoclaved and filter sterilized to 0.2 μm)
50 μl	total reaction volume

- Spin contents to the bottom of the PCR tubes.
- Overlay mix with two drops of mineral oil.

First strand synthesis for reverse transcription polymerase chain reaction (RT-PCR)

Thaw RNA on ice, then mix the following:

X μl	RNA (up to 2μg)
1 μl	reverse primer (50ng/μl)
X μl	DEPC treated water, filter sterilized at 0.2 μm
7 μl	total volume

- Heat denature at 65°C for 10 minutes.
- Snap cool on ice for 5 minutes.
- Add the following:

6 μl	5 X transcription buffer
3 μl	10mM dNTP mix
3 μl	0.1M Dithiothreitol (DTT)

1 µl	M-MLV reverse trancriptase
1 µl	RNA guard (Invitrogen)
9 µl	DEPC treated water, filter sterilized at 0.2 µm
7 µl	RNA mix above
30 µl	total reaction volume

- Incubate at 37°C for at least 1 hour.
- Use 5 µl as template in PCR.

Basic PCR protocol

Notes: Keep Taq polymerase on ice at all times.
Use plugged pipetman tips.

Mix the following:

2.5 µl	10 X PCR buffer
0.75 µl	50mM MgCl
0.5 µl	10mM dNTP mixture
0.25 µl	Taq polymerase
1 µl	forward primer (25 – 50 ng/µl)
1 µl	reverse primer (25 – 50 ng/µl)
X µl	template DNA
X µl	PCR water *
25 µl	total reaction volume

- Spin contents to the bottom of the tubes, and load into thermal cycler.

*PCR water is ddH_2O that has been autoclaved and filter sterilized to 0.2 µm.

Deoxyribonuclease treatment of total RNA
(instructions from Sigma product information insert)

Add the following to an RNAse-free PCR tube:

2 µg	total RNA in 8 µl DEPC-treated water filter sterilized to 0.2 µm
1 µl	10 X Reaction buffer
1 µl	Amplification grade DNAse (1 u/µl)
10 µl	total reaction volume

- Incubate at room temperature for 15 minutes.
- Add 1 µl of Stop solution to inactivate the DNase.
- Heat reaction mixture at 65°C for 10 minutes to denature the RNA and the Dnase.
- Snap cool on ice.

- Proceed with reverse transcription.

Real time RT-PCR protocol

Use first strand generated as above.

General notes:

- Clean bench area and pipetmans with DNAzap (Ambion) before starting.
- Wipe all tubes with 100% ethanol before opening.
- Use plugged tip pipet tips reserved for real time RT-PCR only.
- Shield SYBR® green from light.
- Never pipet into the each well of the 96 well plate more than once.

Add the following:

12.5 µl	iQ SYBR® green supermix (BioRad)
0.5 µl	Forward primer (10 µM)
0.5 µl	Reverse primer (10 µM)
1 µl	Reverse transcribed template cDNA (diluted to half in nuclease-free water (Ambion))
10.5 µl	Nuclease-free water (Ambion)
25 µl	total reaction volume

- Aliquot into 96 well microplates (BioRad) carefully, ensuring that no droplets of water stick to the sides of the plates.
- Perform all reactions in triplicate.
- Cover with optically clear tape (BioRad) and seal evenly with applicator (BioRad).

APPENDIX 2 - REAGENTS AND RECIPES

Tissue culture reagents

Newt media with 10% FCS

250 ml	Minimal essential medium with Earles salts
90 ml	ddH_2O filter sterilized 0.2 μm
40 ml	heat inactivated fetal calf serum
4 ml	100 X Penicillin/streptomycin
4 ml	Insulin
4 ml	100 X L-glutamine

- To heat inactivate FCS, incubate at 56°C for 30 minutes.
- To prepare insulin, dissolve 50 mg insulin in 0.1 M HCl. Add 45 ml A. PBS slowly, shaking. Filter sterilize and aliquot. Store at –20°C.

A. PBS

Dilute 10 X Dulbeccos phosphate buffered saline without calcium and magnesium to 1 X in sterile ddH_2O. Add 25 ml sterile ddH_2O.

Gelatin coated plates

Prepare gelatin by dissolving 0.75 g of gelatin in 100 ml ddH_2O in a 65°C waterbath. Filter sterilize 0.2 μm and store at 4°C. Heat to 37°C to redissolve. Add 2 ml liquid gelatin onto plates, swirl to cover bottom evenly. Aspirate off excess gelatin. Plate cells directly onto liquid or solid gelatin coated plates.

Cloning and sequencing reagents

L-broth

5 g	tryptone peptone
2.5 g	yeast extract
5 g	sodium chloride
500 ml	ddH_2O

Mix well, then autoclave to sterilize. Store at 4°C.

LB-ampicillin/IPTG/X-gal plates

Make 500ml LB according to the recipe above.
Add 7.5 g bacto agar.
Mix well, then autoclave to sterilize.
Cool to 50°C, then add:

250 µl Ampicillin (100mg/ml)
40 mg Xgal in 500 µl di-methyl formamide
250 µl 1M IPTG in ddH_2O

Pour into 100mm sterile petri plates.
Flame the top of the plates with a bunsen burner to remove bubbles.
Store at 4°C inverted.

APPENDIX 3 - PRIMERS

Primer name	Primer sequence 5'→3'	Length
M13 forward	GTAAAACGACGGCCAGT	17
M13 Reverse	CAGGAAACAGCTATGAC	17
5'RACEex	CTGACCTGCTCGTACGGGGACCACTA	26
5'RACEnes	ACAAAGCGTCCAGAGGGGTCACATAGG	27
3'RACEex	AATACTCCCTGCCATCCCCCTGTGACTC	28
3'RACEnes	CGAGAAAGTAAGGCCGAGTCCATGCAGC	28
5'PCRfwd	AGGTCGGGGCTGTAAAAATG	20
5'PCRrev	TCACGACGGGGTCTTTGGAA	20
3'PCRfwd	AATACTCCCTGCCATCCCCCTGTGACTC	28
3'PCRrev	ATGGACTCGGCCTTACTTTCTCGCAG	26
5'UTRex	TATTTTCCAGAGTTCCCAGGGTTTTAGC	28
5'UTRnes	GCGAGCTCTCCTTCACCATCTTCAACTA	28
3'UTRex	TCTGTCCTGCTTAGTCATTTTCTGGGTCAA	30
3'UTRnes	CAAATGTTAGTAAAATGAAGGCCCAAGAAT	30
Notch2F	ACHTGCCTSGACCAGATYGGRGARTTY	27
Notch2R	RAAYTCYCCRATCTGGTCWAGGCAVGT	27
Notch3F	AACACMCCYGACTGYACYGAGAGCTC	26
Notch3R	GAGCTCTCRGTRCAGTCRGGKGTGTT	26
Notch4F	TGYCAGAAYGGHGCYACVTGCACWGAC	27
Notch4R	GTCSGTGCABGTRGCDCCRTTCTGGCA	27
Notch5R	GCGCAGRTCSGCVGCGTCMAGRTGCTG	27
2F4R79midFwd	TCGACAGGATAAATGGCTACC	21
2F4R79midRev	AGAGCTCTCAGTGCAGTCAGGGGTAT	26
4F5R7midFwd	ACGGTCCTGTGGGCAATCTAC	21
4F5R7midRev	CCATTGAATTTTCCAGGGCACAC	23
2F3R26midFwd	CGACAGGATAAATGGCTACGAGT	25
2F3R26midRev	TGTCTTTGCAGGTTCCTCCGTTCAT	23
4F5R26midFwd	GGCAAGCCCTGTAGAAATGGT	21
4F5R26midRev	GGCCGCCATCACCACATACAT	21
4F5R26PrFwd1	GCTGGGACGGTGGCGACTGTT	21
4F5R26PrRev	CGCCGCTTGCTCTTGTTGGTCT	22
NotchRTfwd	ATGGCACCCTGGTTATCGTTGTC	23
NotchRTrev	TACTCGGCTTTGCTGTCCTTCTTG	24
GrooveRTfwd	ACTCCCTGCCATCCCCCTGTGACT	24
GrooveRTrev	GCTGCATGGACTCGGCCTTACTTT	24
NvGAPDH_F1	TGTGGCGTGACGGCAGAGGTG	21
NvGAPDH_R1	TCCAAGCGGCAGGTCAGGTCAAC	23

APPENDIX 4 – PCR PROGRAMS

Basic RACE programs

- RACE experiments used a Perkin Elmer DNA thermal cycler 480.
- Block temperature of the thermal cycler was heated to 94°C before samples were loaded for "hot start".

External RACE
94°C 1 minute
94°C 30 seconds } X 30
68°C 4 minutes }
68°C 10 minutes
Hold 4°C

Nested RACE
94°C 1 minute
94°C 30 seconds } X 20
68°C 4 minutes }
68°C 10 minutes
Hold 4°C

Other PCR programs

- All other PCR programs used a Eppendorf mastercycler gradient thermal cycler
- The lid of the thermal cycler was pre-warmed to 90°C prior to loading to prevent evaporation of the sample.

CTCONDI
95°C 2 minutes
94°C 1 minute
62°C 1 min 30 sec } X 30
72°C 1 min 30 sec
72°C 10 minutes
Hold 4°C

CSPCRSC
95°C 2 minutes
94°C 1 minute
65.5°C 1 min 30 sec } X 30
72°C 1 min 30 sec
72°C 10 minutes
Hold 4°C

3'UTRconf

95°C 2 minutes
94°C 1 min 30 sec
68°C 1 min 30 sec } X 35
72°C 1 min 30 sec
72°C 10 minutes
Hold 4°C

5'UTRconf
95°C 2 minutes
94°C 1 minute
64°C 1 minute } X 35
72°C 1 min 30 sec
72°C 10 minutes
Hold 4°C

UTRcontig
95°C 2 minutes
94°C 1 minute
61 +/- 10°C 1 minute } X 35
72°C 2 minutes
72°C 10 minutes
Hold 4°C

CANDEGN
95°C 2 minutes
94°C 1 minute
66°C 1 minute } X 35
72°C 2 min 30 sec
72°C 10 minutes
Hold 4°C

CSMIDPR
95°C 2 minutes
94°C 1 minute
61 +/- 10°C 1 minute } X 30
72°C 1 min 30 sec
72°C 10 minutes
Hold 4°C

Real time RT-PCR programs

- Real time RT-PCR programs were performed in a BioRad iCycler real time thermal cycler.

Csmelt57

90°C 3 minutes
95°C 30 seconds
57°C 30 seconds } X 40
72°C 30 seconds
72°C 10 minutes
95°C 1 minute
55°C 1 min
55°C + 0.5°C incremental increases, 10 seconds each X 80 increments
Hold 10°C